AD-A033 738 TRW SYSTEMS GROUP REDONDO BEACH CALIF F/G 15/6
HOT WIRE MEASUREMENTS OF TEMPERATURE FIELD STRUCTURE WITHIN GES--ETC(U)
MAR 76 R G BATT DNA001-74-C-0067
UNCLASSIFIED DNA-3936F NL

1 OF 2
AD A033738

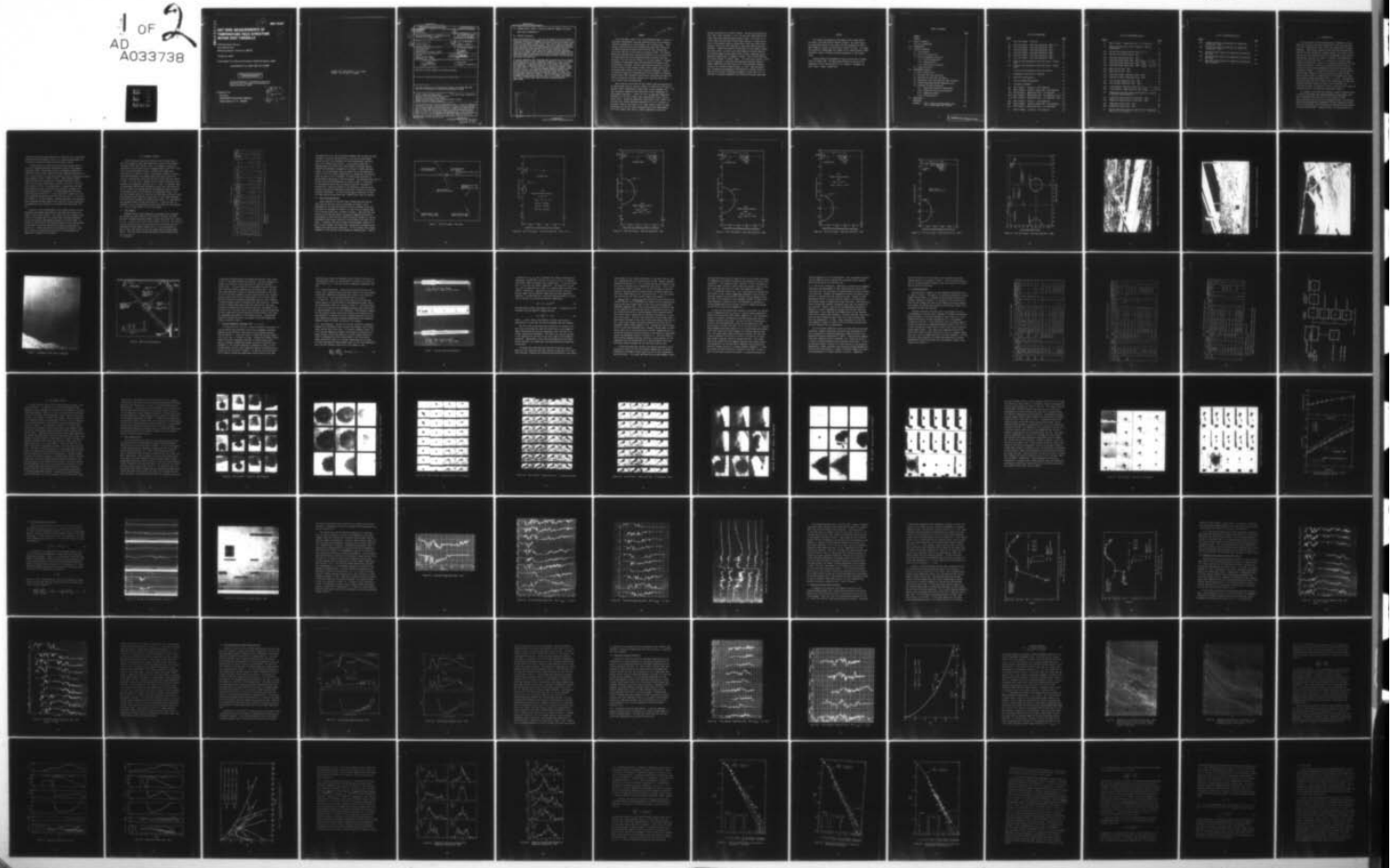

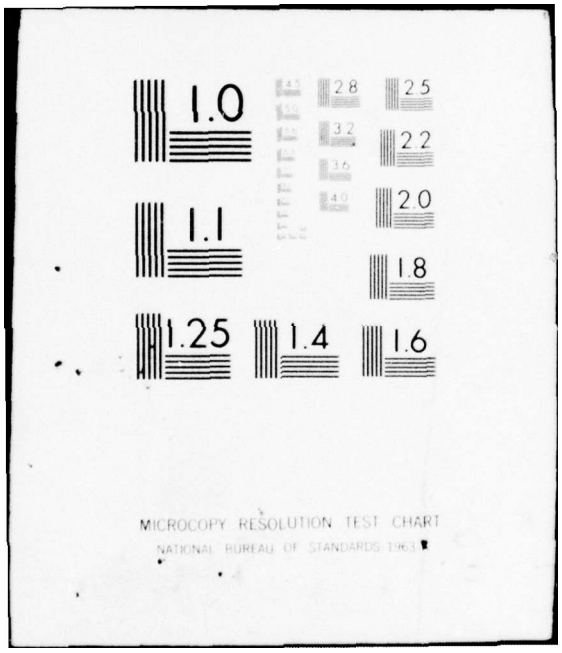
1.0
1.1
1.25
1.4
1.6
1.8
2.0
2.2
2.5
2.8
3.2
3.6
4.0
MICROCOPY RESOLUTION TEST CHART
NATIONAL BUREAU OF STANDARDS 1963

(12)

DNA 3936F

HOT WIRE MEASUREMENTS OF TEMPERATURE FIELD STRUCTURE WITHIN GEST FIREBALLS

TRW Systems Group
One Space Park
Redondo Beach, California 90278

31 March 1976

Final Report for Period 8 October 1973—31 March 1976

CONTRACT No. DNA 001-74-C-0067

THIS WORK SPONSORED BY THE DEFENSE NUCLEAR AGENCY
UNDER RDT&E RMSS CODES B322074462 L25AAXHX63406 AND
B322074464 S99QAXHC06171 H2590D.

Prepared for
Director
DEFENSE NUCLEAR AGENCY
Washington, D. C. 20305

Destroy this report when it is no longer needed. Do not return to sender.

UNCLASSIFIED

SECURITY CLASSIFICATION OF THIS PAGE *(When Data Entered)*

REPORT DOCUMENTATION PAGE

READ INSTRUCTIONS BEFORE COMPLETING FORM

REPORT NUMBER: DNA 3936F	2. GOVT ACCESSION NO.
3. RECIPIENT'S CATALOG NUMBER	
4. TITLE *(and Subtitle)*: HOT WIRE MEASUREMENTS OF TEMPERATURE FIELD STRUCTURE WITHIN GEST FIREBALLS.	5. TYPE OF REPORT & PERIOD COVERED: Final Report for Period 8 Oct 73—31 Mar 76
	6. PERFORMING ORG. REPORT NUMBER
7. AUTHOR(s): Richard G. Batt	8. CONTRACT OR GRANT NUMBER(s): DNA 001-74-C-0067
9. PERFORMING ORGANIZATION NAME AND ADDRESS: TRW Systems Group, One Space Park, Redondo Beach, California 90278	10. PROGRAM ELEMENT, PROJECT, TASK AREA & WORK UNIT NUMBERS: NWET Subtask L25AAXHX634-06
11. CONTROLLING OFFICE NAME AND ADDRESS: Director, Defense Nuclear Agency, Washington, D.C. 20305	12. REPORT DATE: 31 March 1976
	13. NUMBER OF PAGES: 108
14. MONITORING AGENCY NAME & ADDRESS *(if different from Controlling Office)*: 105p.	15. SECURITY CLASS *(of this report)*: UNCLASSIFIED
	15a. DECLASSIFICATION/DOWNGRADING SCHEDULE

16. DISTRIBUTION STATEMENT *(of this Report)*

Approved for public release; distribution unlimited.

17. DISTRIBUTION STATEMENT *(of the abstract entered in Block 20, if different from Report)*

18. SUPPLEMENTARY NOTES

This work sponsored by the Defense Nuclear Agency under RDT&E RMSS Codes B322074462 L25AAXHX63406 and B322074464 S99QAXHC06171 H2590D.

19. KEY WORDS *(Continue on reverse side if necessary and identify by block number)*

Fireball Temperature Measurements
Early Time Fireball Temperature
Buoyant Thermal Temperature Field Structure
Turbulent Structure of Rising Fireball
Temperature Measurements within Simulated Nuclear Fireball
Thermal Structure of GEST Fireballs

20. ABSTRACT *(Continue on reverse side if necessary and identify by block number)*

Using stationary rakes of hot wire anemometer probes, a series of temperature measurements have been conducted within rising fireballs created by detonation of large-diameter, gas-filled balloons. These nuclear simulation tests were performed under DNA's GEST Program at the SANDIA Laboratories Aerial Cable Test Facility, Kirtland AFB, during the late fall of 1973 and early January of 1974. All measurements were performed after pressure equilibrium (t > 1 sec) but prior to completion of the toroid formation process and

DD FORM 1 JAN 73 1473 EDITION OF 1 NOV 65 IS OBSOLETE

UNCLASSIFIED

SECURITY CLASSIFICATION OF THIS PAGE *(When Data Entered)*

10. PROGRAM ELEMENT, PROJECT, TASK AREA & WORK UNIT NUMBERS (Continued)

NWED Subtask S99QAXHC061-71

20. ABSTRACT (Continued)

within the time required ($t < 4$ sec) for the fireball to rise one diameter. Although 70 channels of measurements were activated during the course of the investigation (8 events), fireball data return was partially limited by such factors as wind-induced fireball drift, sensor failure due to balloon debris motion, and signal saturation phenomena. Based on an extensive processing of measured data for two single 10m diameter balloon events (MB-3 and MB-4), unique results describing the mean flow field and turbulent structure statistics for the early-time large-scale fireball have been determined. Final results include: mean velocity and temperature data; temperature and temperature gradient intensities; space, auto- and "eddy lifetime" correlation scales; power spectra densities; probability density distributions and approximate microscale data.

The present temperature data illustrate that the early time rising fireball is characterized by a highly intermittent irregular top or cap, a constant (high) temperature core and a thermal wake exhibiting a linear decay in mean temperature. Normalized intensities at the fireball top and within the thermal wake are substantial ($\cong 0.6$) in contrast to quiescent fireball core levels ($\cong 0.1$). Core leading edge mean temperature gradients compare favorably with HULL code predictions ($10^{o}C/cm$) whereas trailing edge gradients ($0.4^{o}C/cm$) are smaller than predicted results ($3^{o}C/cm$). The fully developed turbulent structure of the GEST fireballs is demonstrated by temperature spectra which exhibit a -5/3's falloff behavior, an eddy lifetime-to-autocorrelation time scale ratio of 4, integral scales equivalent to 5% of fireball mean radius and large turbulence Reynold's number (2000).

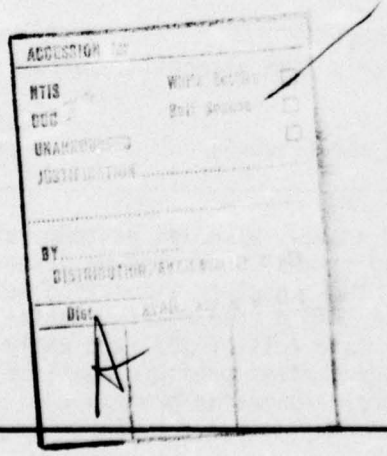

SUMMARY

Using stationary rakes of hot wire anemometer probes, a series of temperature measurements have been conducted within rising fireballs created by detonation of large-diameter, gas-filled balloons. These nuclear simulation tests were performed under DNA's GEST Program at the SANDIA Laboratories Aerial Cable Test Facility, Kirtland AFB, during the late fall of 1973 and early January of 1974. All measurements were performed after pressure equilibrium ($t \gtrsim 1$ sec) but prior to completion of the toroid formation process and within the time required ($t \lesssim 4$ sec) for the fireball to rise one diameter. Although 70 channels of measurement were activated during the course of the investigation (8 events), fireball data return was partially limited by such factors as wind-induced fireball drift, sensor failure due to balloon debris motion, and signal saturation phenomena. Based on an extensive processing of measured data for two single 10 m diameter balloon events (MB-3 and MB-4) unique results describing the mean flow field and turbulent structure statistics for the early-time large-scale fireball have been determined.

Mean convection velocities for the fireball wake were measured to be approximately twice as large as fireball rise velocities (43 ft/sec). Maximum fireball temperatures (1100°C) were in good agreement with peak brightness temperature data determined from an independent IR measurements experiment. Leading and trailing edge mean temperature gradients for the GEST fireballs were approximately 10 and .4°C/cm, respectively. Normalized temperature intensities at the fireball top and within the thermal wake were substantial ($\cong 0.6$) in contrast to quiescent fireball core levels (0.1). Wake integral scales (3 feet), determined from vertical space correlation data, were approximately 5% of the fireball mean radius, a result comparable to optically

derived scale data for a nuclear fireball. Moving frame autocorrelation times ("eddy lifetimes," 0.17 $\pm$ .04 sec) were approximately four times larger than measured autocorrelation times. This result illustrates that the early-time fireball eddy structure is highly persistent, a finding which tends to substantiate those radar models which postulate relatively slow "smearing" of early-time electron density gradients. Probability density distributions for the fireball thermal wake were "spiky" in nature, with some evidence of bimodal behavior, and slightly skewed to the negative side of their normalized values. Normalized spectra data, in general, follow a -5/3's falloff behavior for several decades in spectral power. The noted large "spread" in the inertial subrange is consistent with measured turbulence Reynold's numbers (2000) and with the large scale, fully developed turbulent structure for the GEST fireballs ($Re_D = 3 \times 10^7$). Wake microscale data, estimated from temperature and temperature gradient intensity data and the isotropic turbulence assumption, varied from 2 to 4 cm and were in favorable agreement with predicted microscale magnitudes.

PREFACE

This report was prepared by TRW Systems Group, Redondo Beach, California, under DNA Contract DNA 001-74-0067. The author wishes to acknowledge especially the support and encouragement provided by Major Robert A. Bigoni, the AFWL Project Officer for GEST. The author also gratefully acknowledges the support of Mr. Joseph Quintana (AFWL) and Messrs. Dewey J. Rowland and Harald Rungaldier of TRW Systems Group.

Inclusive dates of performance for this contract were 8 October 1973 to 31 March 1976. The DNA Project Officers at the start and completion of this contract were Lt. Col. Michael F. Monaghan and Capt. Bruce L. Bauer, respectively.

TABLE OF CONTENTS

LIST OF ILLUSTRATIONS

LIST OF ILLUSTRATIONS (Cont.)

LIST OF ILLUSTRATIONS (Cont.)

1.0 INTRODUCTION

The low altitude fireball generated by an atmospheric nuclear detonation produces large radar backscattering cross-sections which give rise to the familiar radar clutter and communications blackout phenomena. Sophisticated numerical codes have been developed which predict not only the behavior of weapon systems in a nuclear environment but also the nature and extent of electromagnetic wave attenuation/scatter caused by the fireball's turbulent, high temperature, electron rich flow field (Ref. 1). Important in validating these predictive capabilities, as well as in clarifying the source for radar clutter and blackout, is the use of measured data quantifying the structure of the turbulent temperature field within the early-time large-scale fireball. To date the availability of required measured data has been limited to either size/rise optical data from atmospheric nuclear events or laboratory results corresponding to small scale buoyant thermal experiments (Refs. 2, 3 and 4). Although some success has been realized in these latter investigations in measuring turbulent structure statistics (Refs. 2 and 3) and mean density profiles (Ref. 4), there still exists a critical lack of detailed turbulence data for the early-time large-scale fireball.

In response to this need for additional fireball turbulence data, a series of multiprobe fast response temperature measurements have been conducted within large scale rising fireballs through use of stationary rakes of hot wire anemometer probes. Such measurements were performed within atmospheric fireballs created by detonation of large diameter gas-filled balloons under DNA's balloon detonation test program (GEST). Reduced results as presented herein are

intended to provide a more extensive set of data for use in clarifying radar backscatter phenomena as well as in supporting development and evaluation of analytical models for the nuclear fireball.

The Gas Explosive Simulation Technique (GEST) program (Refs. 5 and 6) was conducted under DNA sponsorship by the Air Force Weapons Laboratory (AFWL) and involved a series of atmospheric detonation experiments using 10 meter diameter balloons suspended above ground ($h \simeq$ 130 ft.) and filled with a near-stoichiometric mixture of methane and oxygen gases (effective yield: 1500 lb of TNT). These nuclear fireball simulation tests were performed at the SANDIA Laboratories Aerial Cable Test Facility, Kirtland AFB, during the late fall of 1973 and early January of 1974. An overhead cable, at approximately 60 feet above detonation center, was used during the tests to support the required thermal instrumentation. All measurements were performed after pressure equilibrium ($t > 1$ sec) but prior to completion of the toroid formation process and within the time required ($t < 4$ sec) for the fireball to rise one diameter. Reduced temperature data discussed herein therefore provide unique initial condition results quantifying the temperature field structure for the early-time large scale fireball.

Essential to the accomplishment of the stated objective for this temperature measurement experiment was the cooperative support provided to TRW by AFWL personnel. This support not only involved direct field test assistance but also included tape recording of measured results and extensive photographic coverage of all GEST events. In Section 2.0 which follows, the Technical Approach to the investigation is described in detail and Experimental Results are presented in Section 3.0. A brief description of the turbulent structure of the GEST fireballs and important findings from the investigation are summarized in Section 4.0, Conclusions.

2.0 TECHNICAL APPROACH

The Gas Explosive Simulation Technique (GEST) program (Refs. 5 and 6) was conducted under DNA sponsorship by the Air Force Weapons Laboratory (AFWL) and involved a series of atmospheric detonation experiments using 10 meter balloons suspended above ground* and filled with a near-stoichiometric mixture of methane and oxygen gases (effective yield: 1500 lb of TNT). These nuclear fireball simulation tests were performed at the SANDIA Laboratories Aerial Cable Test Facility, Kirtland AFB, during the late fall of 1973 and early January of 1974. This test site is located at an altitude of 6200 feet corresponding to an atmospheric pressure of 12 $\pm$ .1 psi. An overhead cable, at approximately 60 feet above detonation center, was used during the tests to support the required thermal instrumentation which consisted of stationary rakes of calibrated hot wire anemometer probes. This one-inch diameter steel wire cable was installed under a previous field test program and was lowered to ground level to facilitate attachment of the probe strut systems and related sensor cables. All measurements were performed after pressure equilibrium ($t > 1$ sec) but prior to completion of the toroid formation process and within the time required ($t < 4$ sec) for the fireball to rise one diameter.

2.1 Test Schedule

Although multiple probe temperature measurements were attempted on one DMB (dual mylar balloon), four MB (mylar balloon), and three RB (rubber balloon) detonation events, fireball data return was achieved only on four events, RB-11, MB-3, MB-4 and DMB-1 (Table 1). The inability to obtain measured results for the other events was brought about by a combination of wind-induced fireball drift (RB-8, RB-9 and MB-1) as well as early time failure of hot wire sensors due to balloon debris (MB-2). The small rubber balloon experiments (8-foot diameter) were

*h ≈ 130 feet

TABLE 1. Test Matrix Summary

EVENT	TEST DATE	TIME (hours)	BALLOON DIA. (ft)	BALLOON HEIGHT (ft)	CABLE HEIGHT (ft)	STRUT GROUND RANGE[1]		T_{AMB} (^{o}C)	WIND		YIELD 10^9 Joules	SENSORS INSTALLED	SENSOR SURV.	VALIDATED CHS	FIREBALL DATA RETURN	
						AUX. STRUT (ft)	MAIN STRUT (ft)		DIRECTION[2] (degrees)	SPEED $\left(\frac{FT}{SEC}\right)$					FIDU TIME SPAN (sec)	TOTAL CHS
RB-8	10-11-73	0900	8	59	83	3.6	--	--	--	--	--	3	3	1,3	--	0
RB-9	10-11-73	1010	8	59	83	3.6	--	--	--	--	--	3	3	1,3	--	1
RB-11	10-11-73	1455	8	59	83	3.5	--	--	--	--	--	3	3	1,3	0.7-1.6	2
MB-1	11-28-73	0940	33	150	193	2.8	40	-1	330	5	2.86	12	7	1-10	--	0
MB-2	11-30-73	0830	33	140	193	2.8	30	+1	Gusting	3.5	2.93	12	0	1,2,5,7-9,11	--	0
MB-3	12-11-73	0925	33	130	193	2.8	30	+5	Gusting	3.5	3.00	12	9	1-10	1.7-3.8	10
MB-4	12-13-73	0800	33	130	193	17.5	30	+5	135	3.5	2.72	12	10	1-3,5-11	1.4-3.6	10
DMB-1	1-19-74	1000	33	130	193	50	50	+4	60	8.5	1.45/3.20	13	13	5-8,10-12	1.6-4.4	5
											TOTAL	70				

[1]Horizontal Separation from Balloon Center; Auxiliary Strut - Strut Center Separation; Main Strut - Vertical Leg Separation

[2]From True North

performed early-on in the test program (October 1973) as check out measurements to evaluate the feasibility of the overall experimental approach as well as to determine the relative detonation characteristics for different gas mixtures. It was found by AFWL that a methane/oxygen gas mixture (near stoichiometric) provided superior detonation performance as compared to a mixture of carbon monoxide/oxygen. By mixing methane (CH_4) and oxygen (O_2) in the approximate ratio of 1 part to 2 parts, respectively, by volume and inflating the mylar balloons to 10 m in diameter, an energy yield equivalent to approximately 1500 pounds of TNT was achieved. The computed yields (Ref. 6) for the large balloon detonations are noted in Table 1. Detonation of the explosive mixture was initiated by three RP-1 detonators in each balloon. Tracer gas seeding of the detonation cloud was accomplished by wrapping the detonators with plastic containers filled with aluminum oxide powder. All mylar balloons were constructed of three-mil mylar coated on both sides with a 5000 Å thick layer of aluminum.

2.2 Test Site Configuration

Layout drawings for the GEST events showing both the plan and side views for the test sites are presented in Figures 1 and 2. Photographs of the auxiliary and main struts as attached to the overhead cable are presented in Figures 3, 4, and 5 and an assembly drawing of the main probe strut is shown in Figure 6. Note that with the vertical leg of the main strut's triangular framework positioned at approximately 30 feet from the fireball centerline (Figure 2), the two instrumented legs measure data both in the azimuthal and radial directions. In addition, the use of seven and three probes, spaced 18 in. apart on the azimuthal and radial legs, respectively, provided results spanning the expected scale dimensions. All wire sensors were aligned orthogonal to the vertical plane through the overhead cable. Figure 6

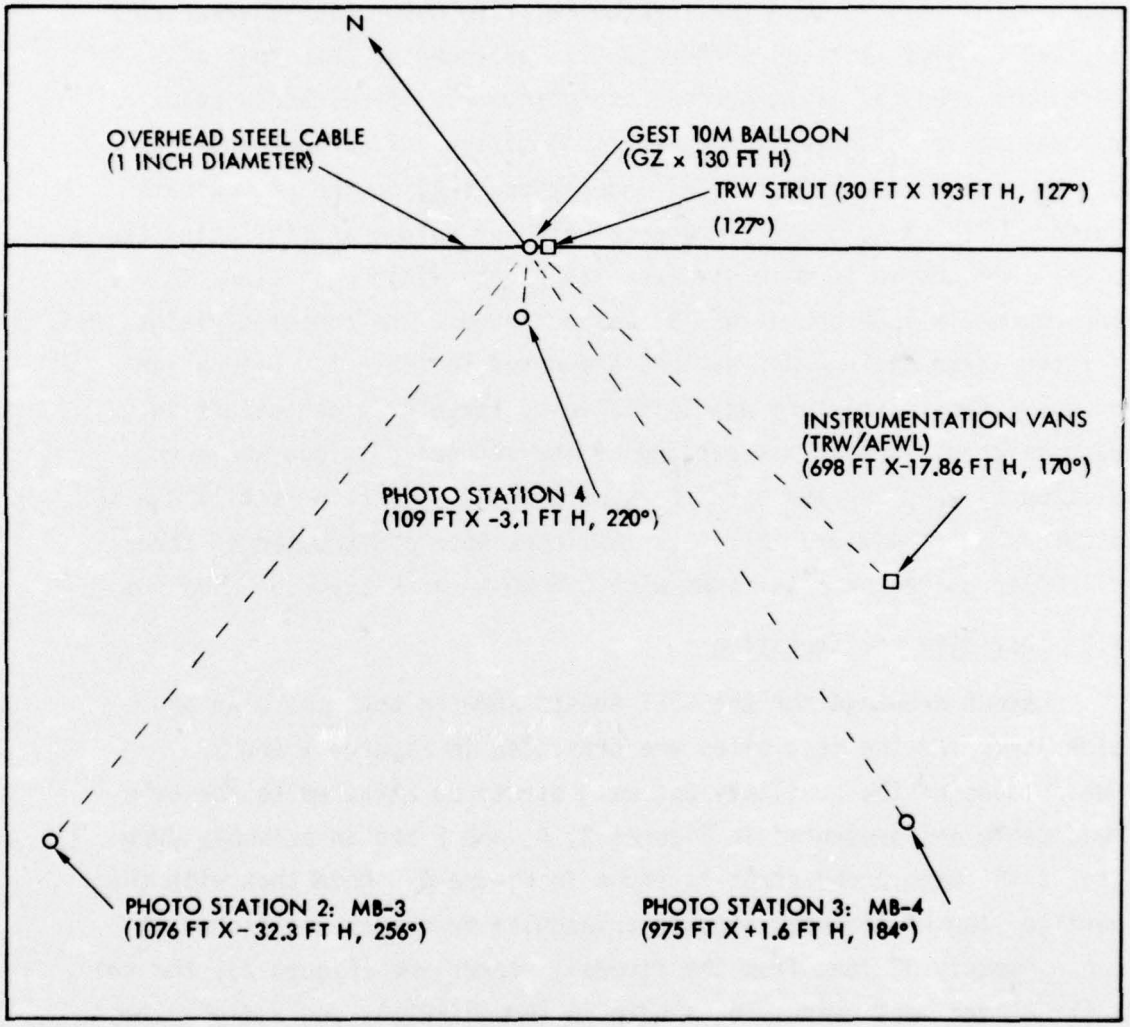

Figure 1. Test Site Layout: Plan View

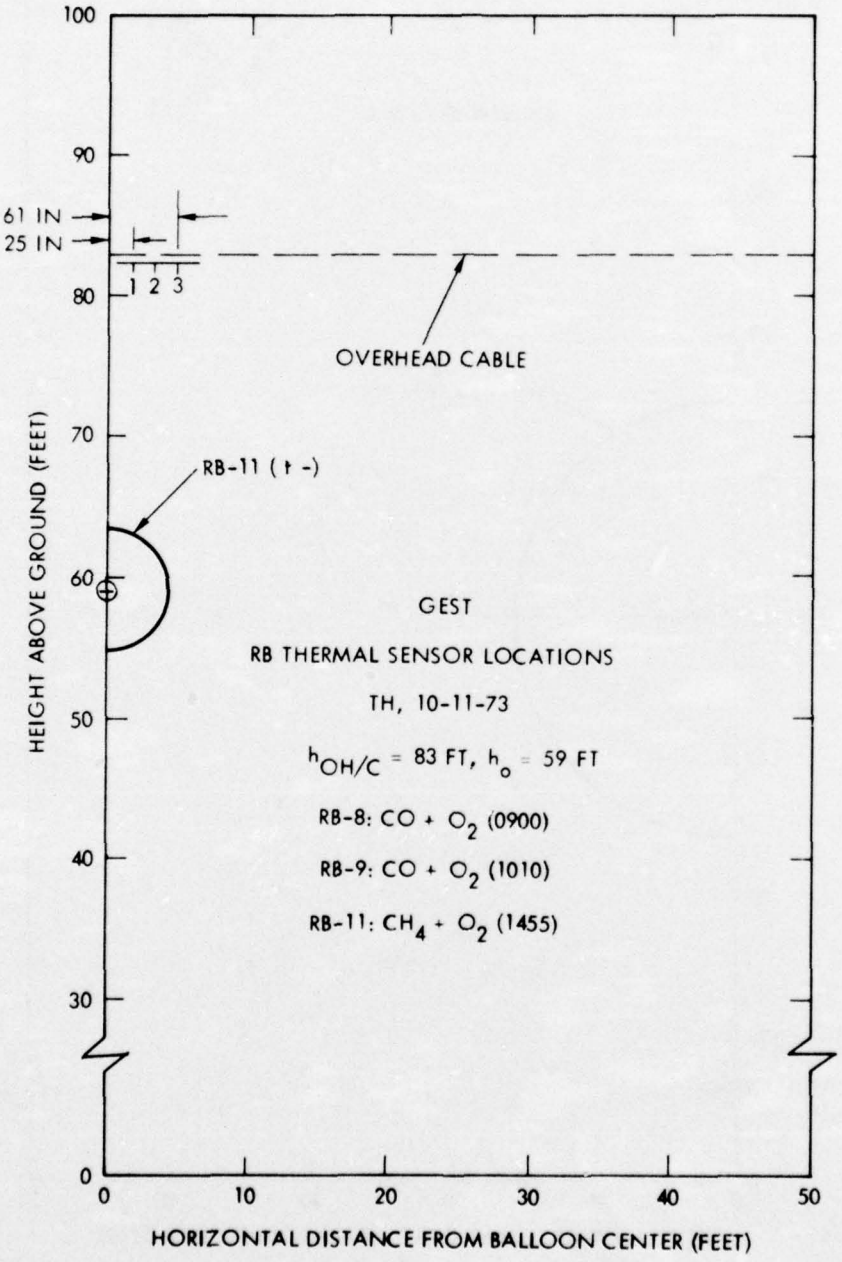

Figure 2a: Test Site Layout: Side View Looking NE - RB-8, -9, -11

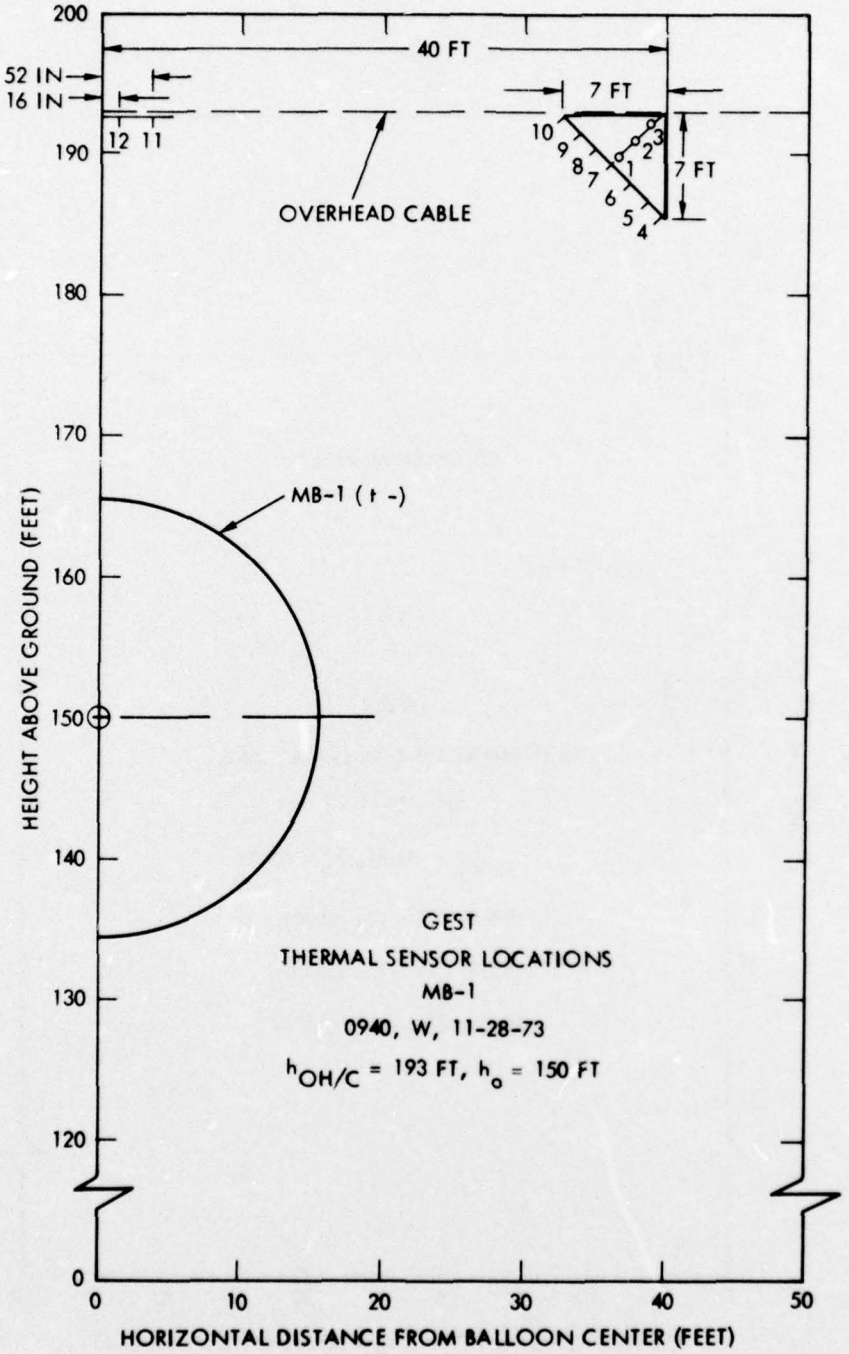

Figure 2b. Test Site Layout: Side View Looking NE - MB-1

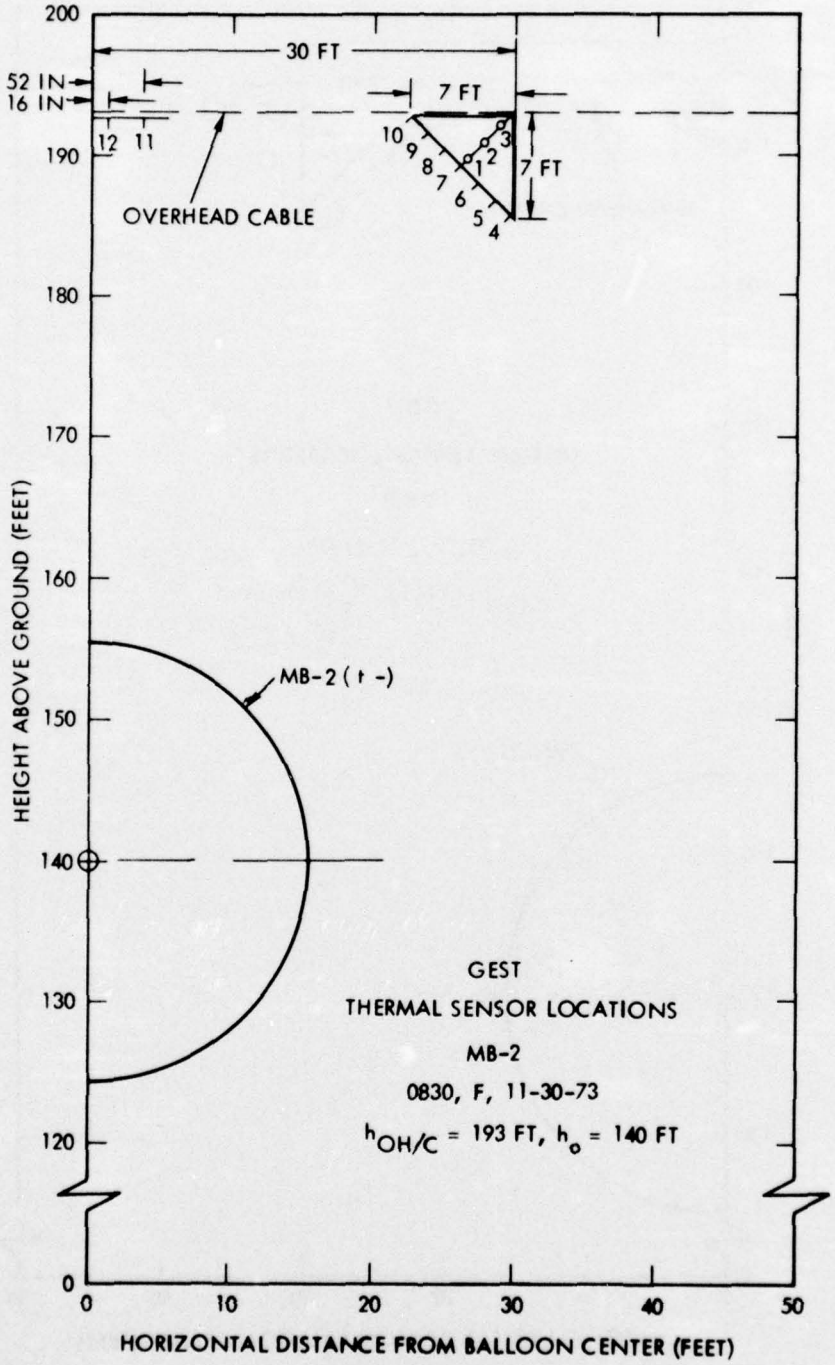

Figure 2c: Test Site Layout: Side View Looking NE - MB-2

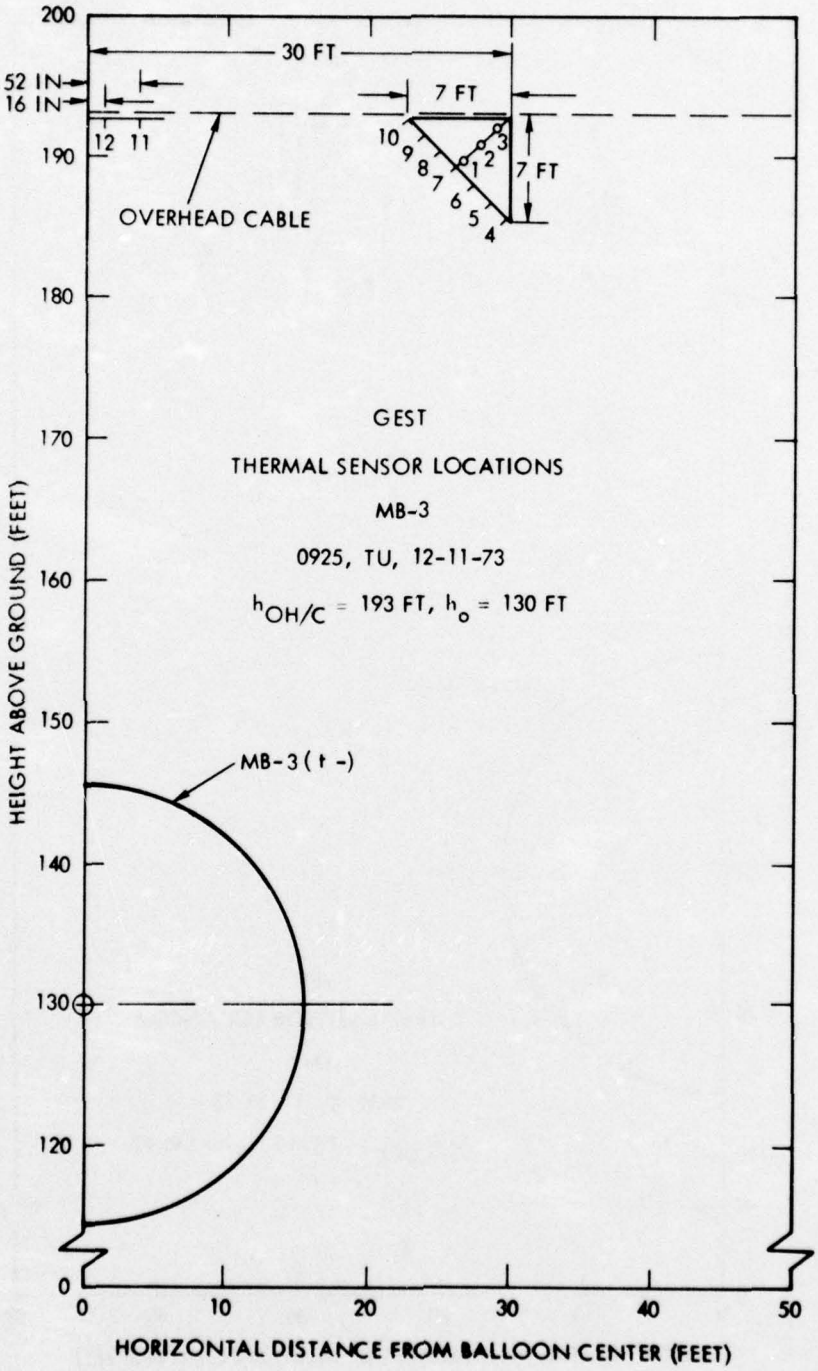

Figure 2d. Test Site Layout: Side View Looking NE - MB-3

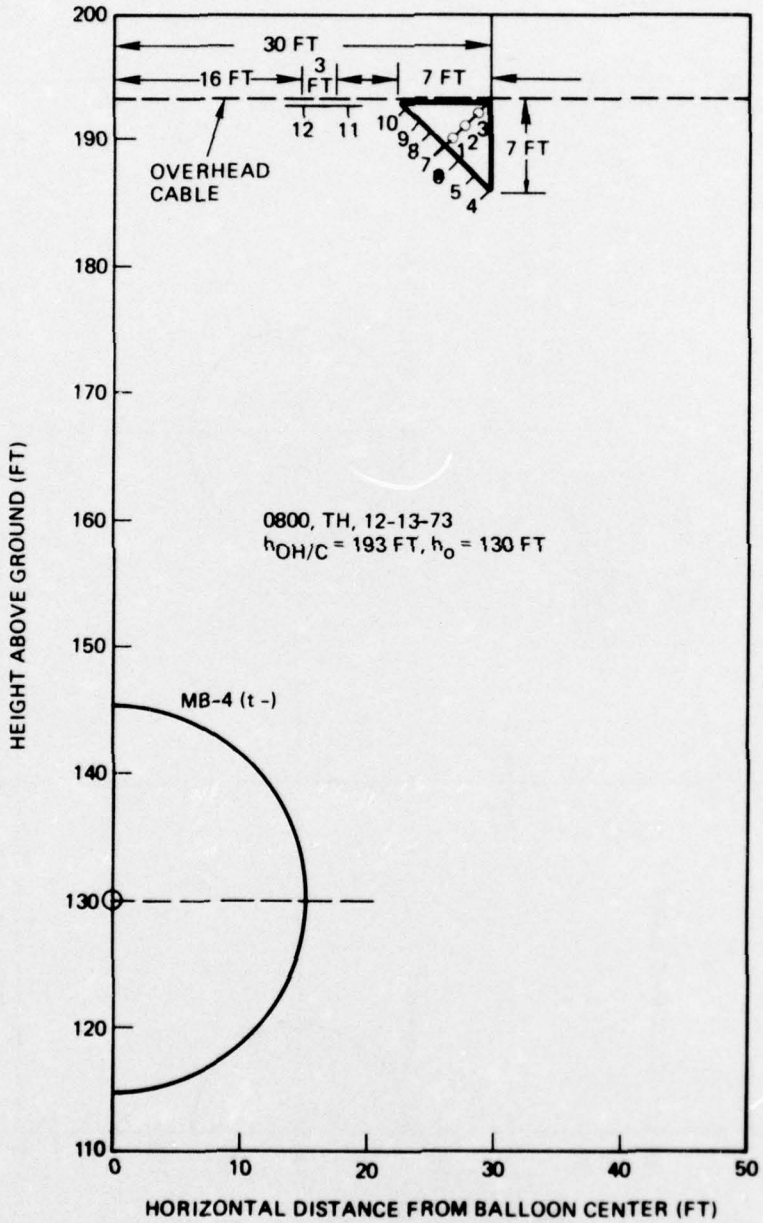

Figure 2e: Test Site Layout: Side View Looking NE - MB-4

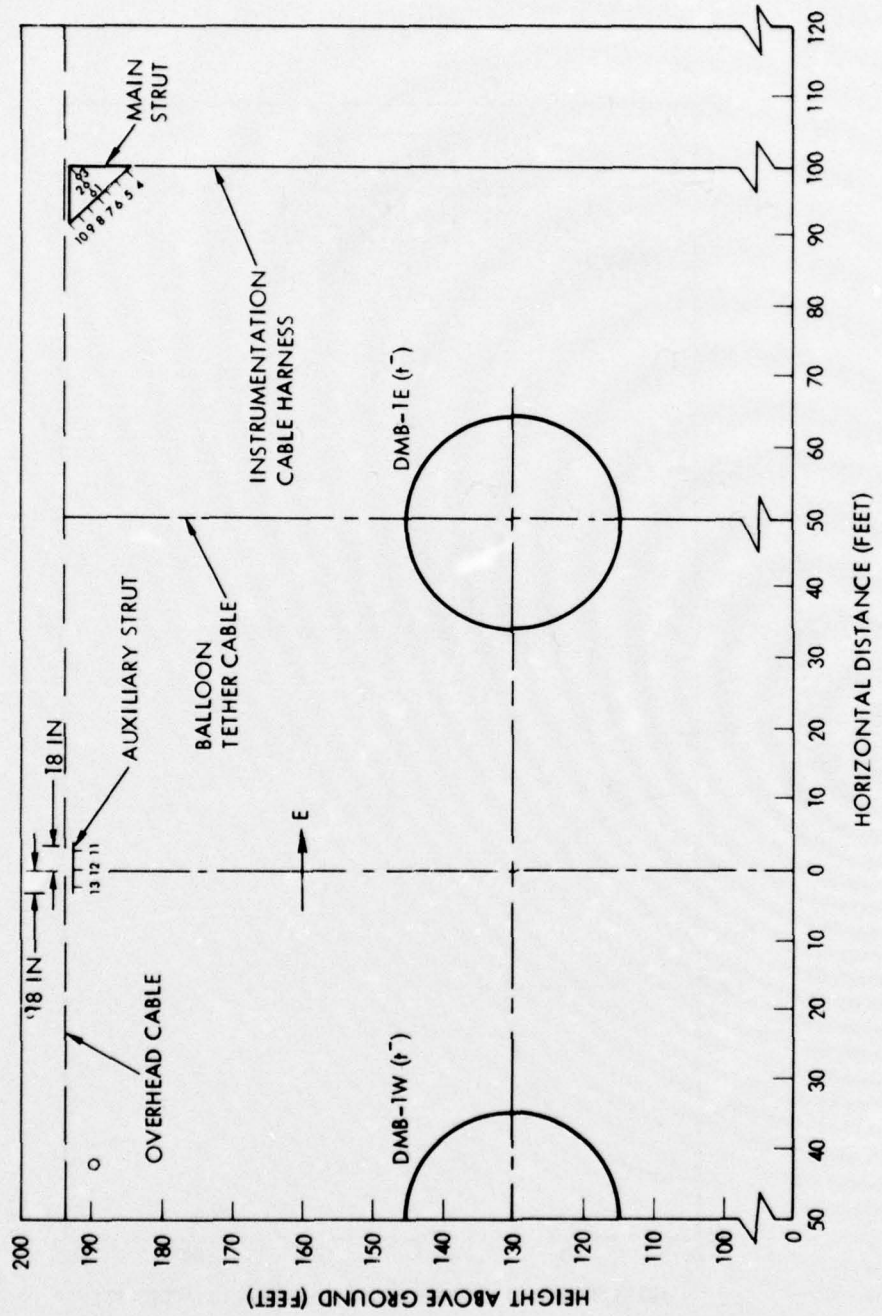

Figure 2f. Test Site Layout: Side View Looking NE - DMB-1

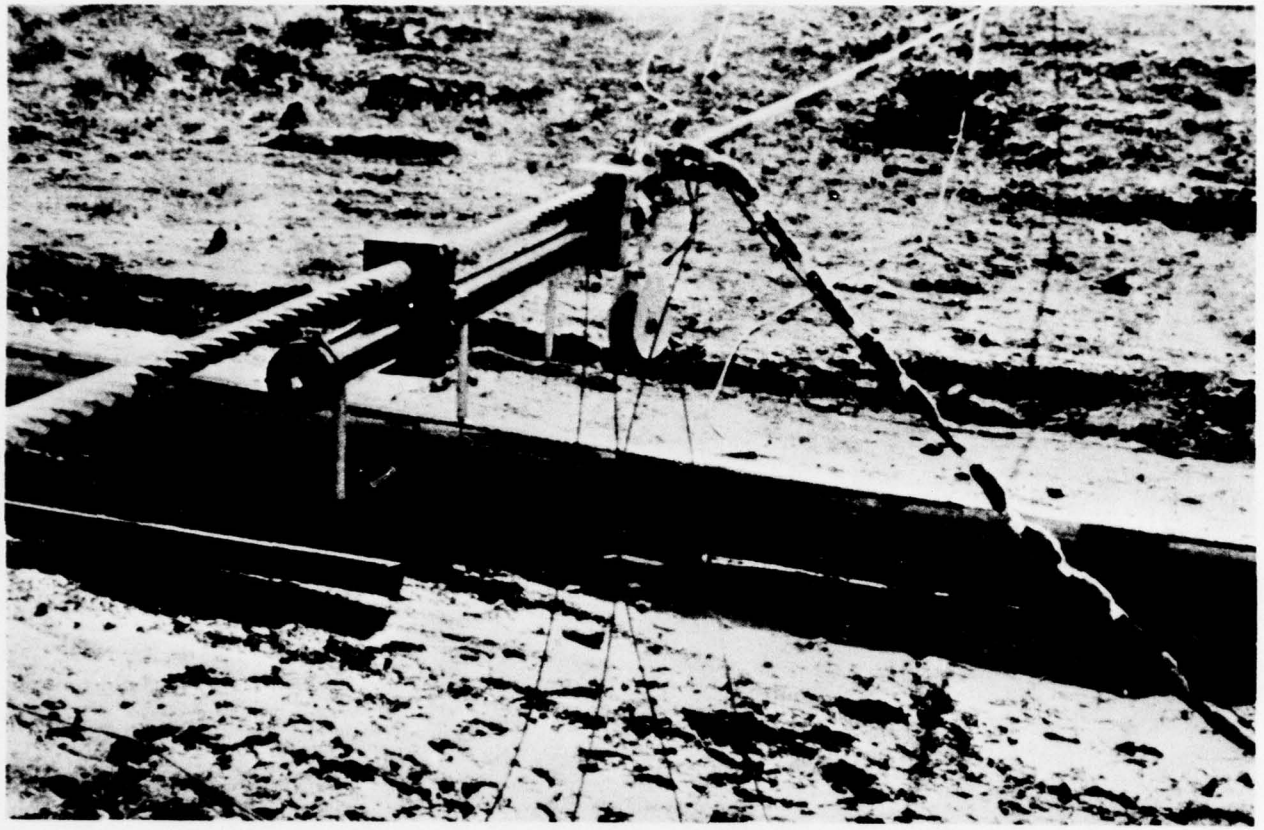

Figure 3a. Close Up View Photograph of Auxiliary Strut - Looking East

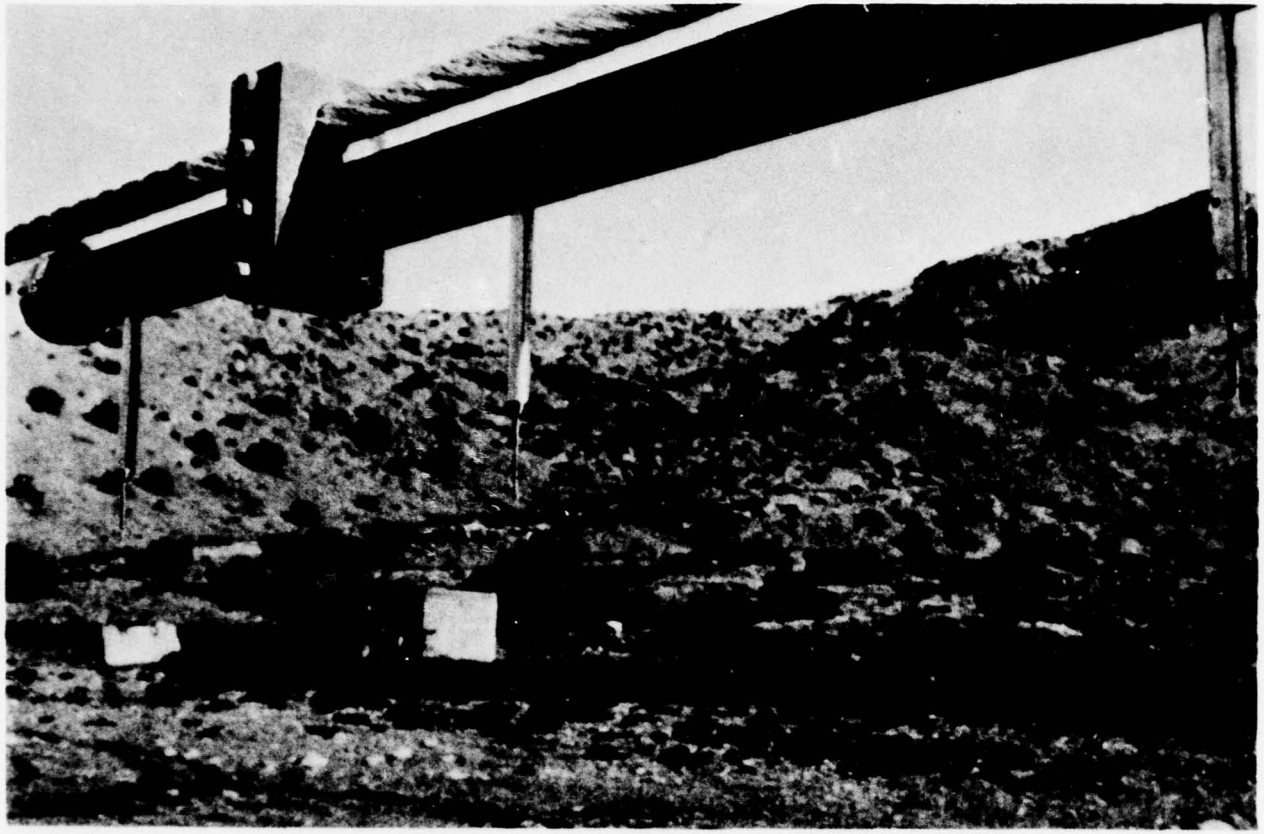

Figure 3b. Close Up View Photograph of Auxiliary Strut - Looking North

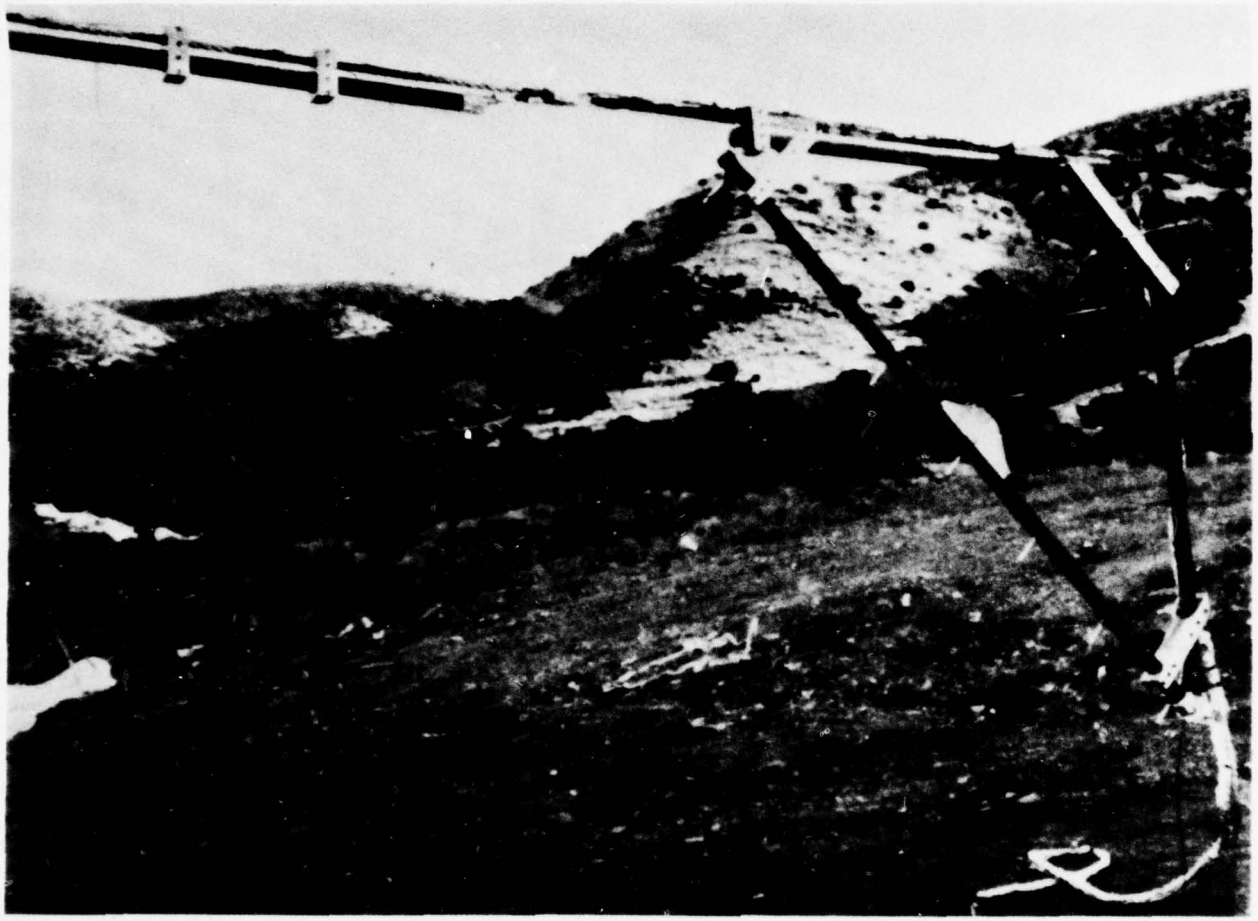

Figure 4. Close Up View Photograph of Main Strut (MB-4)

Figure 5. Photograph of Main Strut as Deployed

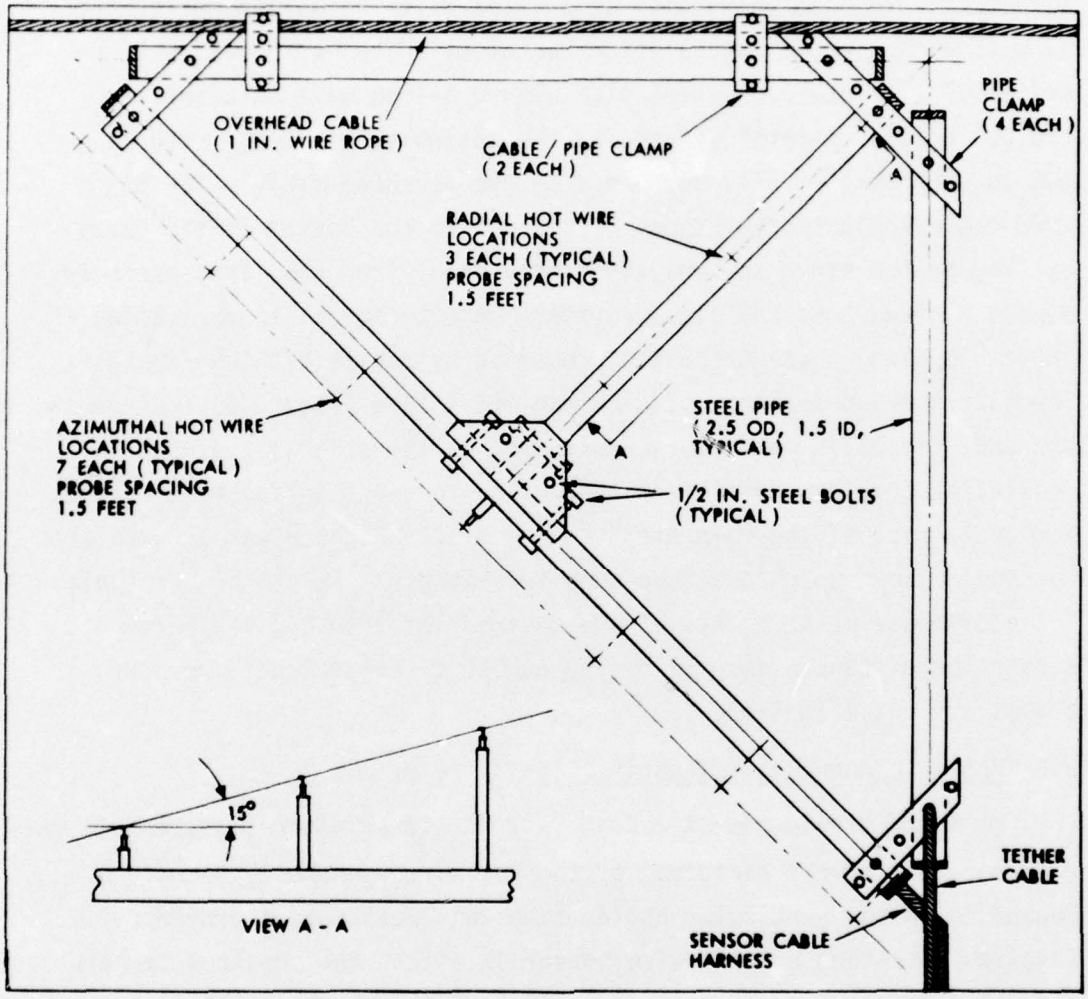

Figure 6. Main Strut Configuration

illustrates the design details associated with the main strut system as well as the probe installation technique. The basic framework consisted of 2.5-inch O.D. steel pipe with 0.5-inch wall thickness (10.68 lb/ft). A total weight for the assembled strut was less than 500 lb which was readily supported by the overhead cable. The tethered cable, indicated in Figure 6 attached to the bottom of the vertical leg of the strut assembly, not only stabilized the strut assembly during a given test but also provided support for all sensor cables. The cable harness was thermally protected by one-inch thick fiberglas insulation wrapped inside of aluminum metal tape (Figure 5). Although the GEST fireballs made contact with the cable harness, the noted insulation provided sufficient thermal protection. Attachment of the horizontal leg of the main strut to the overhead cable was accomplished by steel clamps which could be adjusted along the length of the cable to accommodate measurements at any desired location. Cable/balloon separation distances as well as the number of activated temperature probes are noted in Table 1.

2.3 Hot Wire Anemometry Technique (Refs. 7, 8, and 9)

As noted previously, the fast response temperature measurements carried out herein were performed by the hot wire anemometry technique. Depending on the particular application this measurement procedure involves operating a small wire sensor in either the constant temperature (T_w) or constant current (i_w) mode. Although the constant current sensor (resistance thermometer) provides a voltage output signal directly related to temperature through resistivity calibration data (Appendix I), the constant temperature anemometer provides, as will be shown below, not only local temperature data but also mean velocity results for the rising GEST fireballs. In order to realize the beneficial aspects of measuring temperatures directly while at the same

time providing a means for determining local fireball velocities, an instrumentation matrix was selected which included a mix of both constant current ($i_w \cong 3.7$ ma) and constant temperature anemometer channels.

2.3.1 Probe Configuration. Except for the three cylindrical film sensors (6-mil diameter) used on both RB-8 and RB-9, all probe sensors for the GEST temperature measurements were either 2.5-mil platinum-iridium (PI) or 2-mil platinum-tungsten (PT) wire sensors ($\ell \cong 0.050$ in.). All wires were silver soldered to the probe stem needle supports for the two types of high temperature probes used in the investigation (radial or azimuthal, Figure 7). The noted probes, as well as all other hot wire anemometry equipment were manufactured by Thermo Systems, Inc., St. Paul, Minnesota. The frequency response for the constant current sensors was limited by wire thermal lag to approximately 1 kc whereas the hot wire probes operating in the constant temperature mode were frequency compensated by the anemometer's feedback bridge (TSI 1053B) to provide a 5 kc response.

2.3.2 Data Reduction. The hot wire constant temperature anemometer measures the instantaneous heat transfer rate between a small heated sensor and the local fluid flow. An electronic feedback control circuit (constant temperature bridge), conditioned to provide high frequency response, varies the electrical current flowing through the sensor to compensate for the cooling effect of the fluid motion, always keeping the sensor at a constant temperature and resistance. To reduce the measured bridge voltage signal to flow field temperature data, the heat transfer relation for a wire sensor is used.

$$\left(\frac{e_w}{R_w}\right)_M = \left(\frac{e_w^2}{R_w}\right)_{NF} + Nu\ \pi\ell k(T_w - T) \ldots\ldots \qquad (1)$$

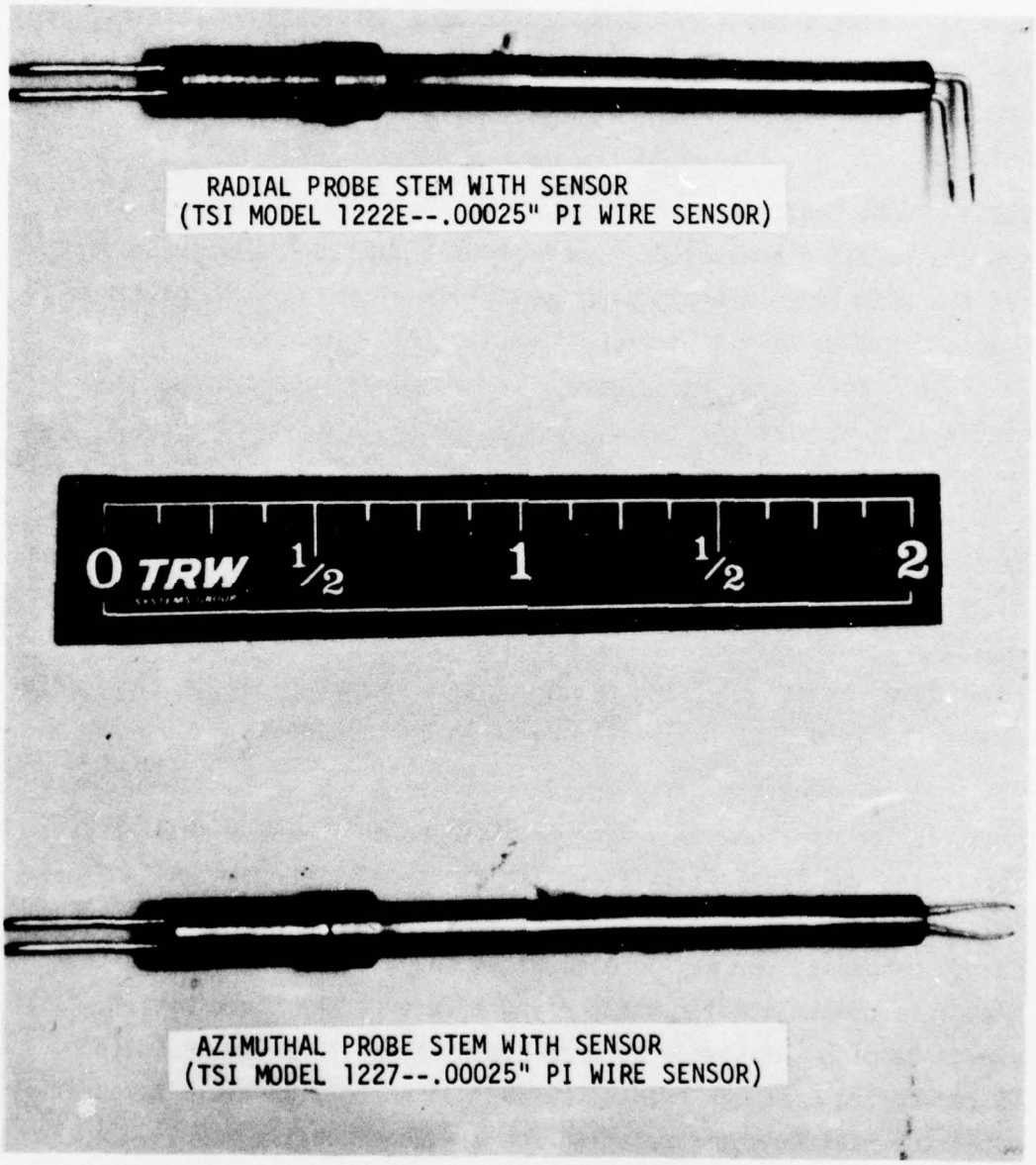

Figure 7. Hot Wire Probe Configurations

In Equation (1), e_w, R_w and T_w represent the voltage, resistance and temperature, respectively, for the wire sensor; Nu and k correspond to the Nusselt number and conductivity, respectively; ℓ is the wire length and T is the local gas dynamic temperature. The subscripts $()_M$ and $()_{NF}$ refer to measured and no flow (i.e., ambient and/or end loss) conditions, respectively. Substantial calibration results relating Nusselt number (Nu) and Reynolds number (Re) have been reported in Reference 9 and the empirical correlation presented therein (as modified to account for an effective reference temperature)

$$Nu = .21 + .46\ Re^{.45} \tag{2}$$

has been used to process the present set of data. In Equation (2), Re represents the wire Reynold's number given by:

$$Re = \frac{\rho u d}{\mu} \ (\simeq 5 - 10) \tag{3}$$

where ρ, u, and μ refer to the density, velocity, and viscosity, respectively, for the local flow and d represents the wire diameter.

The first term on the right side of Equation (1) represents the heat lost to the probe tips (end loss effect) and it was assumed to remain constant during the short measurement times involved in the fireball temperature experiments. This power loss term was measured in the laboratory and verified in the field under no-flow (ambient) conditions. Additionally, sensor operating temperatures and sensor nominal diameters and lengths were also determined during laboratory calibrations.

To enhance data resolution and since wire dimensions could be measured in the laboratory with only limited accuracy due to the small sizes involved, a second flow calibration was performed for each sensor.

Use was made, in this latter calibration, of the result that all fireball temperature data were obtained after the GEST fireball achieved pressure equilibrium ($t > 1$ sec) at which time the wire Reynold's number became a function only of temperature and velocity. Also, as will be discussed further in Section 3.3, the trailing wakes of the GEST fireballs contained vertically moving pockets of unmixed ambient air which were identifiable by their quiescent nature. Since the temperature and velocity for these ambient "eddies" were known, i.e., $T = T_{AMBIENT}$ and $u = u_{CONVECTION}$ (from vertical cross-correlation statistics, Section 3.6.1), corrected wire lengths could be determined by matching the sensor output signal to the local velocity/temperature conditions [Equation (1)]. Thus by flow calibrating a given wire sensor for ambient air conditions just prior to detonation as well as by use of motion statistics for unmixed ambient fluid contained within the fireball wake, a unique pair of calibration constants was arrived at for each sensor. Prior to final processing of the fireball data a determination was made of the local velocity time history (Section 3.3) for a given event by back calculating convection velocities for all detectable ambient eddies [Equation (1)]. Although the resulting mean velocity curves were developed from a somewhat limited number of "data" points, their use in final processing of fireball temperature data is considered satisfactory primarily because of the velocity's approximate square root dependence inherent in Equation (1). Once the fireball's velocity/time dependence had been specified, solving Equation (1) for temperature data was accomplished in an iterative manner using flow calibrated channel constants and the noted mean velocity data.

It should be noted that recorded oscillograph time traces (to be discussed in Section 3.2) for the constant temperature wire sensors correspond to anemometer bridge signals and not to total temperature/velocity directly. The signal developed by the bridge feedback circuit

provides sufficient electrical power to the hot wire sensor to maintain its temperature (resistance) constant during exposure to external cooling effects. Oscillograph raw data, therefore, reflect the amount of electrical power required to offset those heat transfer losses arising due to the combined effects of sensor flow temperature potential (T_w - T) and Nusselt number (Nu). This interpretation of measured output signals for the constant temperature anemometer should be kept in mind when comparing such data with recorded constant current results. Note that for the constant current anemometer, changes in sensor resistance/temperature induced by local flow phenomena are detected as voltage changes which can be directly related to temperature through resistivity calibration data (Appendix I).

To carry out the required data reduction calculations for the two types of temperature data (T_w and i_w), a special purpose temperature conversion program was written (GEST-T, Appendix I). This program was capable of accepting simultaneously digitized multichannel data as prepared from AFWL analog tapes. Not only was GEST-T constructed to provide a digitized temperature output tape corresponding to the simultaneously recorded input data, but it also was set up in a running and/or segmented averaging format so as to calculate mean and standard statistical properties (single channel) for selected sampling intervals. The noted output tape was used both to prepare the time trace histories presented in Section 3.4 as well as to serve as an input tape to TRW's turbulent statistics program (GEST-TS). This latter time series program not only computed complete single channel statistical properties, but also was able to determine cross-correlation statistics between any pair of selected channels (Appendix I). Since the primary data base occurred at frequencies less than 1 kc and in order to avoid data aliasing difficulties, a conservative Nyquist or

folding frequency of 2 kc was established. The corresponding sampling rate was 4000 sps and all statistically processed results reported herein were based on this digitized rate.

2.3.3 Resistivity Calibration. Application of the hot wire anemometry technique to the measurement of local flow properties requires that resistivity data for each sensor be determined during pre-test calibration activities. Normally the dependence of sensor resistance on temperature is obtained from oven calibration tests. Because of probe degradation effects it was not feasible, however, to calibrate the GEST thermal gauges to temperatures higher than 120°C, since the entire probe including the thermally vulnerable probe stem, was subjected to the oven heat. However, from the hot jet measurements described in Reference 10, which independently measured high overheat operating temperatures, it was found that such temperatures not only remained stable after suitable heat treatment ($\cong$ one hour) but that resistivity data from oven calibrations were linear up to and including sensor operating temperatures. In fact, linear extrapolation of the oven data compared in general to within $\pm$ 10°C with sensor operating temperatures based on hot jet measurements.

For the constant temperature sensors utilized during the present experiment, overheat (operating) resistances were determined by linearly extrapolating resistance/temperature calibration data to the appropriate operating temperature ($\cong$ 700°C). These operating temperatures were selected as high as allowable, for a given wire material, in order to minimize expected signal saturation difficulties. As will be discussed further in Section 3.2, even with use of high operating temperatures, channel overrange and corresponding bridge shutdown difficulties were experienced by a number of constant temperature sensors during measurement of fireball top/core conditions. Summarized

resistivity data for all wire sensors used to obtain the present reduced results are presented in Table 2. These calibration data, as well as the noted channel constants, were used directly in the final data processing calculations.

2.4 System Electronics

The electronics schematic for the Temperature Measurements Task is shown in Figure 8. The degree of coordination/cooperation required between TRW and AFWL is illustrated by the equipment responsibility notation indicated in Figure 8. All channels of data from the constant current bridges (TSI 1040 and TSI 1053A) and constant temperature bridges (TSI 1053B) were recorded in the FM mode on AFWL's Bell and Howell VR-3700B Tape Recorder.

Recorder electronics were set up for a tape speed of 60 ips, corresponding to a carrier center frequency of 108 KHz, and with band edge deviations of $\pm$ 40 KHz calibrated for input levels of $\pm$ 7 VDC. Wideband electronics provided recorded data at a 3 db frequency response up to 20 KHz. To use effectively the full dynamic range of the tape recorder while accommodating expected signal levels of 0 to 12 VDC, the bucking voltages noted in Table 2 were used to condition bridge output signals. Each sensor was connected to bridge electronics with either TSI triax cable (.011 Ω/ft, 18 Ω standard impedance, Chs 2 and 7) or RG58U coax cable (all other channels). All TRW electronics were contained in an AFWL instrumentation van located approximately 700 feet due South of GZ and adjacent to AFWL's tape recorder van (Figure 1).

TABLE 2. Channel Calibration/Performance Summary

EVENT	CH	BRIDGE		BUCK. VOLT. (VDC)	PROBE		R_o (Ω)	dR/dT (Ω/°C)	R_{op} (Ω)	T_{op} (°C)	e_{AMB} (VDC)	SURVIVAL TIME (sec)	FIREBALL DATA RETURN		
		Model	Type[1]		Type	S/N							FIREBALL DATA[2]	FIDU TIME SPAN (sec)	CH PERF[3]
RB-8	1	1053B	T_w	10.0	1220.60	6659	4.34	.0090	8.84	500	7.05	∞	NA	--	S
	2	10534	i_w	8.0		6667	4.83	.0096	--	--	1.41	∞	NA	--	M-B
	3	10533	T_w	10.0		6664	5.43	.0103	10.37	500	11.0	∞	NA	--	S
RB-9	1	10533	T_w	10.0	1220.60	6654	4.34	.0090	8.84	500	7.0	∞	NA	--	S
	2	1053A	i_w	8.0		6667	4.83	.0096	--	--	1.4	∞	NA	--	M-B
	3	1053B	T_w	10.0		6664	5.43	.0103	10.37	500	11.0	∞	NA	--	S
RB-11	1	1053B	T_w	10.0	1227-PI2.5	8106	13.35	.0116	21.93	741	4.29	∞	A	.68-1.24	S
	2	1053A	i_w	8.0		8105	16.13	.0121	--	--	1.75	∞	NA	--	M-B
	3	1053B	T_w	10.0		8107	11.52	.0118	19.30	661	3.85	∞	A	.71-1.58	S
MB-3	1	1053B	T_w	5	1222E-PI2.5	9119	11.66	.0127	21.40	770	4.8	∞	A	1.73-3.78	S*
	2	1040A	i_w	5	1222E-PT2.0	9117	4.98	.0172	--	--	- .44	∞	A	1.86-3.80	S
	3	1053B	T_w	5	1222E-PI2.5	9116	10.45	.0118	17.33	585	4.1	∞	A	2.20-3.84	S*
	4				1227-PI2.5	8955	12.18	.0126	21.52	742	4.9	∞	A	1.90-3.63	S*
	5					8106	11.56	.0119	19.28	650	4.4	∞	A	1.98-3.70	S*
	6					9113	12.20	.0116	21.05	765	4.8	∞	A	1.88-3.76	S*
	7	1053A	i_w	7		8957	10.94	.0122	--	--	9.98	2.25	A	1.74-2.25	S*
	8	1053B	T_w	5		8958	11.28	.0110	18.02	614	4.2	∞	A	1.86-3.80	S*
	9	1053B	T_w	5		8959	11.82	.0133	20.43	650	4.5	∞	A	1.85-3.86	S*

TABLE 2. Channel Calibration/Performance Summary (Cont.)

EVENT	CH	BRIDGE		BUCK. VOLT. (VDC)	PROBE		R_o (Ω)	dR/dT (Ω/°C)	R_{op} (Ω)	T_{op} (°C)	e_{AMB} (VDC)	SURVIVAL TIME (sec)	FIREBALL DATA RETURN		
		Model	Type[1]		Type	S/N							FIREBALL DATA[2]	FIDU TIME SPAN (sec)	CH PERF[3]
MB-3 Cont	10	1053B	T_w	5	1227-PI2.5	8960	11.39	.0112	18.43	650	4.4	∞	A	1.86-3.90	S*
	11	1040A	i_w		1227-PT2.0	6673	5.03	.0178	--	--	-.18	.78	NA	.74-.78	M-S
	12	1053B	T_w		1222E-PI2.5	9115	11.99	.0126	21.91	780	4.6	.004	NA	--	M-S
MB-4	1	1053B	T_w	5.0	1222E-PI2.5	9119	11.66	.0127	21.55	795	4.5	∞	A	1.79-3.50	S
	2	1040A	i_w		1222E-PT2.0	9117	4.98	.0180	--	--	.07	∞	A	1.80-3.60	S
	3	1053B	T_w		1222E-PI2.5	9116	10.45	.0118	19.33	750	4.35	∞	A	1.70-2.55	S
	4				1227-PI2.5	8959	11.82	.0132	21.92	755	4.70	.0105	NA	--	M-S
	5					9114	11.83	.0144	22.35	700	4.45	∞	A	1.89-3.50	S*
	6					9113	12.20	.0116	21.25	780	4.50	∞	A	1.89-3.40	S*
	7	1053A	i_w	7.0		8956	11.40	.0123	--	--	14.00	∞	A	1.52-3.40	S
	8	1053B	T_w	5.0		8960	12.71	.0129	22.75	770	4.36	∞	A	1.60-2.95	S*
	9					8958	11.28	.0106	18.70	790	4.32	∞	A	1.58-2.94	S*
	10					9111	11.06	.0130	20.70	745	4.36	∞	A	1.53-2.94	S*
	11	1040A	i_w		1227-PT2.0	6668	6.04	.020	--	--	-.40	∞	A	1.42-2.60	S*
	12	1053B	T_w		1227 PI2.5	9115	12.26	.0133	22.11	735	4.20	.135	NA	--	M-S

TABLE 2. Channel Calibration/Performance Summary (Cont.)

EVENT	CH	BRIDGE		BUCK. VOLT. (VDC)	PROBE		R_o (Ω)	dR/dT (Ω/°C)	R_{op} (Ω)	T_{op} (°C)	e_{AMB} (VDC)	SURVIVAL TIME (sec)	FIREBALL DATA RETURN		
		Model	Type[1]		Type	S/N							FIREBALL DATA[2]	FIDU TIME SPAN (sec)	CH PERF[3]
DMB-1	1	1053B	T_w	5.0	1222E-PI2.5	9119	11.49	.0127	20.49	770	4.5	∞	NA	--	M-N
	2	1040A	i_w	7.0		9116	10.54	.0118	--	--	.15	∞	NA	--	M-N
	3	1053B	T_w	5.0		9118	12.85	.0140	22.76	770	4.7	∞	NA	--	M-N
	4				1227 PI2.5	9116	13.73	.0128	22.77	645	4.5	∞	NA	--	M-N
	5					9114	15.11	.0137	24.96	710	4.8	∞	A	1.55-4.03	F
	6					9113	12.45	.0116	21.10	748	5.2	∞	A	1.65-4.15	F*
	7	1053A	i_w	7.0	1220-T-2.5	8957	20.42	.0100	--	--	14.2	∞	A	1.56-4.40	F*
	8	1053B	T_w	5.0	1227-PI2.5	9111	11.24	.0130	20.50	715	4.6	∞	A	1.62-4.40	F*
	9	1040A	i_w	7.0	1220-PT2.0	6664	5.40	.0184	--	--	-1.2	∞	NA	--	M-B
	10	1053B	T_w	5.0	1227-PI2.5	8960	13.06	.0129	22.18	770	4.5	∞	A	1.62-4.40	F*
	11					8956	11.48	.0123	20.15	620	4.3	∞	NA	--	F
	12					8106	11.70	.0119	20.16	746	4.4	∞	NA	--	F
	13					8958	11.37	.0110	19.18	653	--	∞	NA	--	M-B

[1] T_w: constant temperature; i_w: constant current

[2] A: available; NA: not available

[3] S: satisfactory; F: fair; M: malfunction (B: Bridge; N: Noise; S: Sensor)

*Moderate to substantial signal saturation for fireball top and/or core.

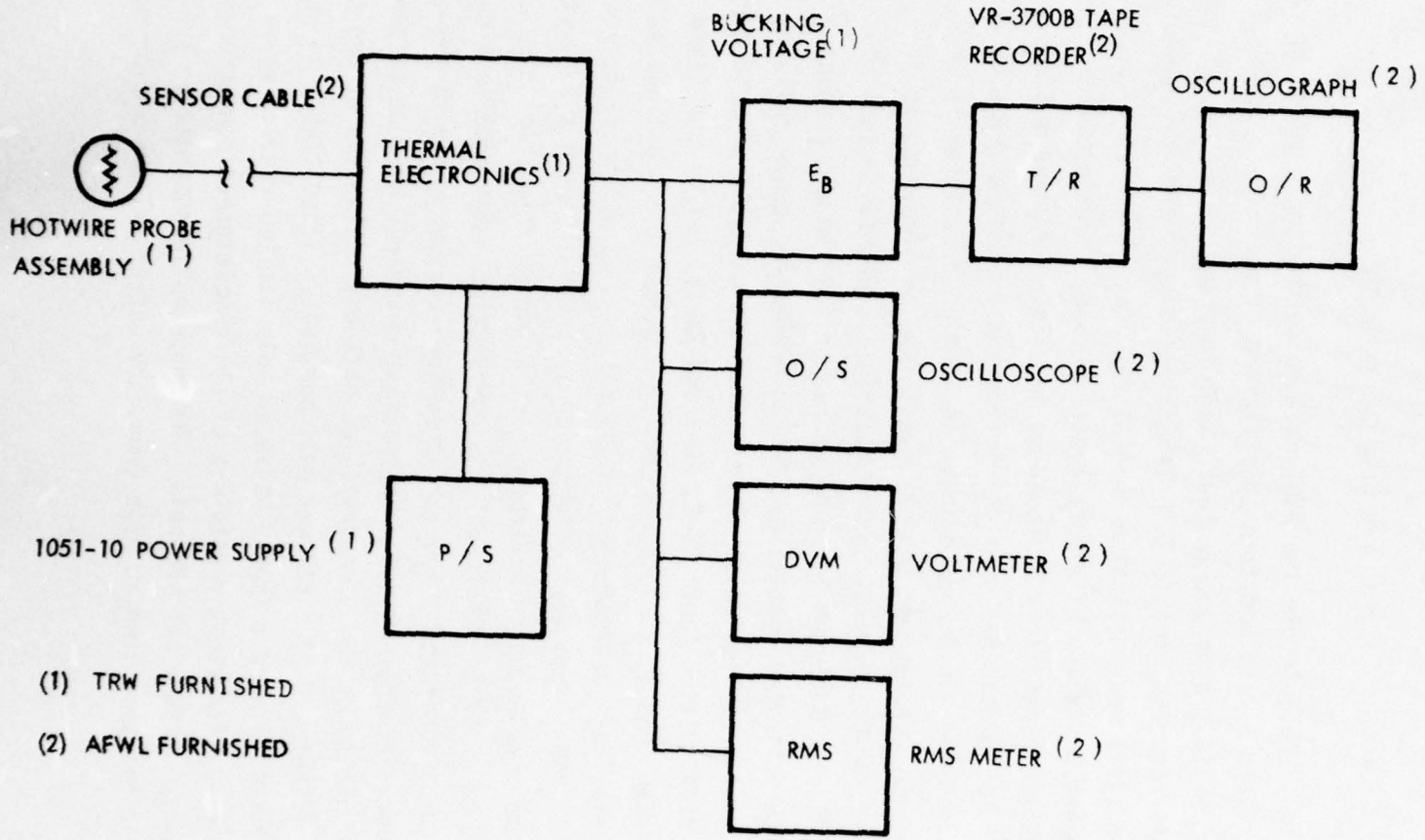

Figure 8. Electronics Schematic

3.0 EXPERIMENTAL RESULTS

The test schedule for the GEST balloon detonation program is presented in Table 1. In addition to a listing of performance dates, detonation yields, atmospheric test conditions and number of activated temperature channels (total: 70), Table 1 also specifies balloon/strut separation distances, validated channel results, sensor survival performance, and a summary of fireball data return. Specific probe location/orientation details are presented in Section 2.0 and a summary of sensor/bridge operational characteristics and instrumentation matrix is given in Table 2. As noted above in Section 2.1, fireball data return was not achieved on several events due to wind-induced fireball drift (RB-8, RB-9 and MB-1) and/or substantial debris-induced sensor failure (MB-2). Although the primary reason certain other channels did not achieve validated results was due to premature sensor failure, some channels also were limited in signal return as a result of bridge performance difficulties (CH2: RB-8, RB-9 and RB-11) and/or excessive channel noise (CHS 1, 2, 3, and 4 DMB-1). Except for DMB-1 the validated channel data corresponded in general to a 40 db signal-to-noise ratio. All DMB-1 data were affected by an intermittent but persistent ground loop problem which developed just prior to detonation time and which was observed on other GEST instrumentation. A gradual buildup of gusty wind conditions, however, precluded further delay in the detonation time, in order to pursue corrective measures, because of the hazardous nature of the already-filled balloons. Also one of the two balloons (DMB-1W, Figure 2f) was only partially filled (Table 1) due to a malfunctioning gas supply valve so only limited results were expected from this event regardless of the completeness/performance of activated measurement channels. Although noise suppression processing techniques, such as high frequency cutoff filters and/or noise

subtraction using reference signal channels can be used to upgrade recorded DMB-1 data, this effort has not been pursued herein primarily because of the noted disparity in detonation yield between the two DMB-1 balloons. Since the main purpose of DMB-1 was to provide a controlled experiment evaluating shock torusing and fireball coupling arising between two large atmospheric detonations of equal yield, only limited usefulness in reduced temperature data could be realized with the off-nominal performance for DMB-1. It should also be noted that the reduction of RB-11 fireball data has similarly been limited because of the small yield/scale nature of this RB detonation. Thus although fireball data return was realized on RB-11, MB-3, MB-4 and DMB-1, processing and reduction of measured results to determine temperatures and turbulent statistics for the GEST fireballs have concentrated herein on the MB-3 and MB-4 results.

3.1 GEST Size/Rise Data

Prior to discussing the details of measured temperature results for MB-3 and MB-4 it is appropriate to assess general performance characteristics for the rising GEST fireballs. To this end reference is made to the extensive photographic coverage carried out by AFWL for the GEST program (Ref. 6). Typical side-view motion picture results obtained by AFWL are shown in Figures 9a and 10a for MB-3 and MB-4, respectively. These sequential film clips were prepared from 16 mm color films (400 frames/sec) taken by Fastex cameras located approximately 1000 feet from GZ (Figure 1). Note that sensor-detected fireball leading/trailing edge times were 1.7/3.8 sec and 1.4/3.6 sec for MB-3 and MB-4, respectively (Table 1). In addition to the fireball cloud, also visible in Figures 9a and 10a are the overhead cable, a black and white scaling marker, the sensor cable harness and the main probe strut. The 15-foot scaling marker was suspended vertically

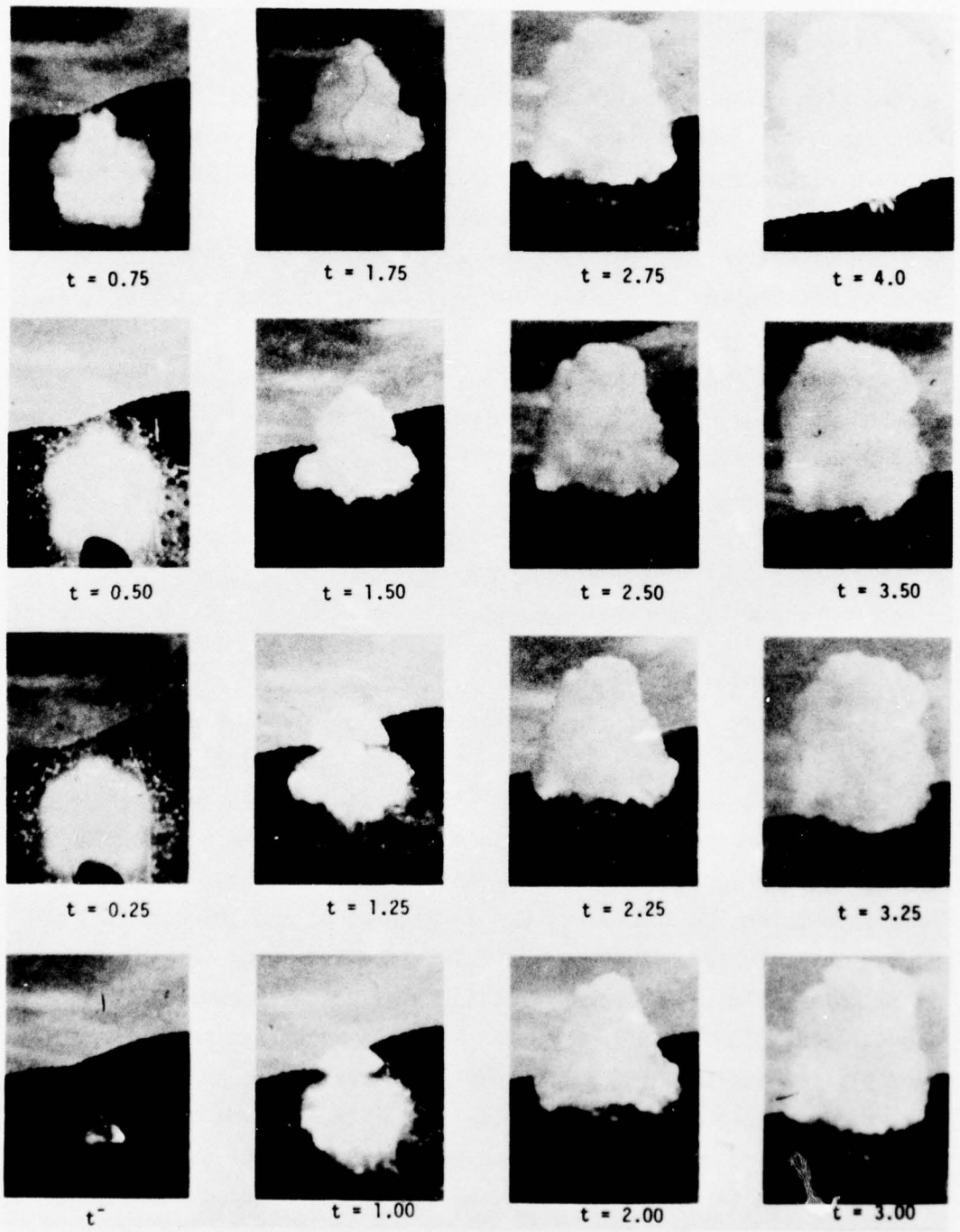

Figure 9a. MB-3 Fireball: Station 2 - 400 frames/sec

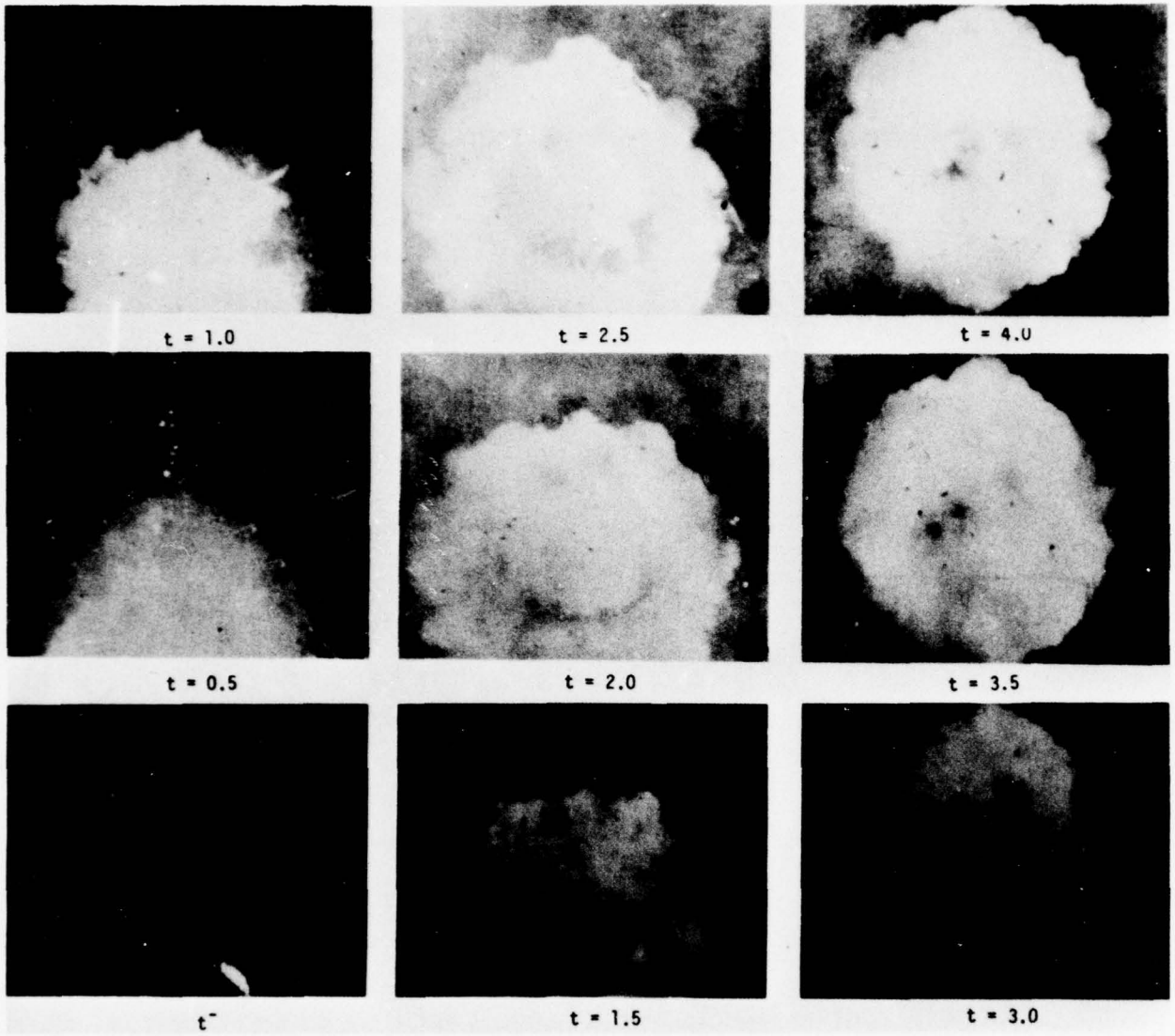

Figure 9b. MB-3 Fireball: Station 4 (Base View) - 48 frames/sec

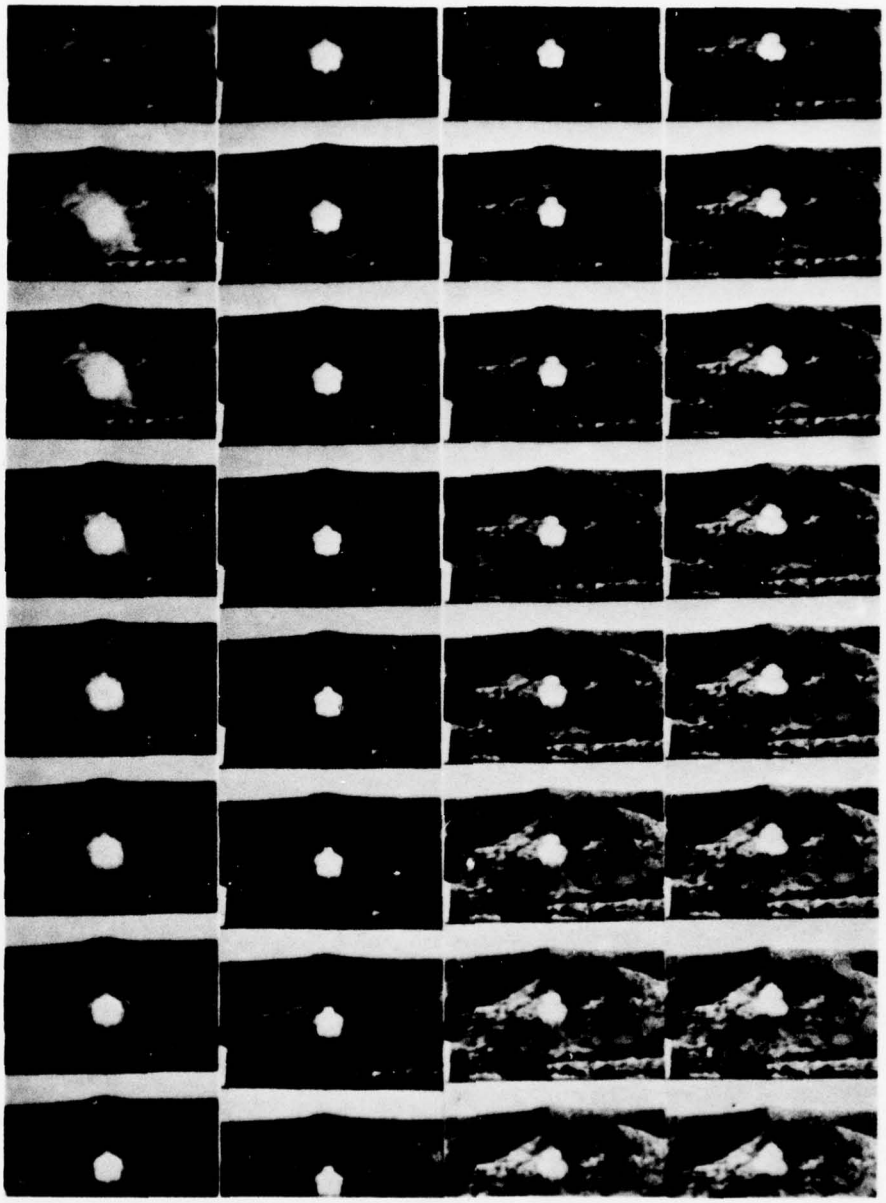

Figure 9c-1. MB-3 Fireball: Observation Area - 24 frames/sec

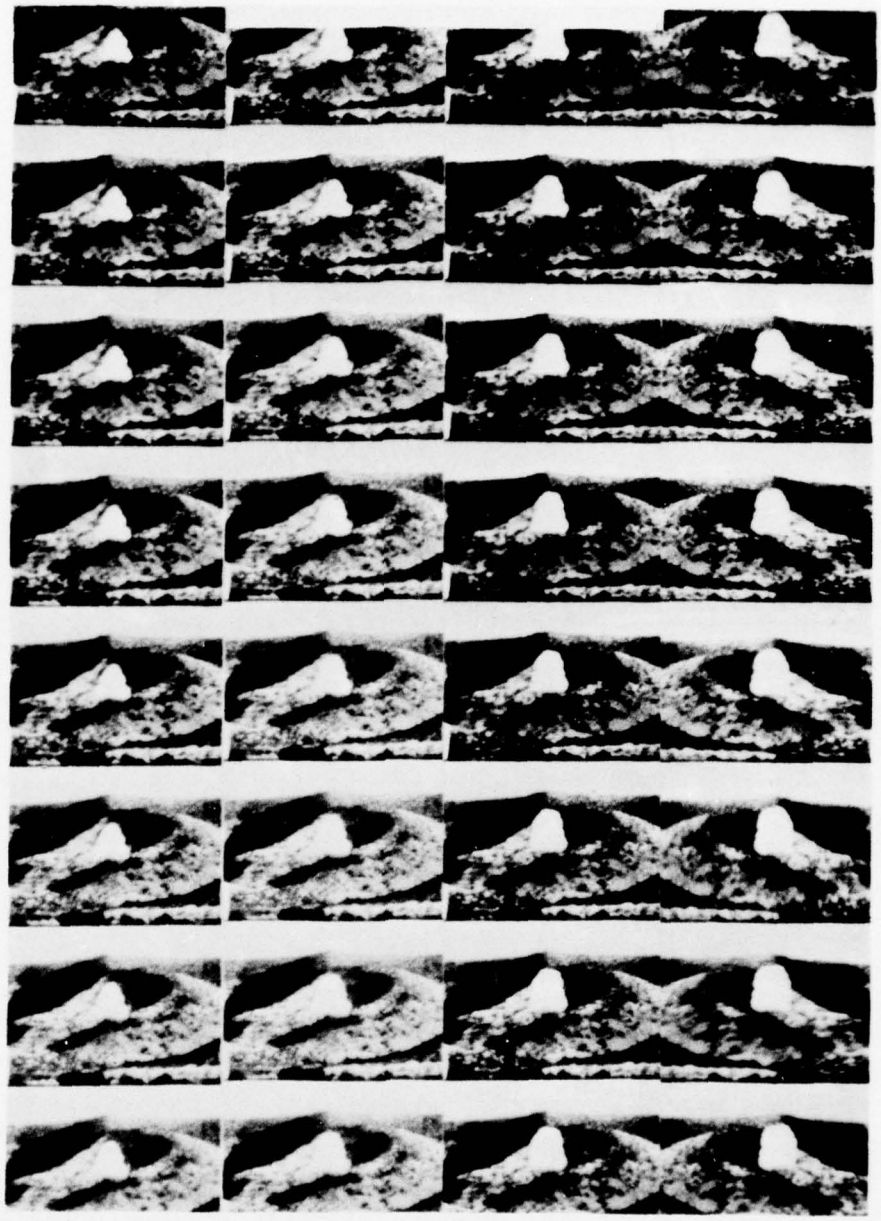

Figure 9c-2. MB-3 Fireball: Observation Area - 24 frames/sec (Cont.)

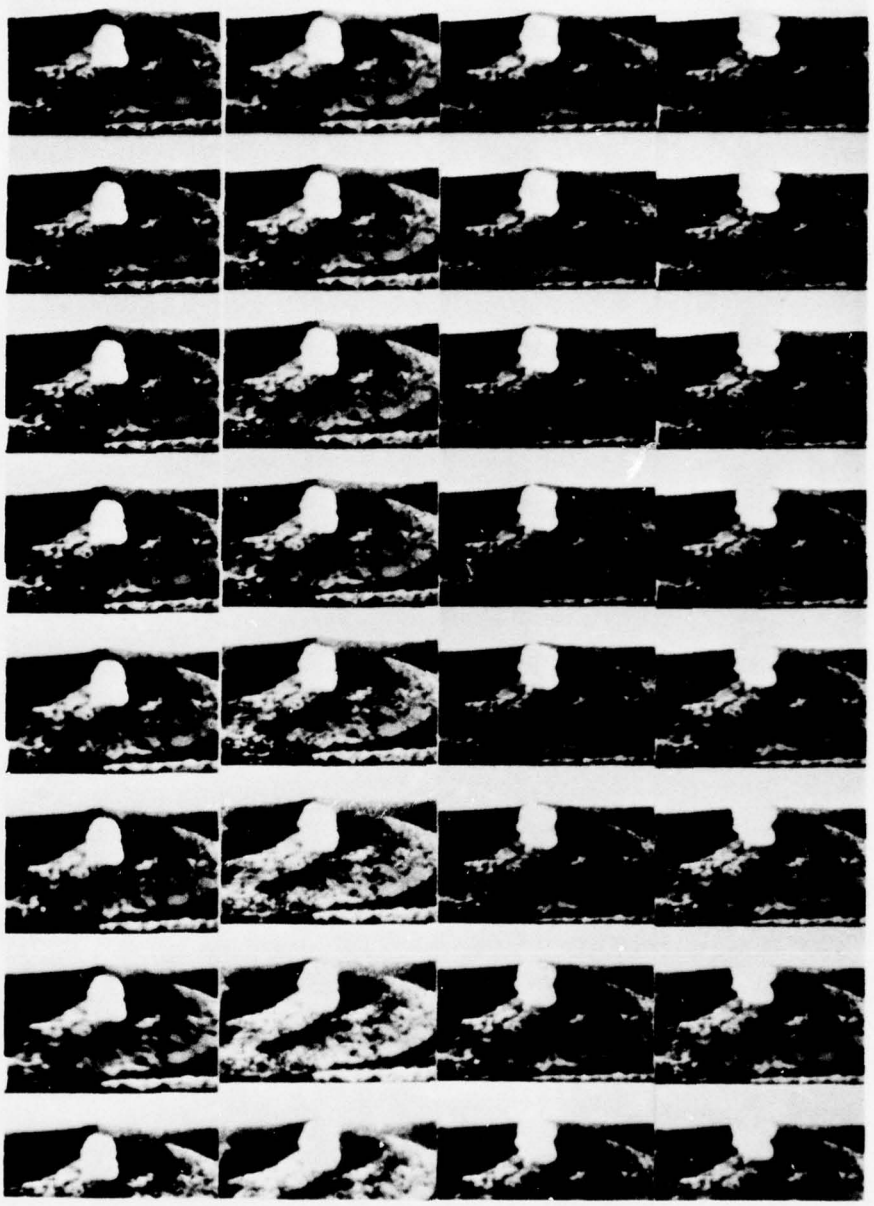

Figure 9c-3. MB-3 Fireball: Observation Area - 24 frames/sec (Cont.)

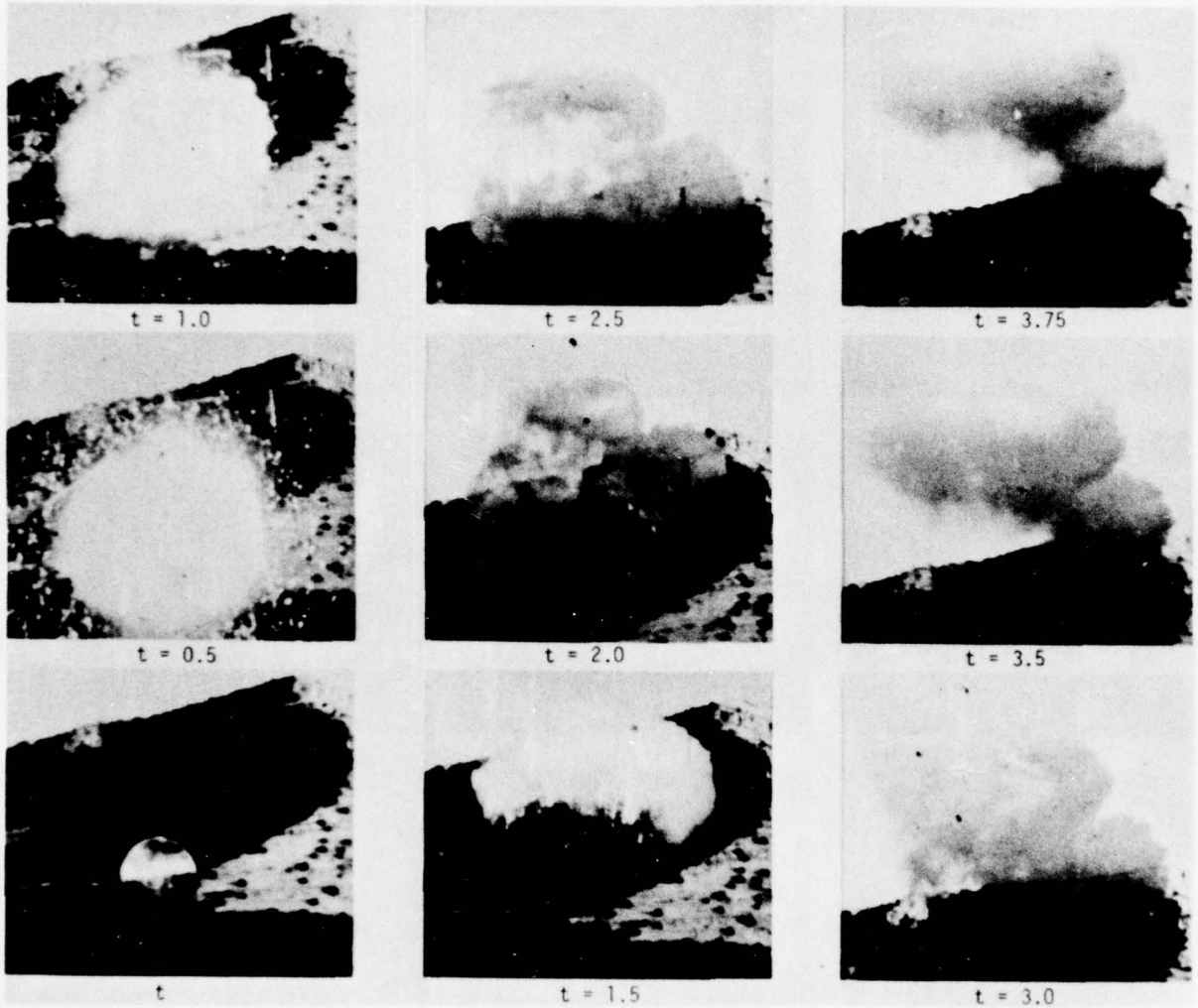

Figure 10a. MB-4 Fireball: Station 3 - 400 frames/sec

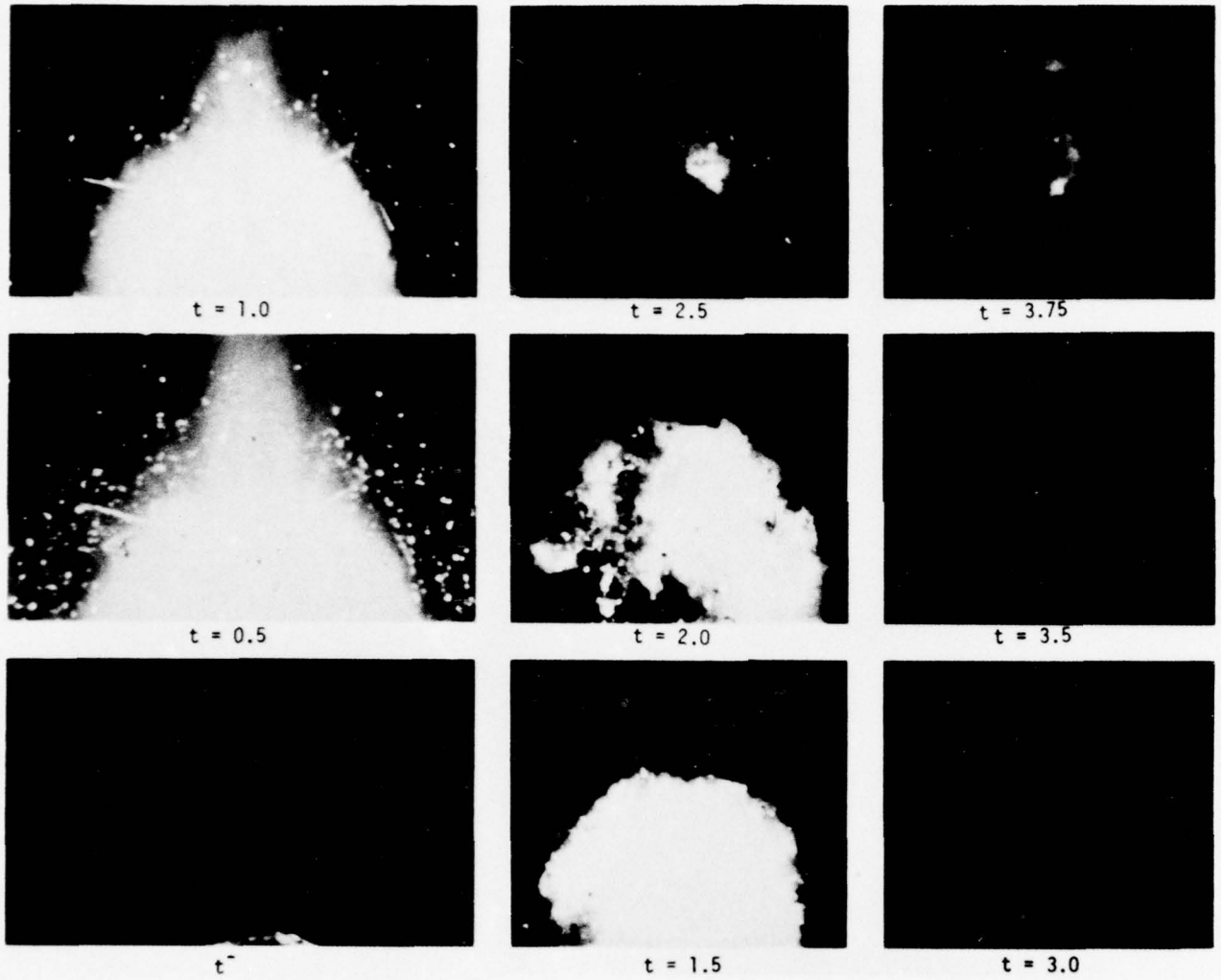

Figure 10b. MB-4 Fireball: Station 4(Base View) - 48 frames/sec

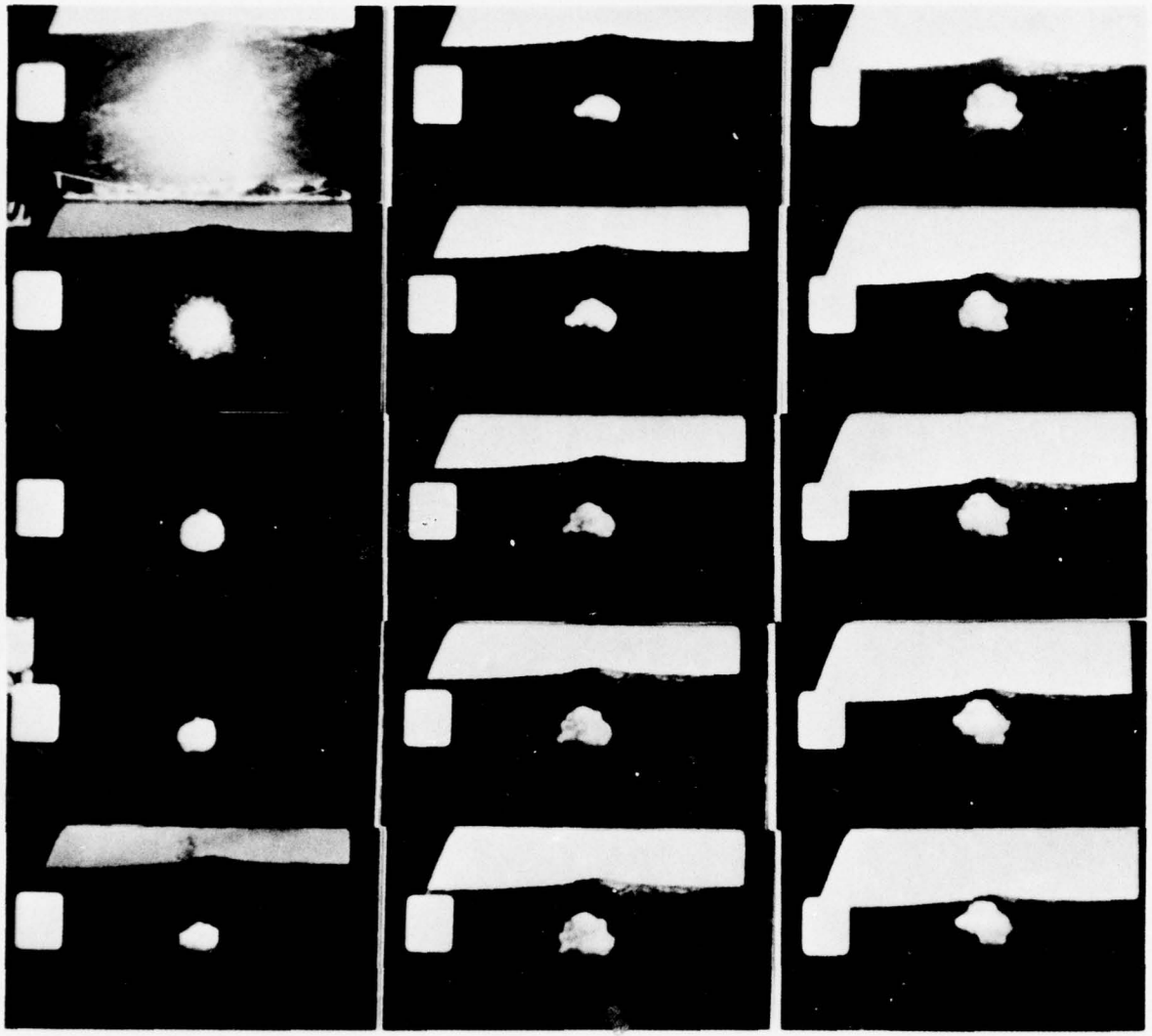

Figure 10c. MB-4 Fireball: Observation Area - 4.8 frames/sec

from the overhead cable at a radial distance from GZ (127°) of 50 feet. This marker was used by AFWL as a calibration "scale" to determine the size/rise data presented in Figure 13 (Ref. 6). These data illustrate that the MB-3 and MB-4 fireballs rose vertically at a velocity of approximately 43 ft/sec and were nearly 108 feet in diameter during the time GEST temperature data were measured. Corresponding fireball Reynolds numbers based on these diameter and velocity data and ambient conditions were of the order of 3×10^7. From motion picture films taken by cameras positioned directly below balloon center, vortex formation became evident at approximately 4 to 5 sec after detonation (Figures 9b and 10b - 48 frames/sec). These photographic results illustrate that the main probe strut for the temperature task was positioned at approximately the half maximum radius location. The resulting data correspond to a vertical slice through the rising fireball, thus providing multiprobe temperature measurements for the fireball top, central core and trailing wake. Evident in Figures 9 and 10 are the fast rising center "cap", vortical motion around the fireball perimeter and the early time turbulent structure for the GEST fireballs. Intermittent "pockets" of ambient air are also observed to be entrained by the turbulent fireball and subsequently to pass through the temperature probe locations. Additional motion picture film "clips" of rising GEST fireballs are shown in Figures 9c, 10c, 11 and 12 for MB-3, MB-4, RB-25 and DMB-1, respectively. These photographic results were obtained with a standard super 8 motion picture camera (24 frames/sec) positioned at the TRW van location (RB-25) or at the GEST observation area (4800 ft @ 220°, MB-3, MB-4 and DMB-1).

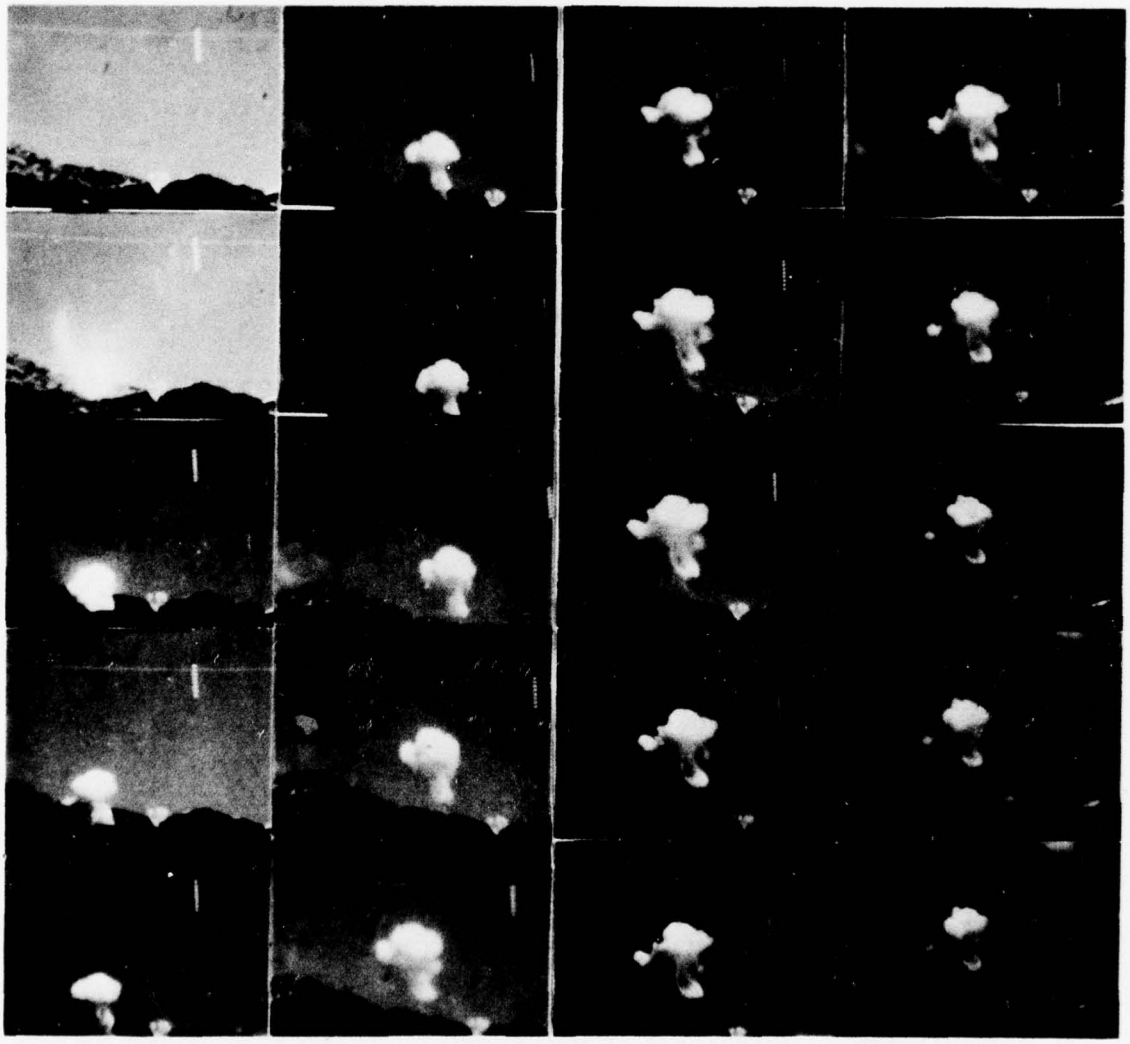

Figure 11. RB-25 Fireball: Van Area - 48 frames/sec

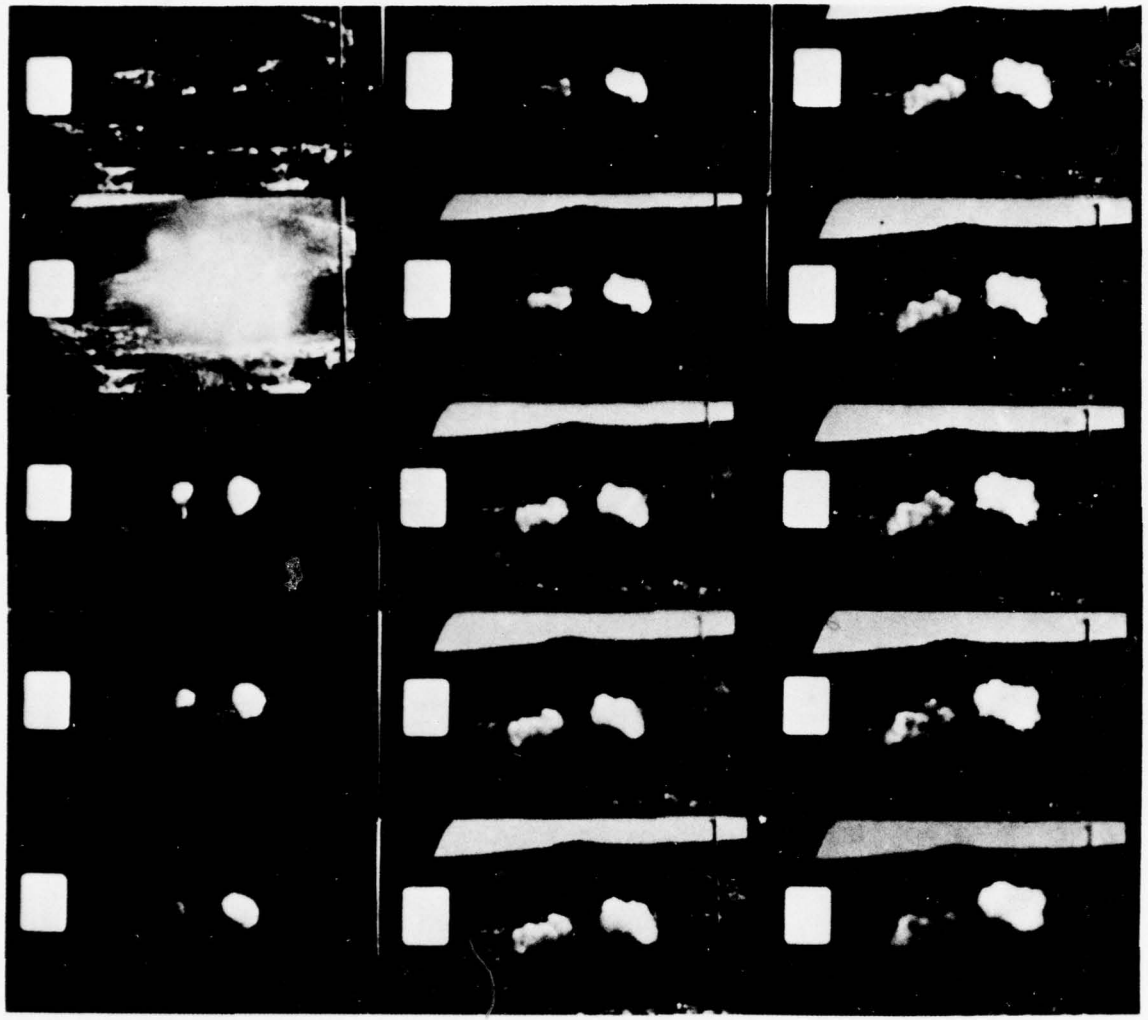

Figure 12. DMB-1 Fireball: Observation Area - 4.8 frames/sec

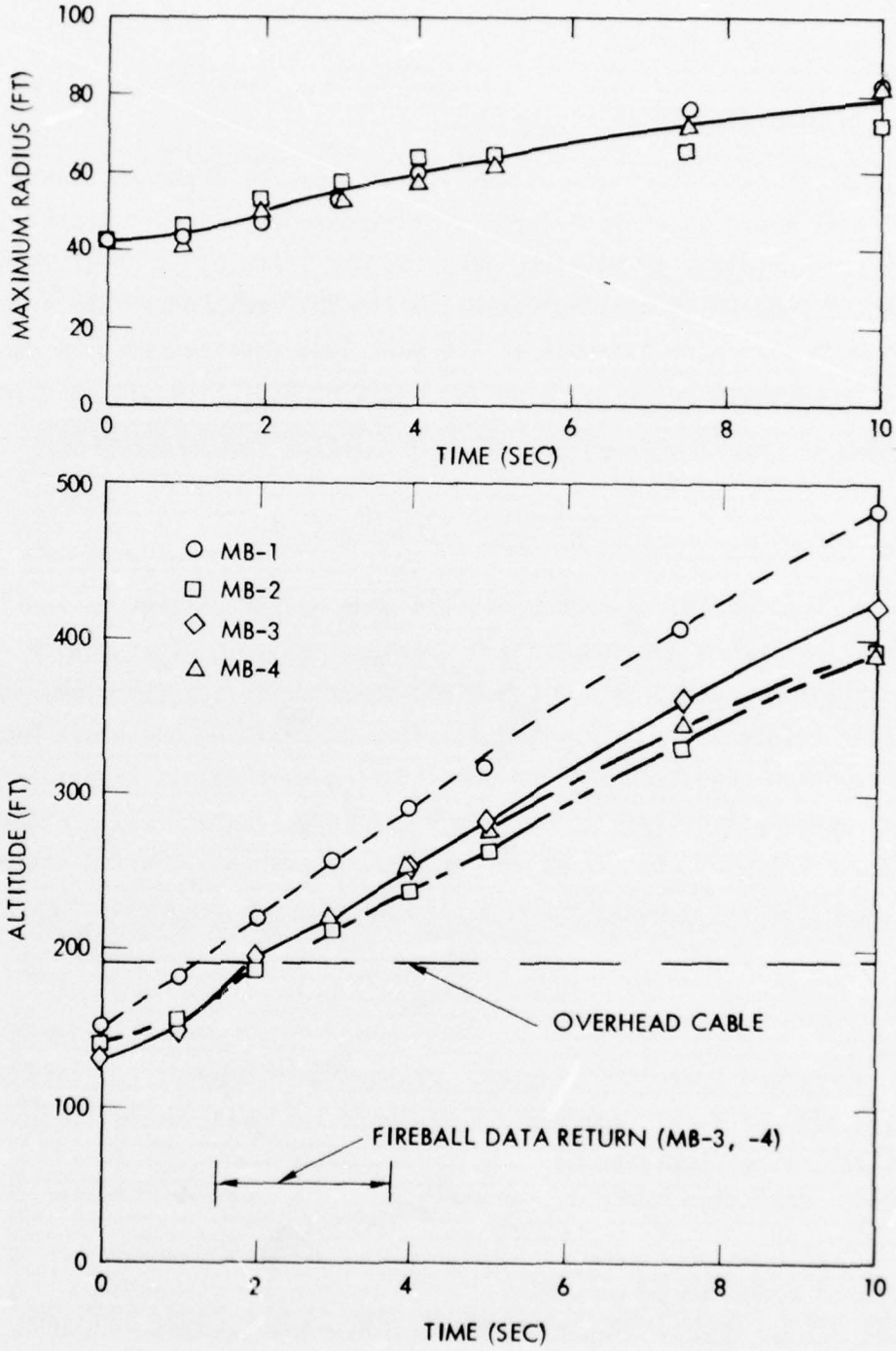

Figure 13. Radius/Altitude Data for GEST Fireballs - Optical Measurements (Ref. 6)

3.2 Raw Data Time Trace Histories

Typical raw data time-trace histories for the three RB events and for MB-4 are shown in Figure 14. Response of the heat transfer gauge (constant temperature sensors, Chs 1 and 3) to shock front motion is seen to be distinct from the fireball response. The noted difference is a direct result of the heat loss equation for the constant temperature hot wire which for a rising GEST fireball is given approximately by

$$e_w^2 \dot{\sim} (CT + \sqrt{u})(T_w - T) \qquad (4)$$

In Equation (4) e_w represents the wire output voltage, u and T the local velocity and temperature, respectively, and T_w the wire temperature (constant, $\cong$ 700°C). This formulation for the wire heat transfer relationship is arrived at after simplifying the basic hot wire equation [Equation (1)] by substituting the Nusselt/Reynold's number correlation given in Section 2.3.2 into Equation (1). After some rearrangement and making use of the pressure equilibrium condition as well as the perfect gas relationship

$$\rho = \frac{p}{RT}$$

where ρ, p, and T are the density, pressure and temperature, respectively, for the local flow and R represents the gas constant, Equation (1) can be rewritten as

$$\left(\frac{e_w^2}{R_w}\right) = \left(\frac{e_w^2}{R_w}\right)_{NF} + \pi \ell k \left[.21 + .49 \left(\frac{p}{RT} \frac{ud}{\mu}\right)^{.45}\right](T_w - T) \qquad (5)$$

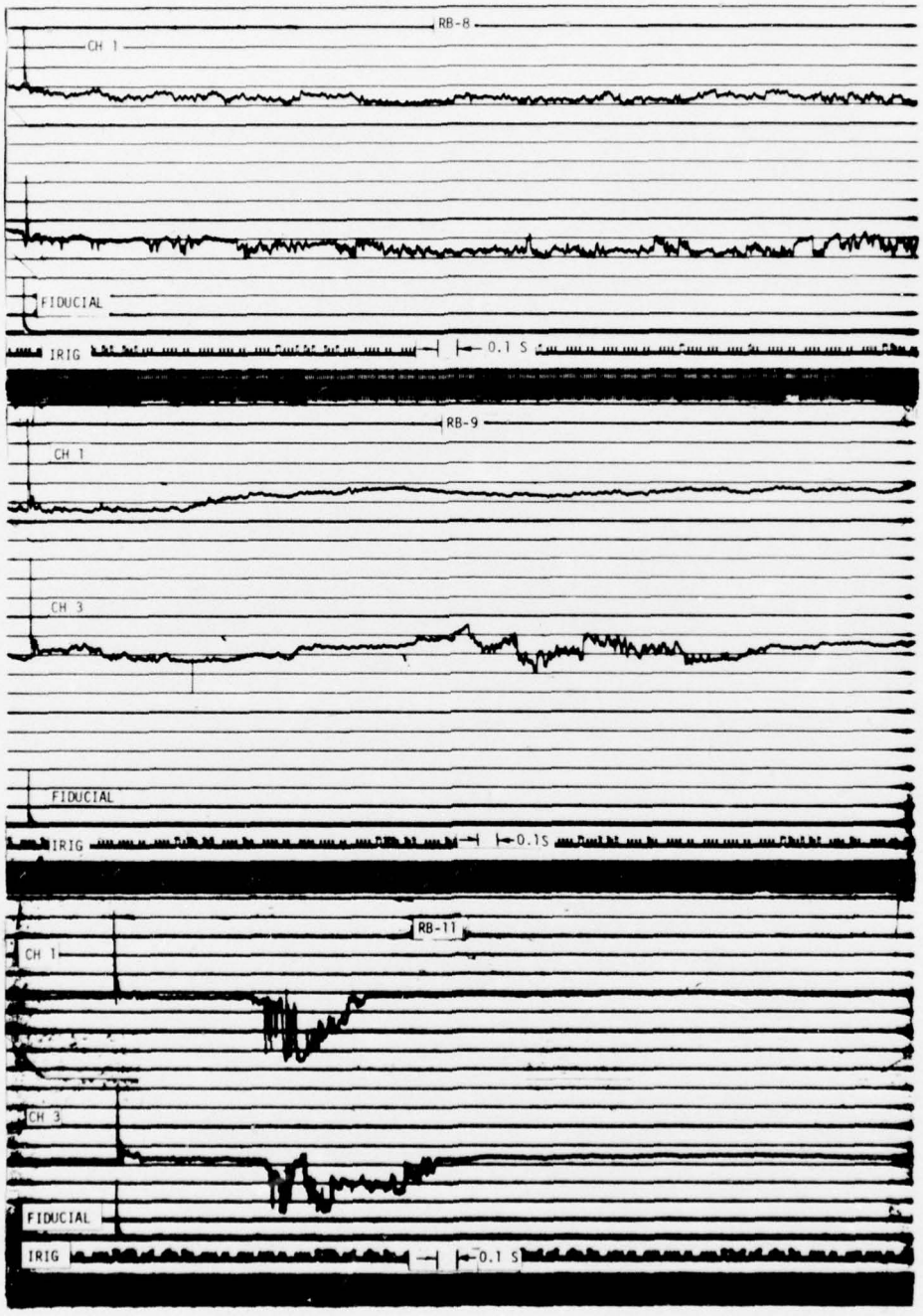

Figure 14a. Raw Data Oscillograph Records: RB-8,-9,-11

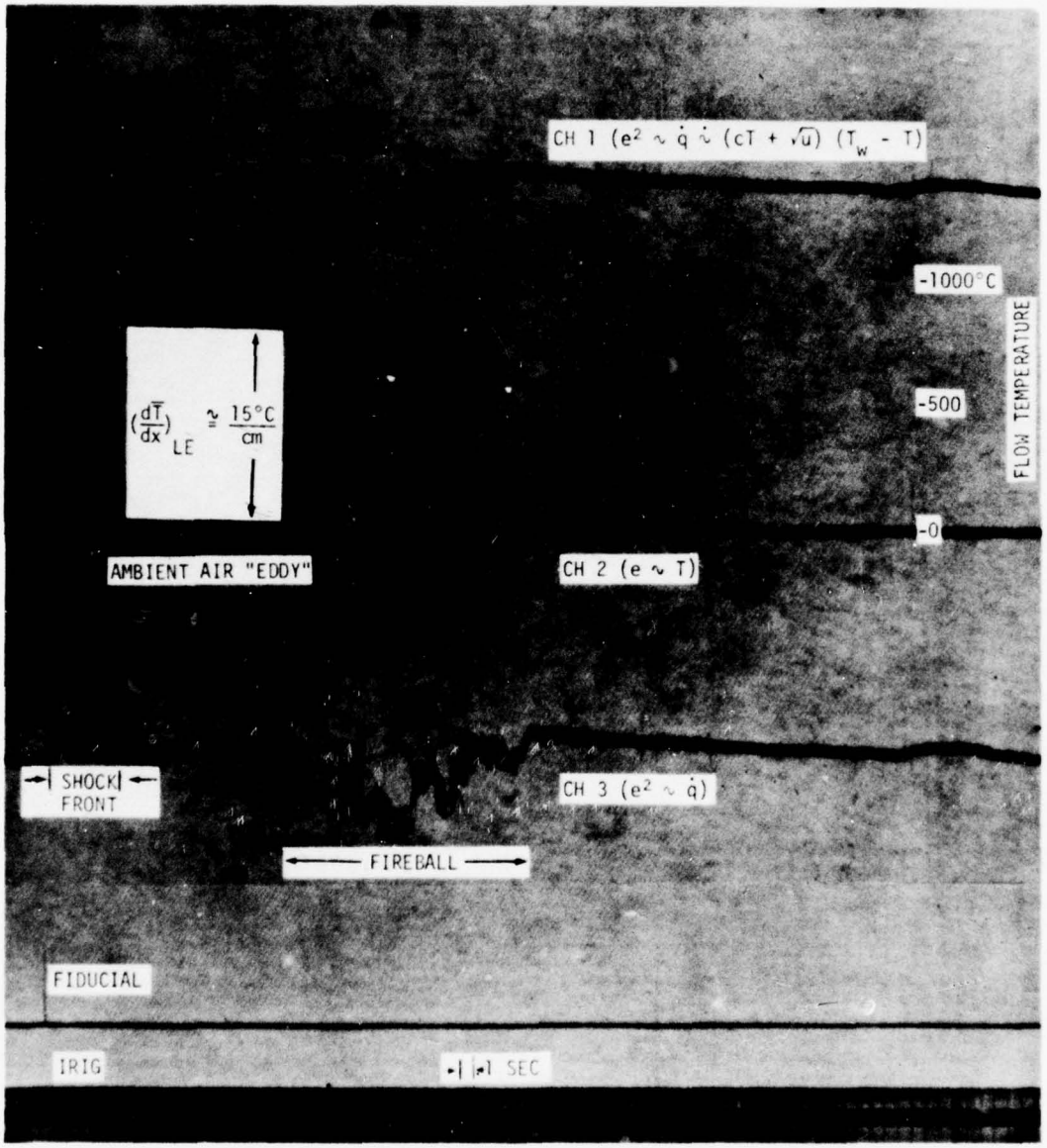

Figure 14b. Raw Data Oscillograph Records: MB-4

By further assuming that the viscosity (μ) and conductivity are proportional to temperature, Equation (5) reduces to the approximate form given by Equation (4)

The reduced heat transfer equation [Equation (4)] illustrates that, in order to maintain a constant wire temperature, the bridge feedback power must increase with increasing velocity when flow temperature changes are negligible. Similarly, when velocity changes are small but substantial temperature increases occur, as within the fireball, feedback power is reduced. Although the bridge power signal represents the combined effects of both the velocity and temperature field within the fireball, its dependence on velocity is relatively small because of the velocity's square root behavior. Once an approximate determination has been made of the fireball's mean velocity field (Section 3.3), solution of the constant temperature hot wire heat transfer equation can be accomplished to provide fireball temperature data (Section 2.3.2). The resulting reduced temperatures represent data corresponding to a 5 KHz frequency response as provided by the anemometer feedback bridge. Such data therefore complement results obtained with constant current sensors (e.g., Ch 2, Figure 14b) which, because of thermal response characteristics, were limited to an upper frequency response of 1 KHz. Additional raw data time history results, as digitized (4000 cps) and without adjustment for bucking voltage offsets, are presented in Figure 15. In Figures 14 and 15 Channels 2, 7, and 11 correspond to constant current sensors, wherein the output signal is proportional to temperature ($e \sim T$) while all other channels represent sensor heat transfer data as measured by constant temperature bridges (Table 2).

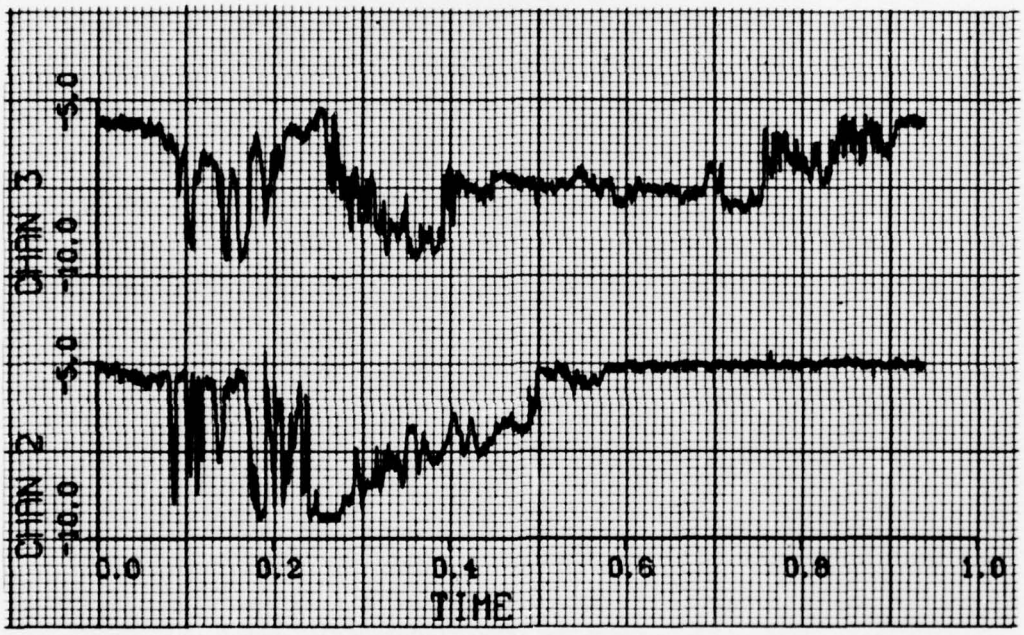

Figure 15a. Digitized Bridge Output Data: RB-11

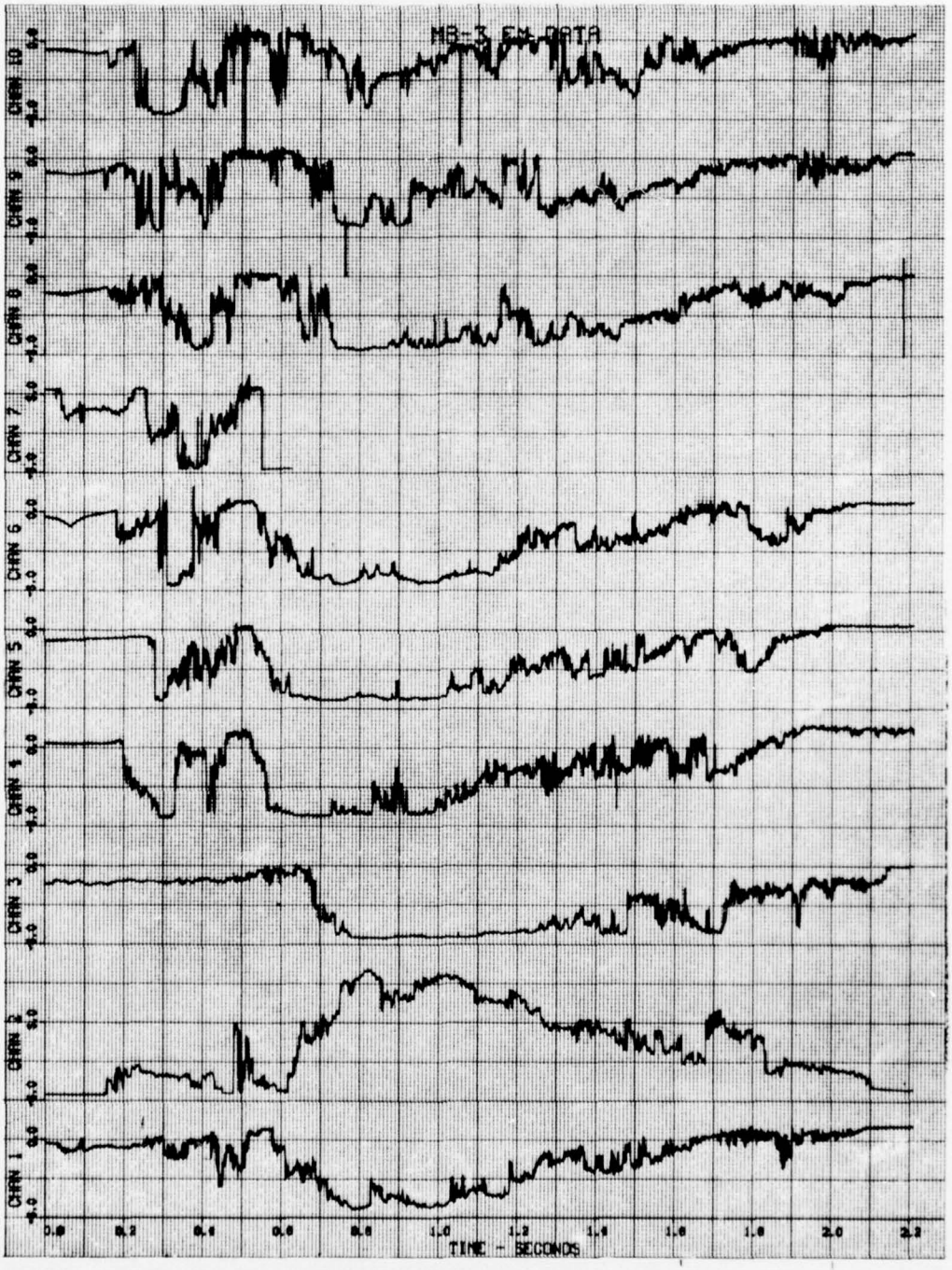

Figure 15b. Digitized Bridge Output Data: MB-3 (t_{FIDU} = -1.7 sec)

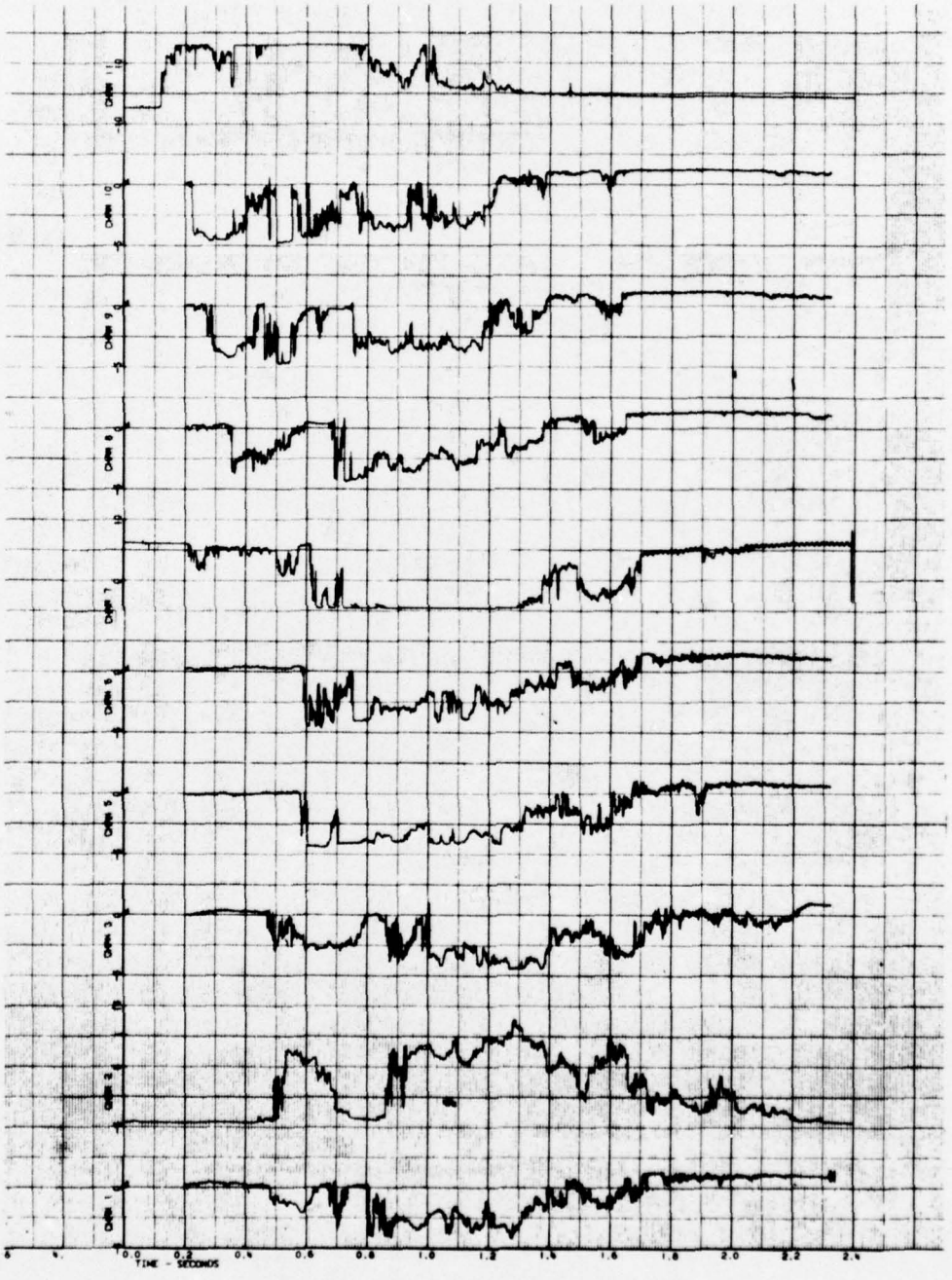

Figure 15c. Digitized Bridge Output Data: MB-4 (t_{FIDU} = -1.3 sec)

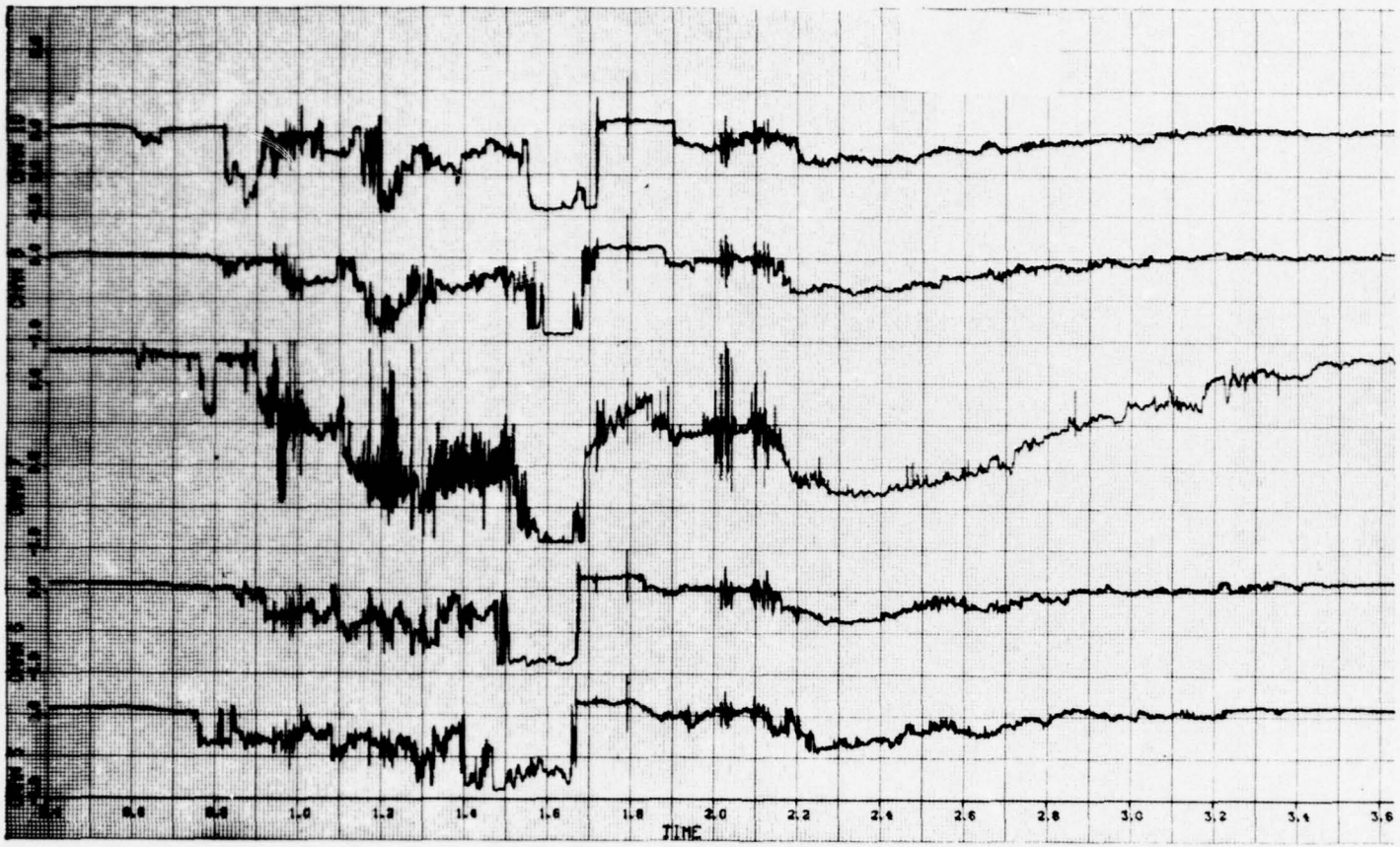

Figure 15d. Digitized Bridge Output Data: DMB-1 (t_{FIDU} = -0.8 sec)

The present digitized results illustrate that a number of channels experienced signal saturation difficulties during exposure to leading edge (top) and mid-fireball (core) conditions. For MB-3 and MB-4, on the other hand, all Channel 2 data for both events as well as trailing wake results for all other channels provided high resolution data in the absence of channel crosstalk. When evaluating this overrange question and the corresponding limited data return experienced by some channels, it should also be recognized, however, that the MB-3 and MB-4 events represent, in fact, the first such large scale atmospheric detonation events where even some "in-situ" temperature data were successfully measured. The short stand-down time between events three and four (one day, Table 1) necessitated that corrective measures to reduce this signal saturation problem for MB-4 be restricted only to raising operating temperatures to somewhat higher levels (Table 2). In spite of the data return limitations imposed by the noted channel overrange effects, the present validated temperature results provide a useful "first cut" measurement of the temperature field structure for the early-time, large-scale fireball. Future multiprobe experiments for the rising fireball problem can now benefit from the experience gained with the current set of prototype temperature measurements and consider greater use of fast response resistance thermometer probes as used for Channel 2 (MB-3, MB-4) as well as larger probe/balloon separation distances compatible with a "cooler" fireball.

3.3 Mean Velocity Data (MB-3 and MB-4)

In scoping out the original instrumentation matrix for the Temperature Measurements Task, consideration was given to the need to measure local flow velocities as well as to optimize the use of available equipment. Thus, the final test configuration consisted of a mix of "direct" and "derived" temperature measurement channels. Both types

of measurement employed hot wire anemometry techniques in either the constant current mode ("direct," resistant thermometer) or constant temperature mode ("derived"-heat transfer) (Section 2.3). This latter anemometry procedure permits a determination to be made of the mean velocity field by "backing out" local velocities from measured heat transfer data associated with the motion of ambient air. Since unmixed ambient fluid is identifiable by its quiescent nature, local velocity data can be derived directly from the sensor heat transfer equation (Section 2.3.2). In this manner, reduced velocity results for both MB-3 and MB-4 have been "measured" and are shown as open-symbol data in Figures 16a and 16b, respectively. Shown also on Figures 16a and 16b are local convection velocities as determined by "eddy" time delays between vertically adjacent channels. For MB-3 the noted velocities were matched (to determine flow calibration constants) at a time from detonation of $t = 3.8$ sec, whereas the corresponding calibration time for MB-4 was $t = 3.2$ sec.

To assist in evaluating these velocity data, annotation entries for the mean rise velocity derived from optical data (Section 3.1) as well as relative locations for the fireball core and thermal wake (based on mean temperature results to be discussed shortly) are also shown on Figures 16a and 16b. The noted data especially the MB-3 results, provide evidence that the fireball leading edge is moving vertically at a velocity comparable to the optically derived mean rise velocity (43 ft/sec). On the other hand, velocity results for the fireball thermal wake illustrate that velocities as high as twice the core velocities were experienced. Such a result compares favorably, however, with the maximum flow velocities for Hill's spherical vortex model (Ref. 11) which predicts maximum velocities 2.5 times larger than the mean rise velocity. It thus would appear that the noted velocity enhancement evident in the thermal wake can be attributed

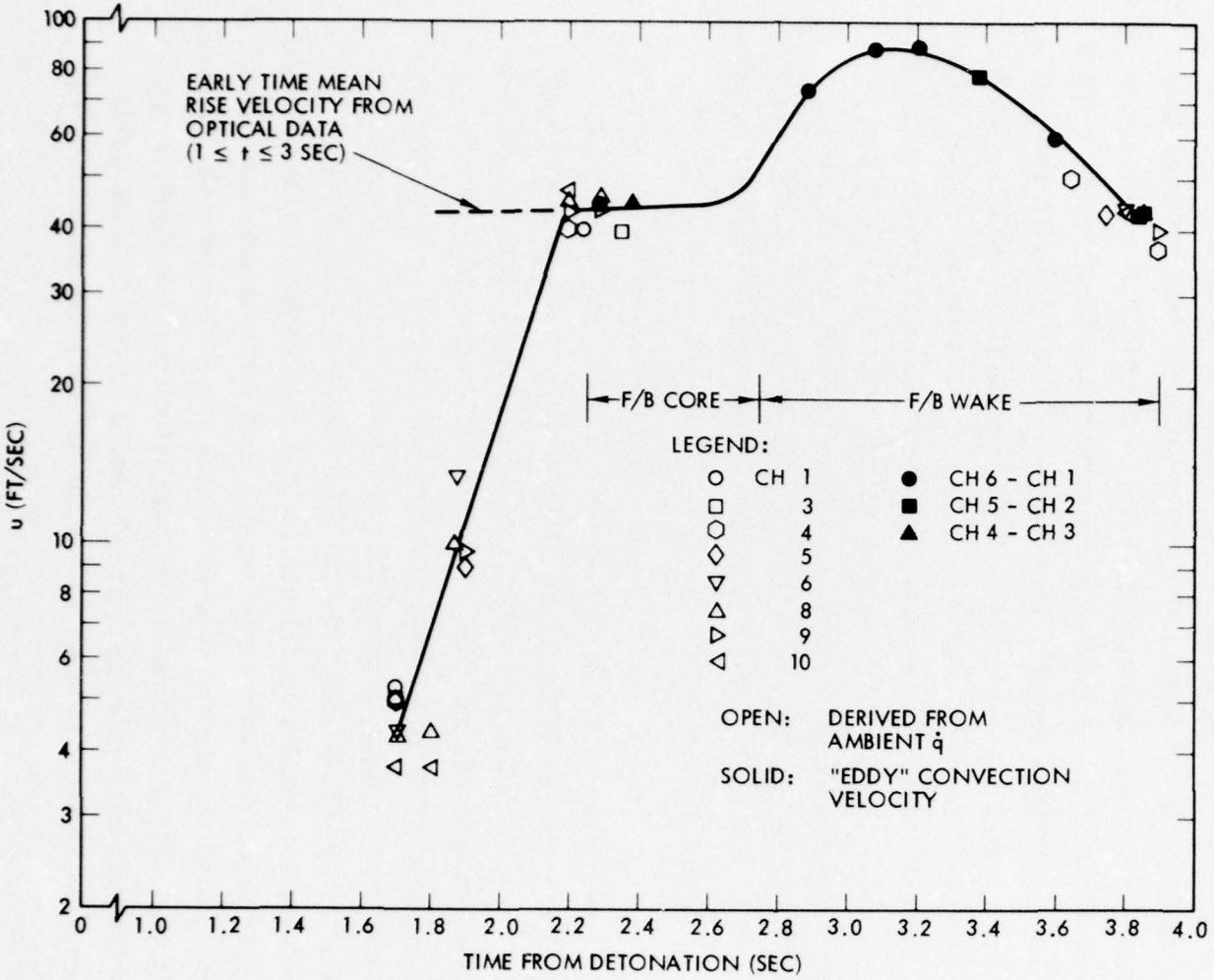

Figure 16a. Mean Velocity Data: MB-3

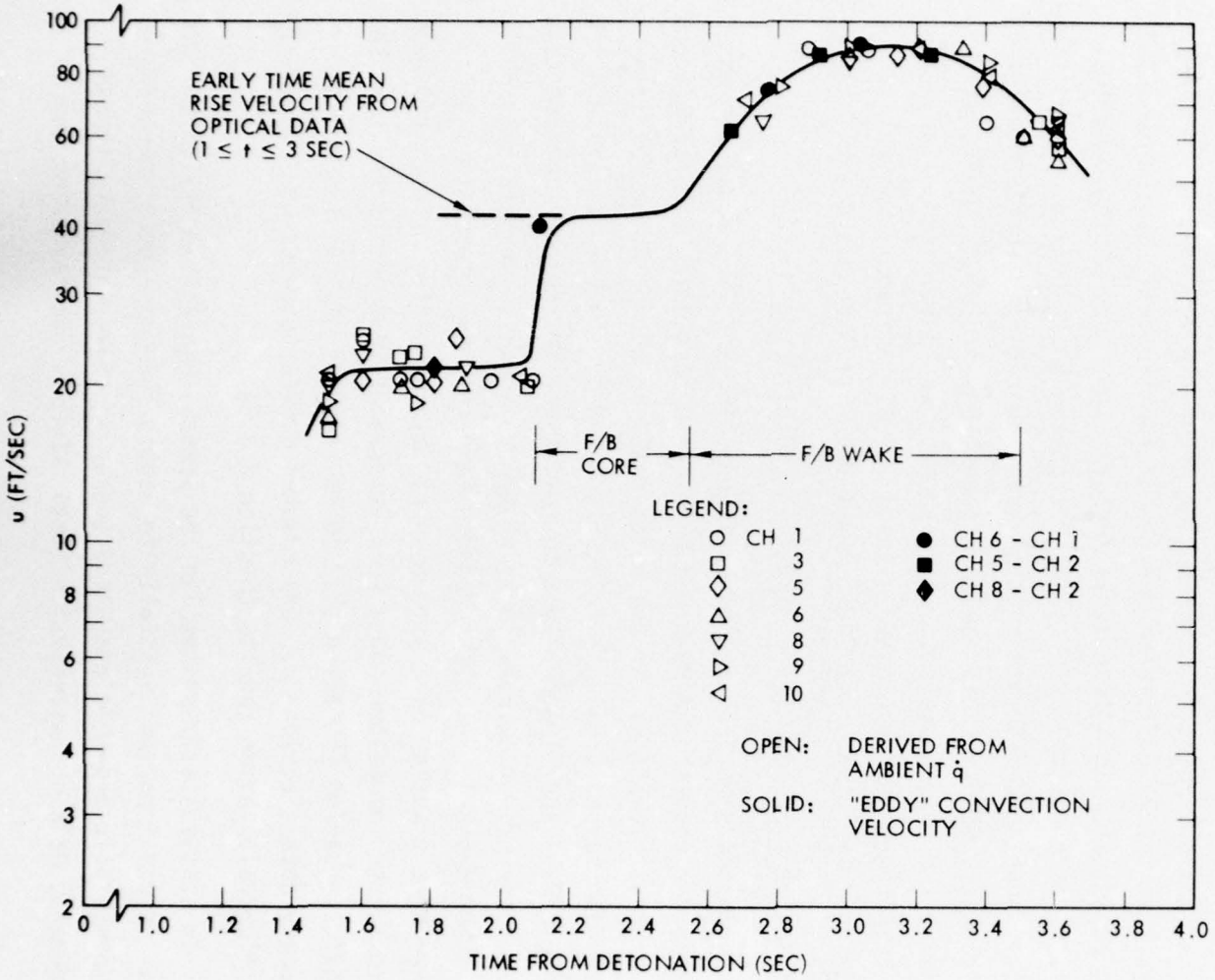

Figure 16b. Mean Velocity Data: MB-4

primarily to the fireball's vortex motion. In addition, the present data base further substantiates the use of the spherical vortex model to approximate the velocity field within rising fireballs.

As a final point relative to the Figure 16 results, it should be noted that the velocities at the top of the fireball for the MB-3 and MB-4 events are significantly different. This contrasting behavior, however, is consistent when it is recognized that portions of the fireball top/cap for MB-4 were initially moving radially (horizontally) at substantial speeds. This radial motion behavior, which tentatively explains the present velocity differences, was determined after reviewing high speed motion picture results for GEST fireballs as well as radially correlating "cap" turbulence data for Channels 8 and 2 of MB-4.

3.4 Temperature Time Trace Histories (MB-3, MB-4)

From the digitized raw data (Figures 15b and 15c) final processed temperature results for MB-3 and MB-4 are presented in Figures 17a and 17b. Sensor locations for the noted data are shown in the test configuration layout drawings of Figures 2 and 6. In Figures 17a and 17b, Channels 2, 7 and 11 correspond to resistance thermometer measurements, wherein the bridge output signal is proportional to temperature, while all other channels represent reduced temperatures determined from sensor heat transfer data as "measured" by anemometer bridge voltages. These latter temperature data were determined through the hot wire heat transfer equation [Equation (1)] in an iterative manner using mean velocity data (Section 3.3) and channel constants based on laboratory and flow calibration results (Section 2.3.3).

In statistically processing the present non-stationary turbulence data, it was important initially to assess the presence of repeatable (deterministic ensemble averages) and/or locally stationary (trend phenomena) data characteristics (Refs. 12-15). In reviewing the

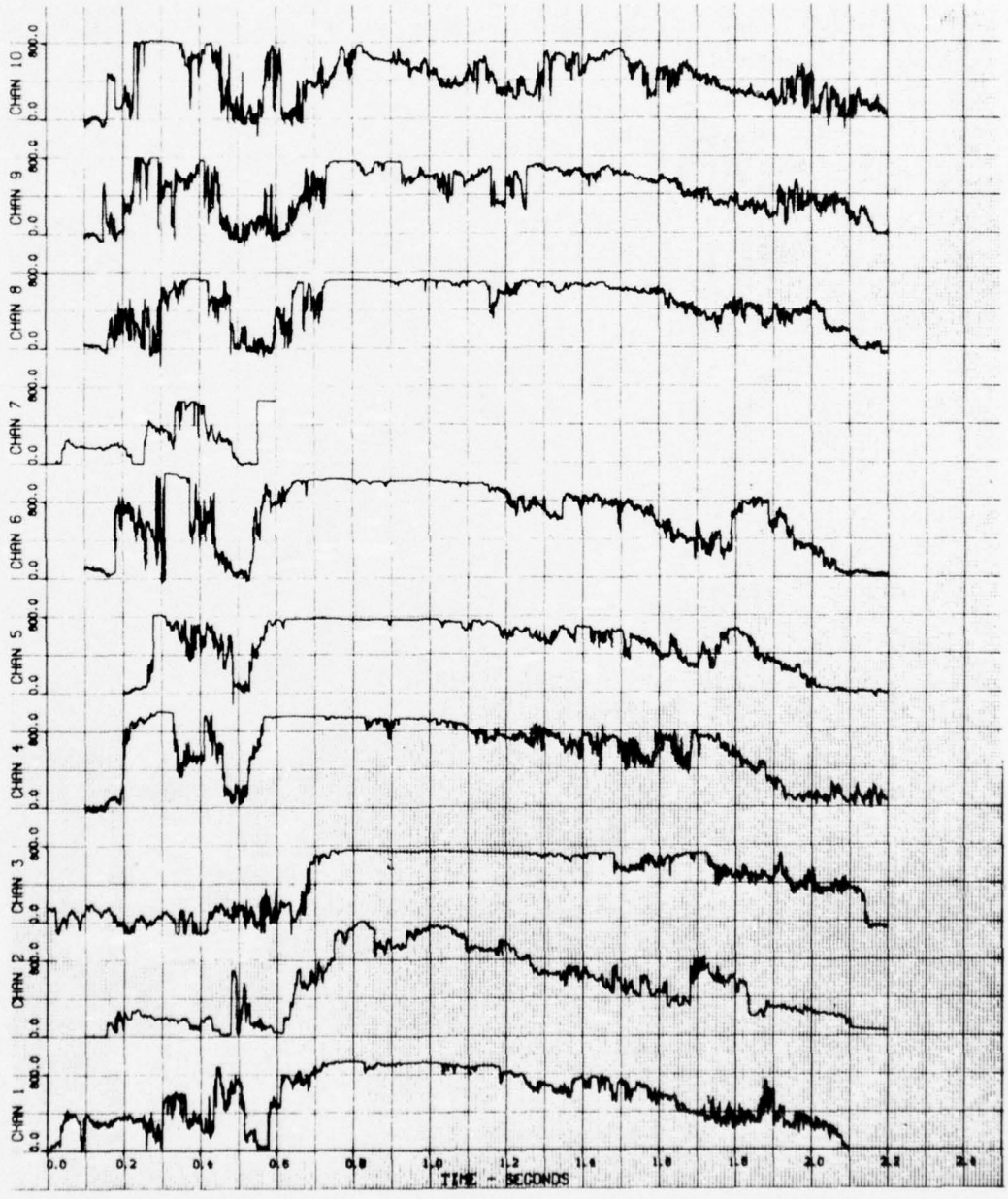

Figure 17a. Digitized Fireball Temperature Data: MB-3
(t_{FIDU} = -1.7 sec)

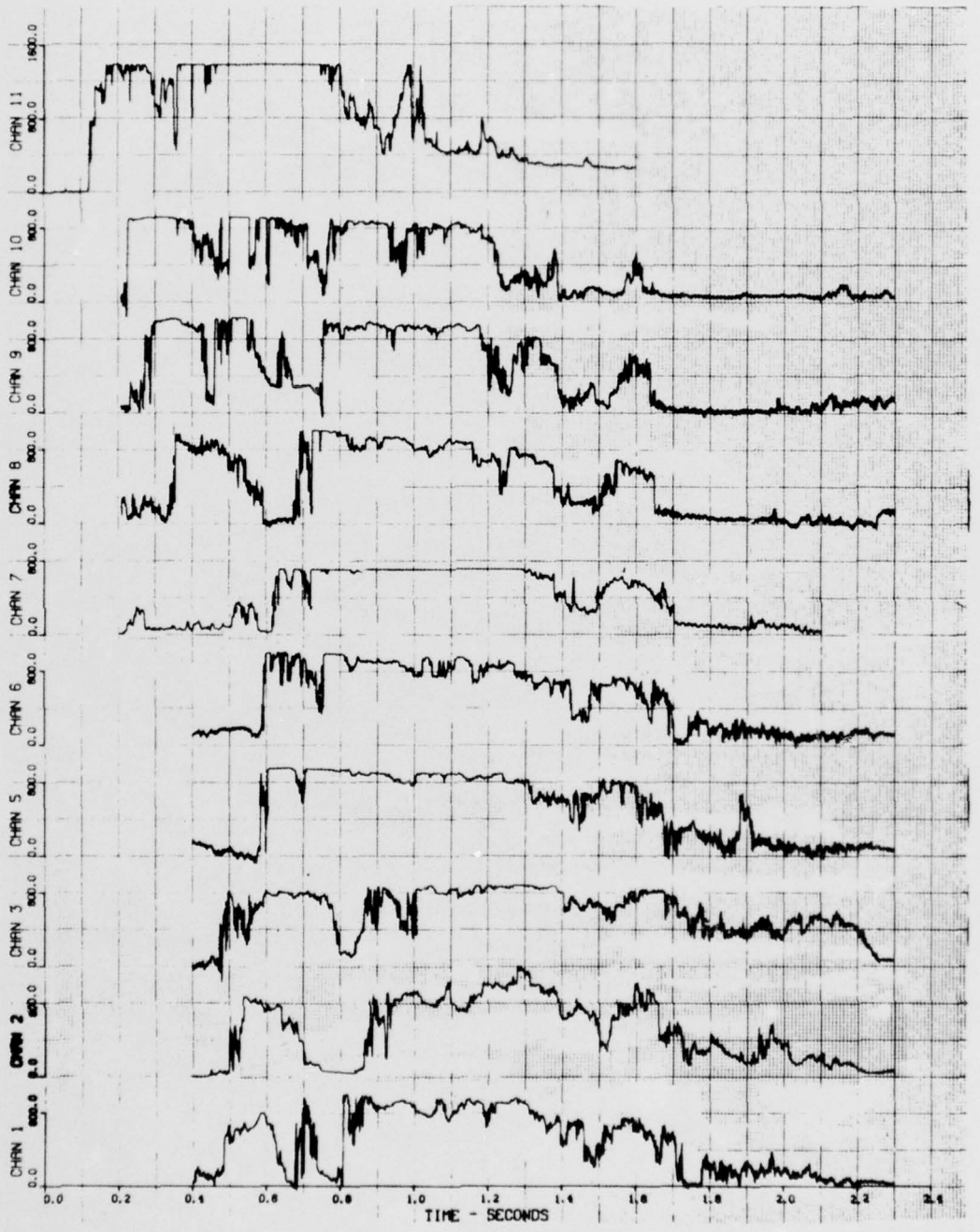

Figure 17b. Digitized Fireball Temperature Data: MB-4
(t_{FIDU} = -1.3 sec)

present temperature history data and in spite of the signal overrange difficulties already discussed in Section 3.2, a relatively consistent model for the GEST fireball does indeed become apparent. To a first approximation the noted data illustrate that the early time rising fireball is characterized by a highly intermittent irregular fireball top or cap, a relatively constant, high temperature core and a thermal wake exhibiting (approximately) a linear decay in mean temperature. Not only are temperature fluctuations near the fireball "top" and "bottom" of the same order as the mean temperature, but these fluctuations, as well as temperatures and temperature gradients, are all higher at the leading edge of the fireball compared to corresponding values at the trailing edge. Note. for example, the rather "sudden" growth in temperature/intensity at the top of the fireball as compared to the gradual decay at the bottom. Leading edges of "hot" eddies and the fireball core are, in general, characterized by steep temperature gradients relative to trailing edges which contain relatively shallow gradients. Hot fluid motion at the fireball top consists of large scale structure in combination with random pockets of intense turbulent activity. The presence of ambient air eddies (pockets) embedded/entrained within the fireball flow field is evident in the time trace data of Figure 17, a finding consistent with results from the GEST photographic coverage. This first order thermal "picture" of a rising fireball agrees favorably with available laboratory data for buoyant thermals (Refs. 2 and 3), as well as with fireball radar models which consider the fireball top to be "hard shelled" (capped) relative to the fireball base. The existence of such a cap, where substantial temperature (electron densities) fluctuations are present, plays a significant role when computing signal transmission and/or radar backscatter for the full-scale nuclear fireball.

3.5 Time Averaged Mean and RMS Temperature Data

Summarized results for mean and RMS temperature data for MB-3 and MB-4 are presented in Figures 18a and 18b, respectively. The core and wake data shown represent reduced results as validated for only those channels/times where flow turbulence is established (i.e., non-intermittent) and where signal saturation difficulties are not present. Only limited data are presented for fireball top conditions since such measured data are highly irregular and intermittent. All data have been shifted in time such that core leading edges are aligned with the core leading edge for Channel 1. This time adjustment corresponds to the assumption that spatial changes in fireball characteristics occur "slowly" relative to the fireball rise velocity. For the data of Figures 18a and 18b, averaging interval times of .2 sec and .05 sec were used for the core/wake and top, respectively. All data, as shown, are plotted as a function of mid-interval times. The noted time intervals were chosen after a study was completed showing that such times were sufficient to provide approximate invariance of averaged temperature data with interval size. Processing of random non-stationary data requires that such an analysis be carried out to minimize the effects of data processing procedure on reduced results. This becomes particularly important when evaluating spectra, correlations and probability distribution functions from measured turbulence data. Completion of this optimum interval study made it possible to proceed with ensemble averaging and trend removal operations on the present temperature data.

Examination of the results of Figures 17a and 17b provides further confirmation that the GEST fireballs do indeed exhibit consistent and reproducible behavior. From the mean temperature data in particular, it becomes apparent that the approximate locations for the fireball

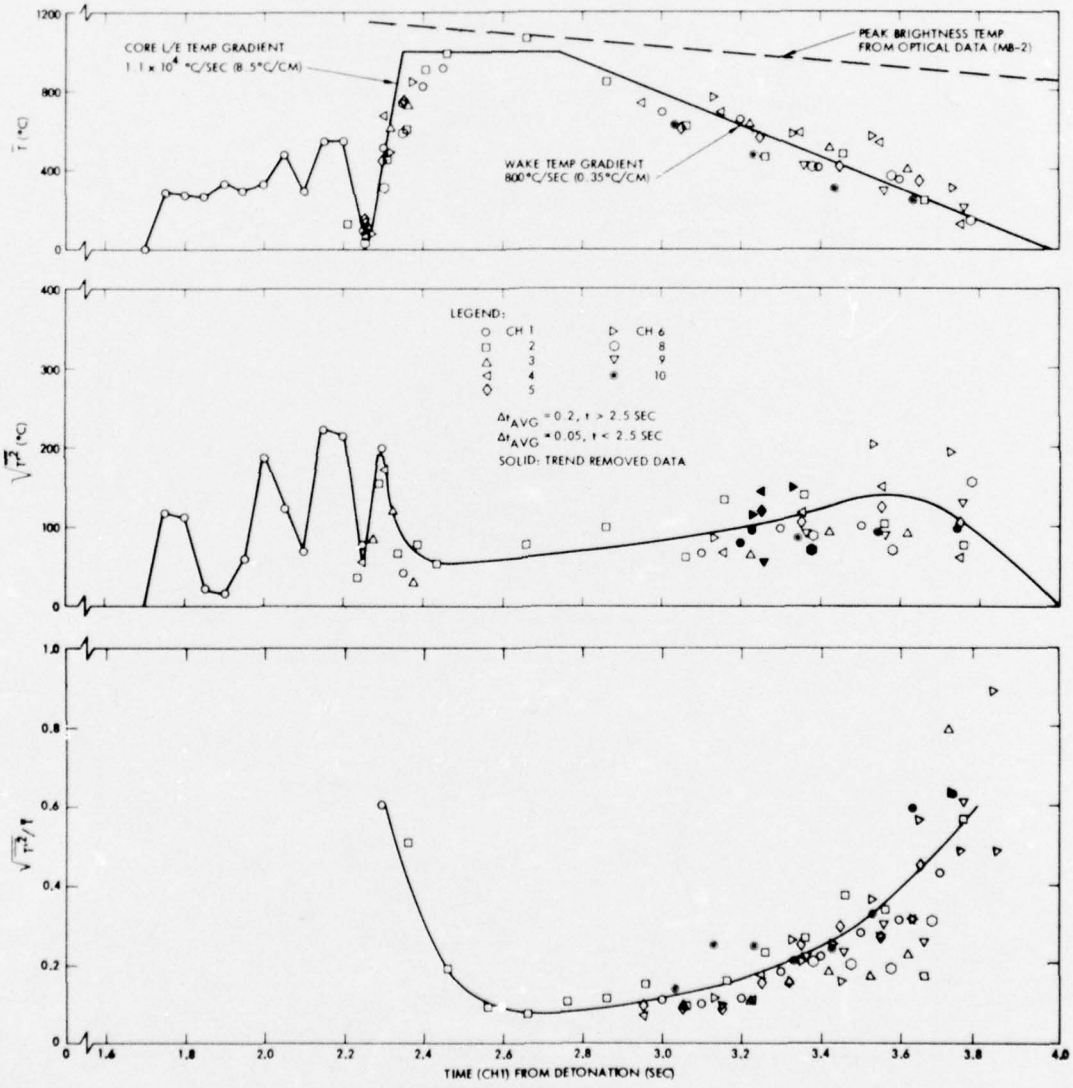

Figure 18a. Time Averaged Temperature Data: MB-3

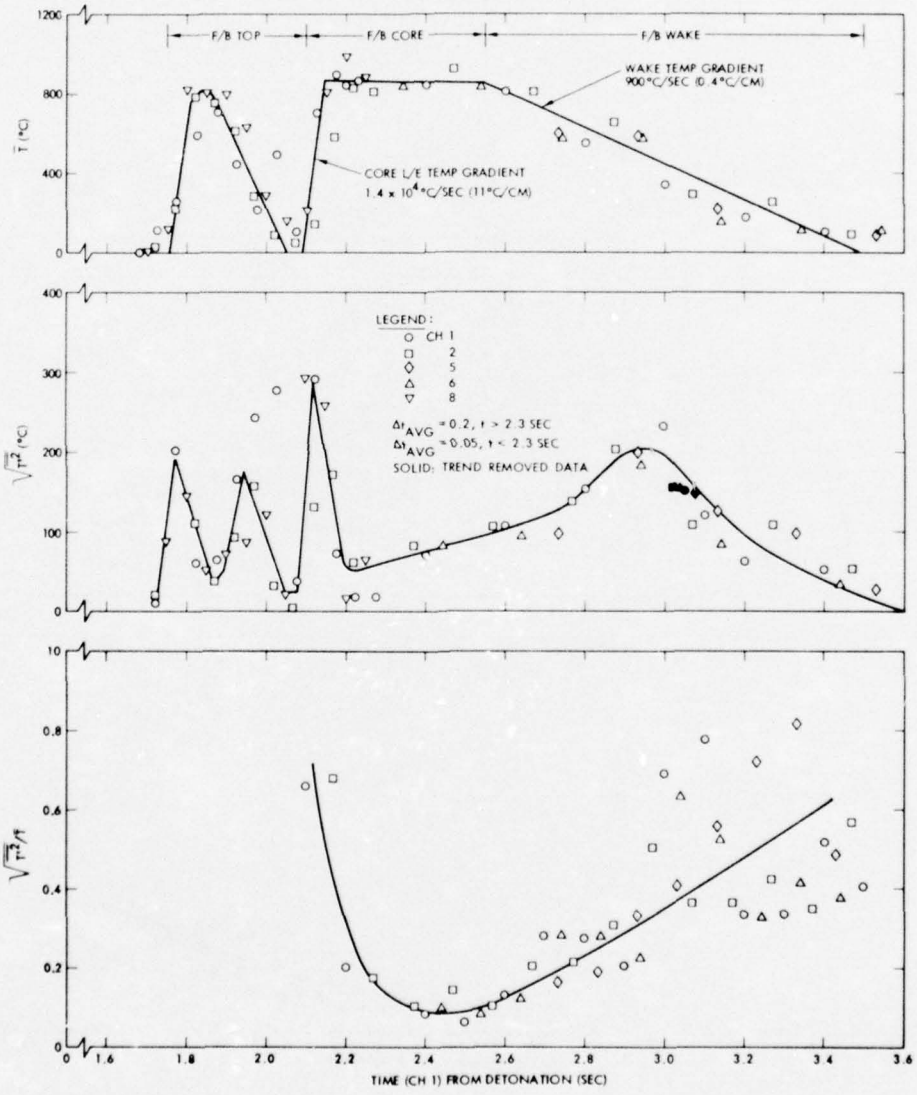

Figure 18b. Time Averaged Temperature Data: MB-4

top, core and wake can be clearly designated. The peak brightness temperature data from optical measurements for MB-2 (Ref. 6) are also shown on Figure 17a and favorable comparison is evident. Since the detonation yields for MB-2 and MB-3 were similar ($\cong$ 3.00 Joules), the noted agreement provides a consistency check between two separate experiments. In addition, such a field test comparison substantiates the temperature measurement accuracy of the IR scanning technique and further justifies its use in measuring peak temperature data on other large scale detonation events. Some decrease in temperature is evident between events MB-3 and MB-4 and this result is consistent with the fact that the detonation yield for MB-4 was about 10% lower than the yield for MB-3 (Table 1). Trailing edge mean temperature gradients for both events are approximately .4°C/cm whereas core leading edge gradients are 8.5°C/cm and 11°C/cm for MB-3 and MB-4, respectively. These mean gradient results contrast with instantaneous gradient data which were measured to be as high as 300°C/cm. Although MB-3 leading edge gradients are low relative to HULL code predictions (11°C/cm, Ref. 6), the MB-4 data are seen to compare favorably. Predicted temperatures for HULL code calculations (Ref. 6), on the other hand, compare poorly with the present temperature data in terms of maximum temperature (2000°C) and trailing edge gradients ($\cong$ 3°C/cm). Although these differences may be partially explained by substantial temperature attenuation due to turbulent mixing as well as the dependence of temperature data on the relative location of the probe strut within the fireball perimeter ($R_{STRUT} \cong R_{FB}/2$), this question will require additional study before a satisfactory explanation is available. As shown by the normalized intensity data in Figure 17, the RMS temperature intensities for the fireball wake are large and become comparable to mean temperature levels whereas core intensities are relatively small. Apparently for these early fireball times, penetration of entrained ambient air into the fireball core region was limited

as compared to the substantial mixing experienced by the fireball wake. Additional review of the temperature time trace histories is consistent with this viewpoint.

3.6 Turbulent Structure Statistics

Statistical processing of the MB-3 and MB-4 temperatures was performed herein on selected segments of instantaneous temperature data as well as on validated wake data which had been redigitized into the locally stationary form (Ref. 12). These latter "adjusted" data were obtained by subtracting the linear decay trend for mean temperature (Figures 17a and 17b) from the instantaneous ("raw") temperature data. Typical results from this processing procedure are shown in Figures 19a and 19b and the assumption of a constant mean temperature over the noted time segments is seen to be a reasonable approximation. Based on these "trend removed" data, the sections which follow present such computed statistics as auto and cross correlations, histograms (pdf), skewness and flatness factors and power spectra densities (psd). Integral length scales, as well as eddy lifetimes based on moving frame autocorrelation results, are also presented. Although these locally stationary data were computed from TRW's turbulent statistics program, some "raw" temperature results, also shown in the following sections for comparison purposes, were calculated both by the time series program as well as by the temperature conversion program (Section 2.3.2).

3.6.1 Space/Time Correlation Measurements. Figure 20 summarizes spatial correlation data as measured by vertically aligned probes for the MB-3 and MB-4 events. The noted data, which show the variation of the zero time-delay cross-correlation coefficient

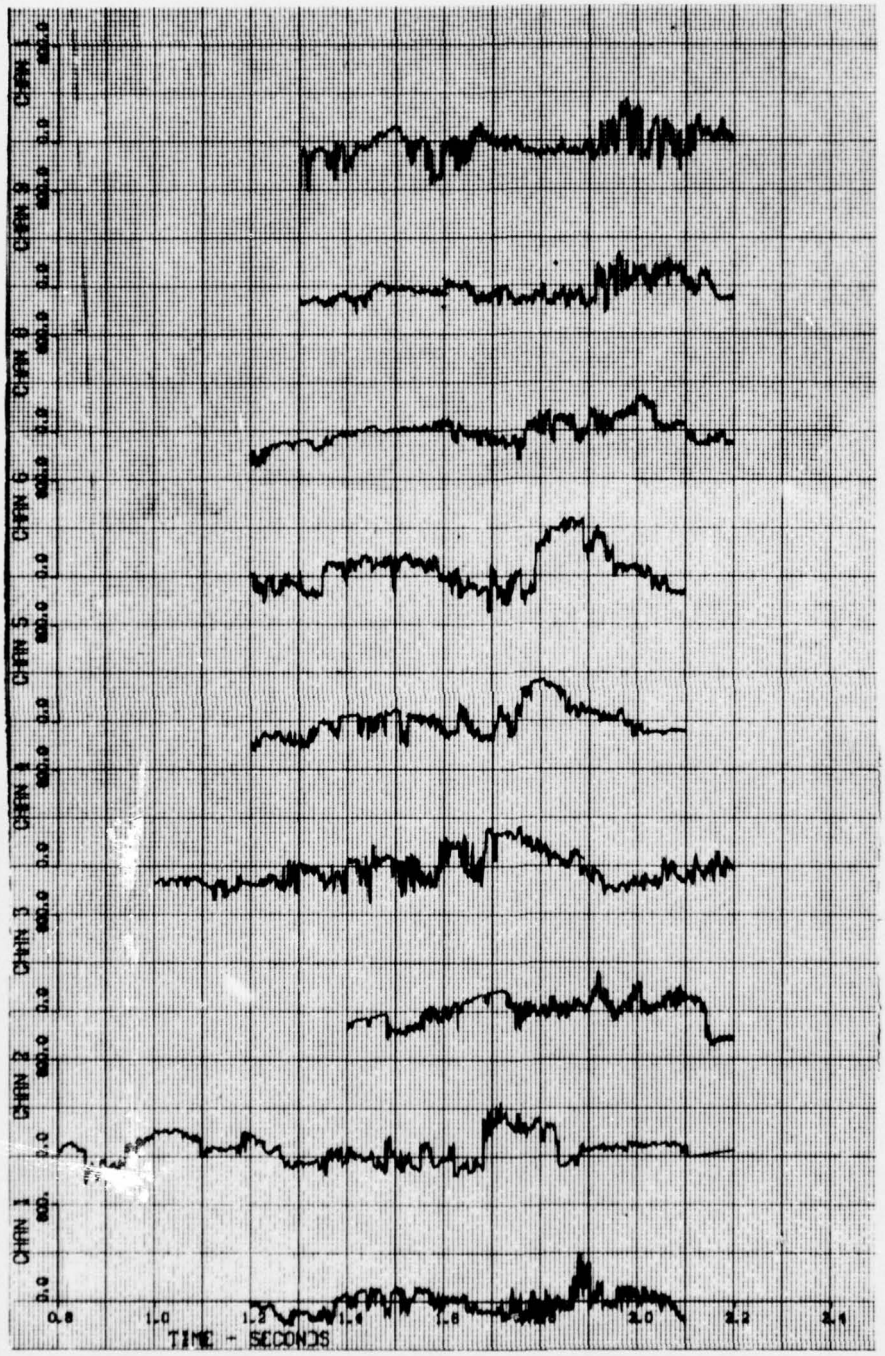

Figure 19a. "Trend Removed" Temperature Data: MB-3 (t_{FIDU} = -1.7 sec)

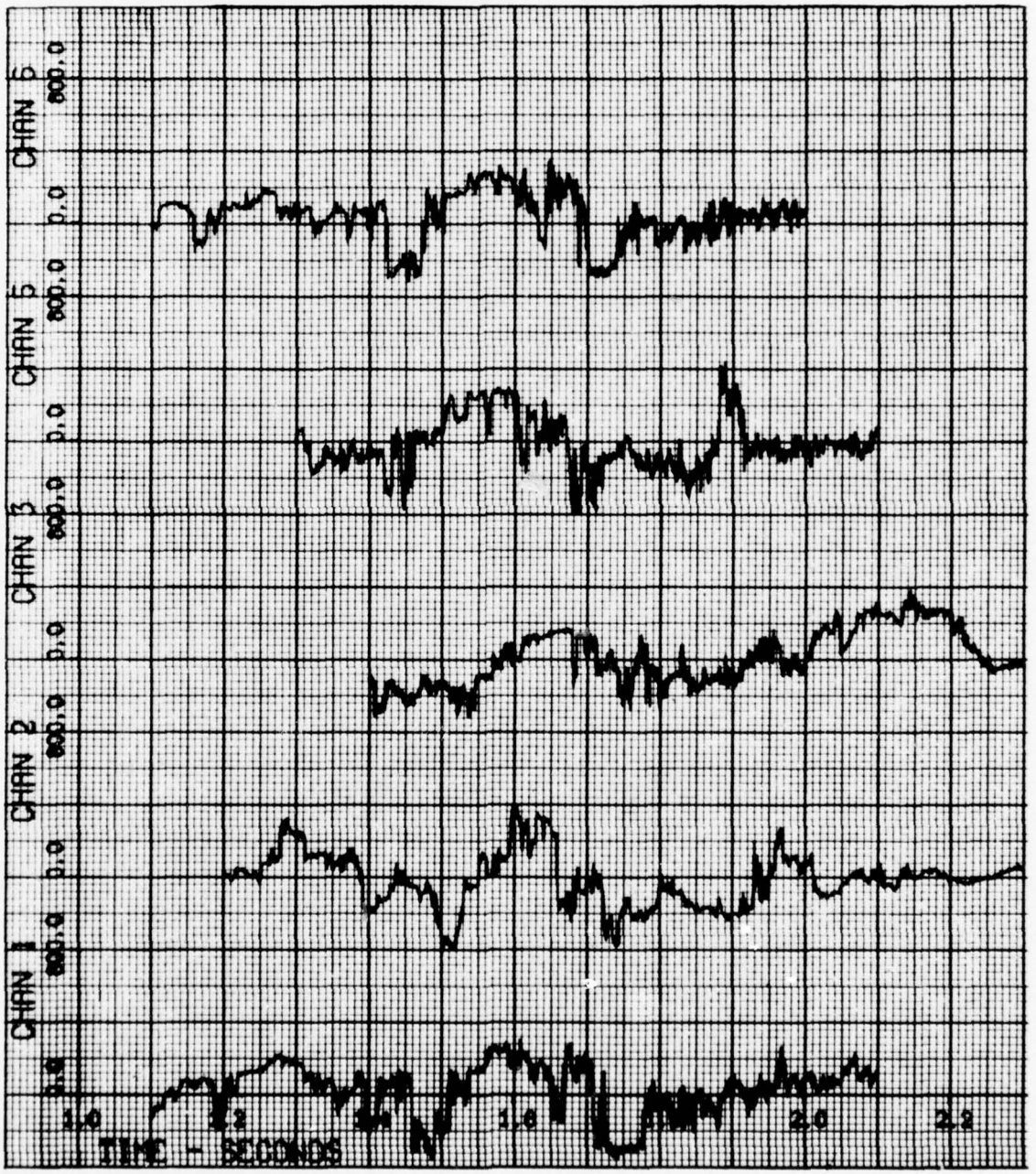

Figure 19b. "Trend Removed" Temperature Data: MB-4 (t_{FIDU} = -1.3 sec)

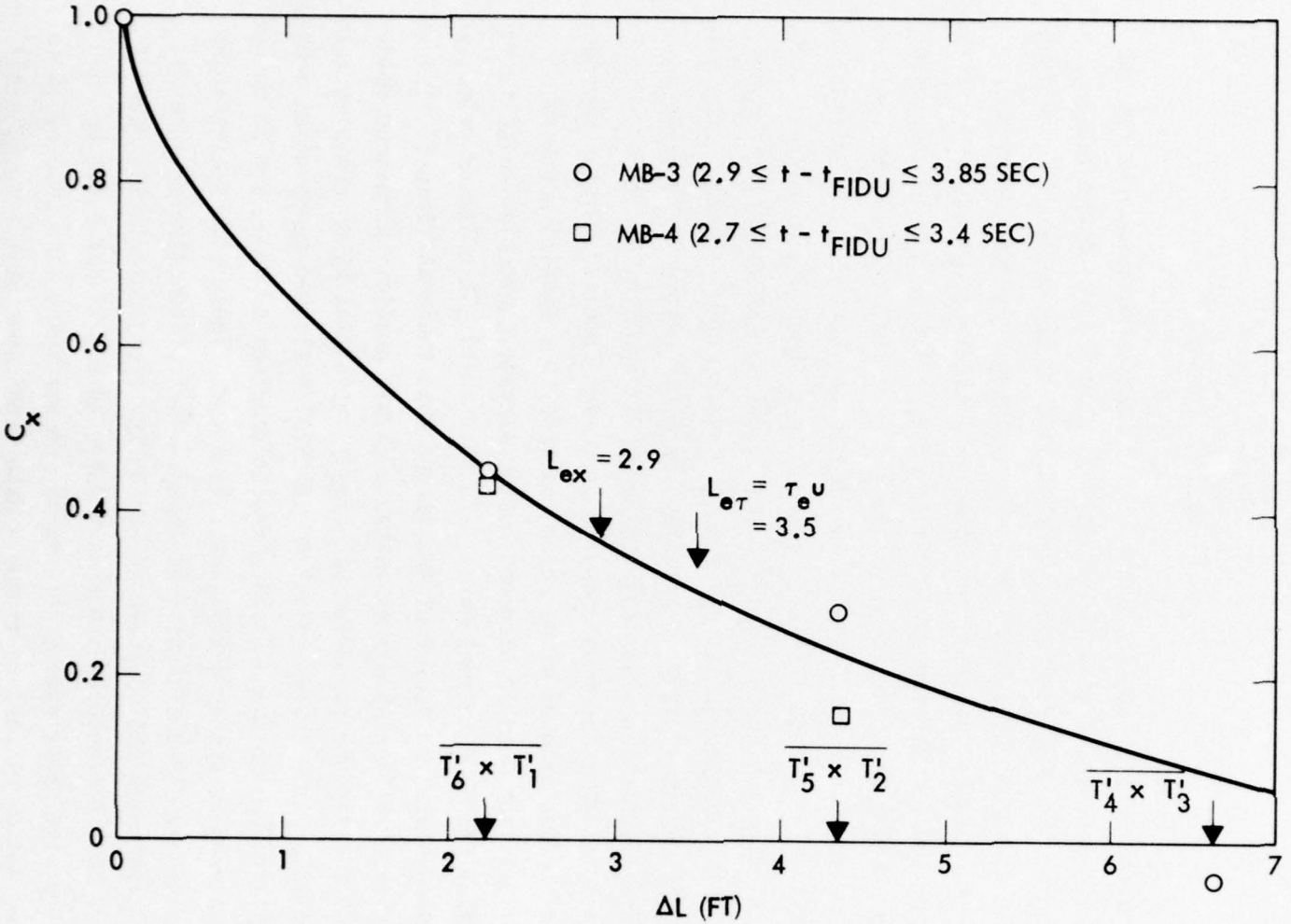

Figure 20. Temperature Cross-Correlation Coefficient as a Function of Vertical Probe Separation

$$c_{xT} = \frac{\overline{T'(o,t)\ T'(\Delta x,t)}}{[T'(o,t)^2\ T'(\Delta x,t)^2]^{1/2}} \qquad (6)$$

with probe separation, represent primary measurement results for the present temperature measurements task. From Figure 20 the integral scale for the GEST fireballs is seen to be of the order of three feet (L_{ex} = 2.9 $\pm$ .5 feet) based on an "e" folding distance definition. Since turbulence investigators often estimate integral scales by transforming the "e" folding autocorrelation time scale to a length scale through the local convection velocity ($L_{e\tau} = \tau u$), this length scale is also noted on Figure 20 and it is seen to be about 20% larger than the spatial scale. Such a result is consistent, however, with other turbulent flows which are similarly "non-frozen" and where Taylor's hypothesis is expected to be only a rough approximation at best. The autocorrelation times used in this time scale calculation were based on averaging autocorrelation data (Figures 21a and 21b) for eight channels on MB-3 and five channels on MB-4. Combined results provide a correlation time of 41 ms which converts to a spatial scale of L_{ex} = 3.5 feet when transformed by the average convection velocity for the MB-3 and MB-4 thermal wakes, u $\cong$ 85 ft/sec. This latter velocity is approximately a factor of two larger than the mean fireball rise velocity. (Hill's spherical vortex analysis predicts a maximum velocity 2.5 times the mean rise velocity.) Note that by determining autocorrelation time scales only from vertically aligned temperature probes (Ch 6 and Ch 1; Ch 5 and Ch 2) correlation times of 48 ms and 33 ms for MB-3 and MB-4, respectively, are calculated. These time scales transform into length scales of 4.05 and 2.8 feet, respectively, a result consistent with the observed spread in the cross-correlation data of Figure 20. All results shown in Figures 20 and 21 are based on the locally stationary data of Figure 19, an averaging time span of .6 to .7 sec and correspond to fireball wake conditions at t - t_{FIDU} = 3.2

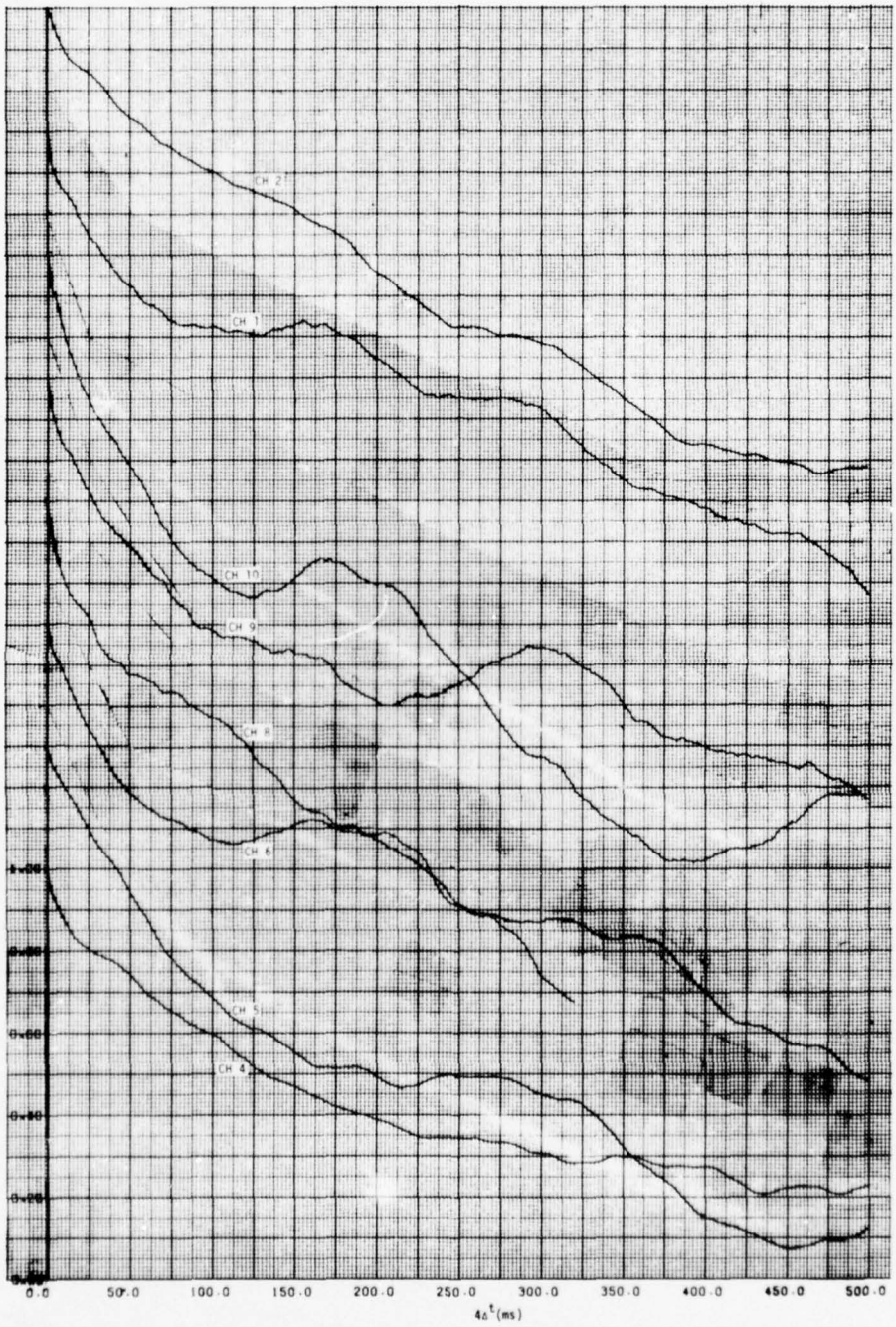

Figure 21a. Temperature Autocorrelation Coefficient: MB-3 (t_1/t_2; CH 1, 2, 4, 5, 6, 8, 9, 10: 2.9/3.5, 2.9/3.5, 2.9/3.5, 2.9/3.5, 2.9/3.5, 3.2/3.6, 3.0/3.6, 3.0/3.6 sec).

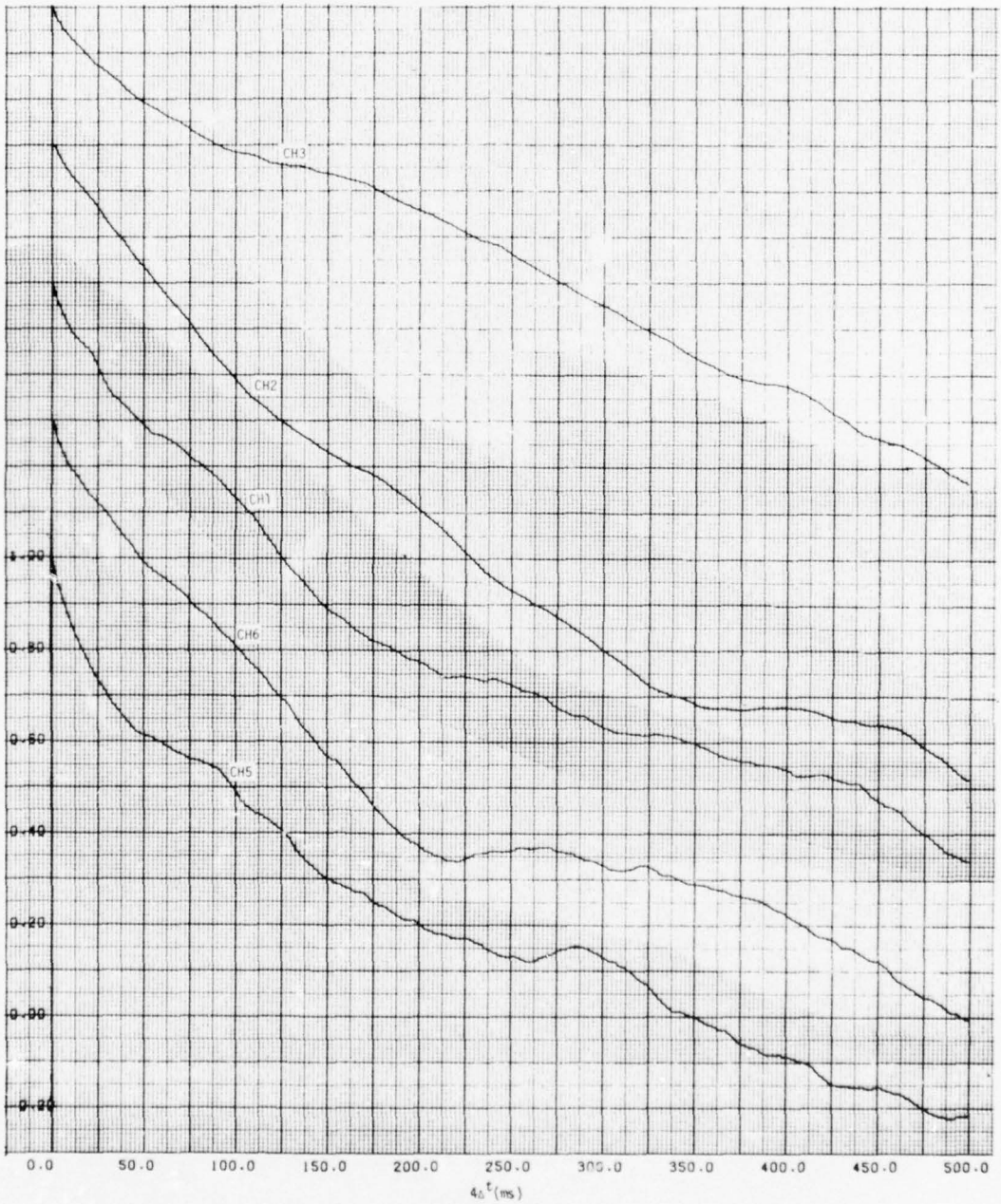

Figure 21b. Temperature Autocorrelation Coefficient: MB-4 (t_1/t_2; CH 1, 2, 3, 5, 6: 2.7/3.4, 2.7/3.4, 2.7/3.45, 2.7/3.4, 2.7/3.3 sec).

and 3.0 sec for MB-3 and MB-4, respectively. Probe separation distances are also shown on Figure 20 and illustrate that the data as measured amply span the required scale dimensions, a result which substantiates the probe strut design as used for the GEST fireballs. Using the fireball radius data of Reference 6, a normalized integral scale of

$$\left(\frac{L_{ex}}{R_{FB}} \cong .054\right)$$

is calculated (Figure 22). This result compares favorably with integral scale data deduced from processing of optical data for a full scale nuclear fireball. In addition to summarized velocity and temperature results, Figure 22b also presents normalized scale data for MB-4 Channel 2 based on measured autocorrelation times and mean velocity data. Again, the transformed time scale, although, comparable, is seen to be somewhat larger than the measured spatial scale. It is believed that the current scale data represent the first such large scale fireball measurements obtained to date through the use of in-situ instrumentation. Since investigators applying turbulence modeling techniques to treatment of large scale fireballs (buoyant thermals) require normalized scale data, the present measurements may provide important inputs to aid in satisfactory code development work.

Moving frame autocorrelation results for MB-3 and MB-4 are shown in Figure 23. These data typically provide a measure of eddy lifetime for a given turbulent flow. This time scale ($\overline{\tau}_e = .17 \pm .04$ sec) quantifies the decay (breakdown) behavior of the large eddies and thus represents a characteristic input to fireball dispersion and chemistry calculations. The ratio of moving frame to autocorrelation time scales ($\cong 4$) is comparable to results corresponding to data for other

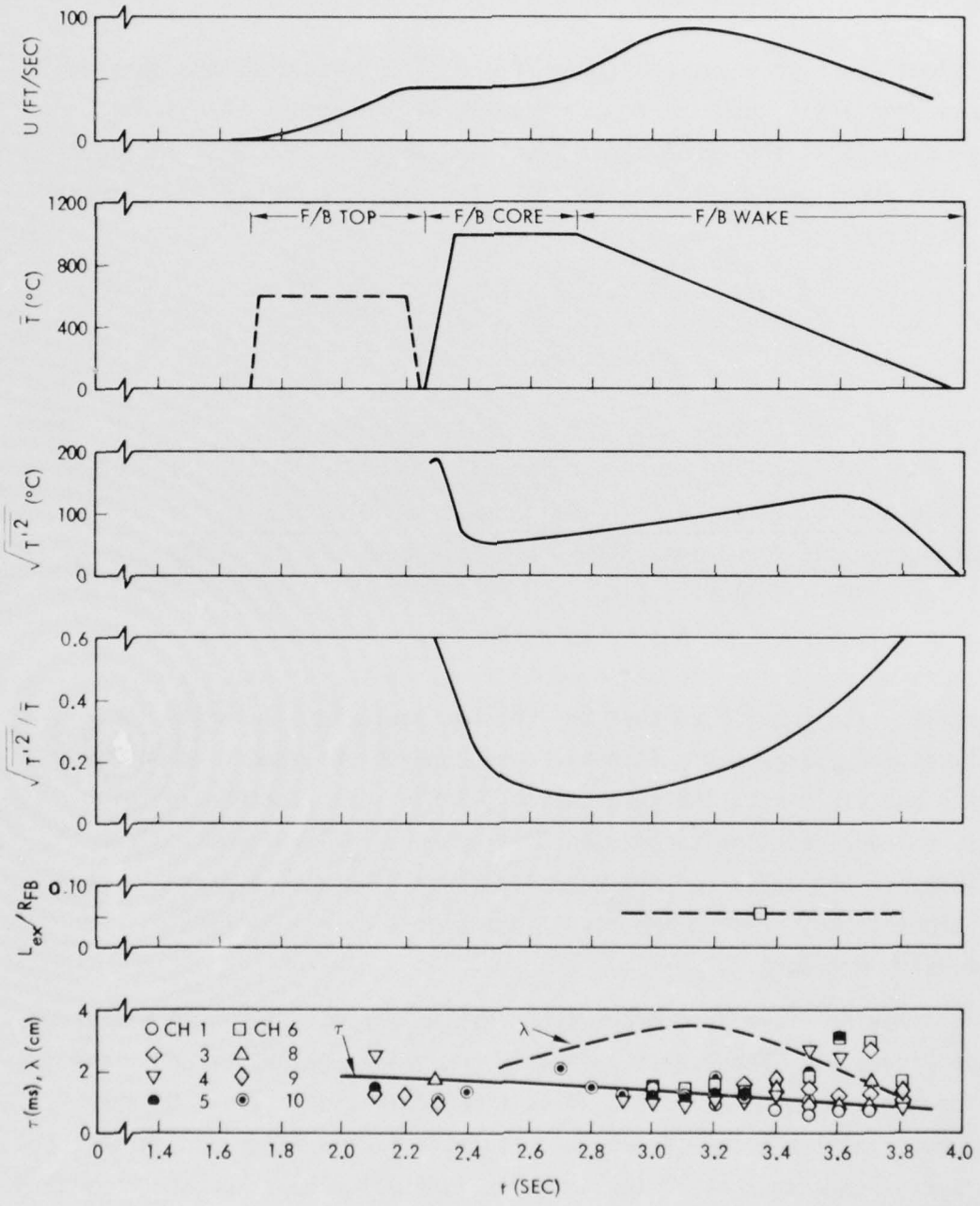

Figure 22a. Summarized Fireball Data: MB-3

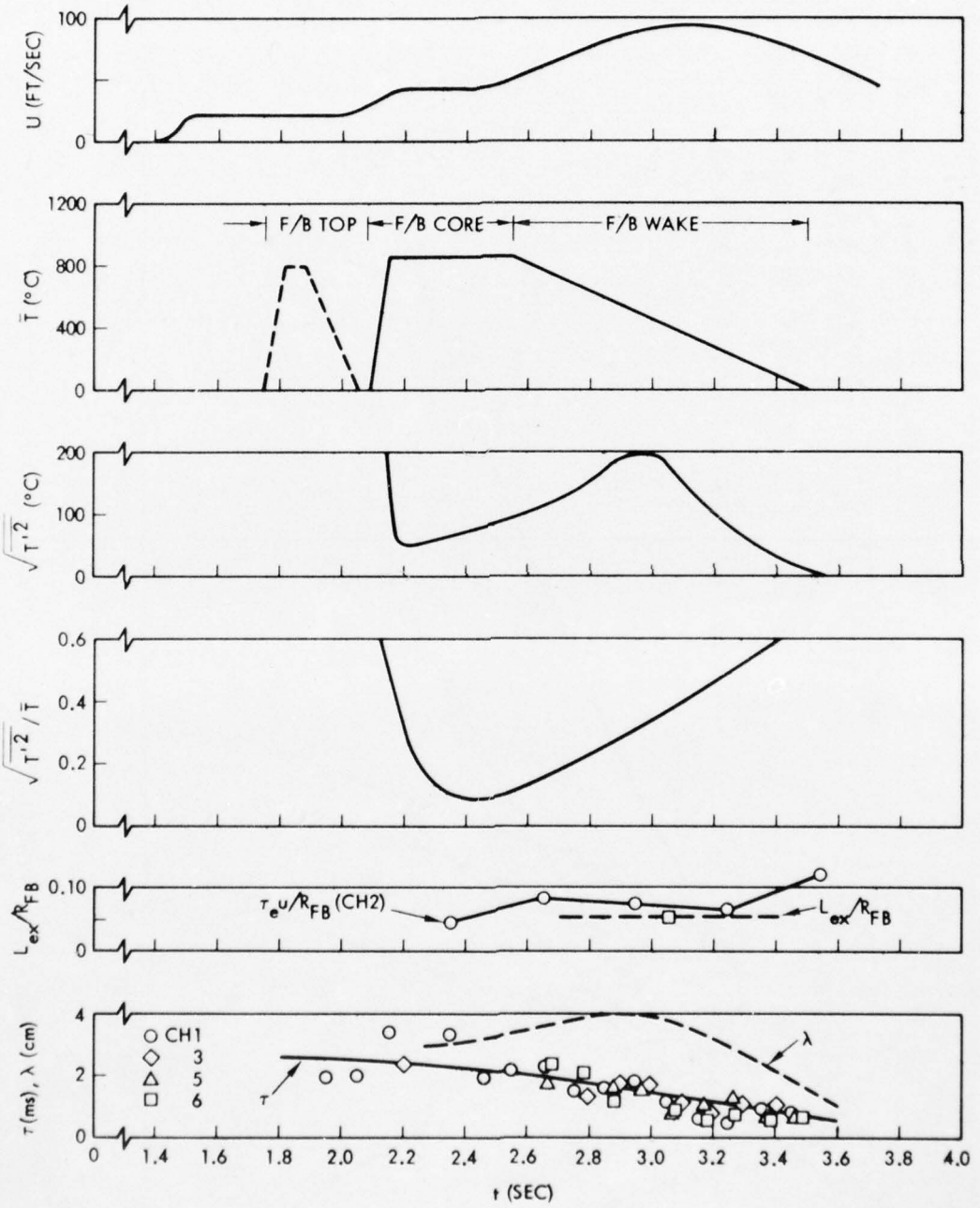

Figure 22b. Summarized Fireball Data: MB-4

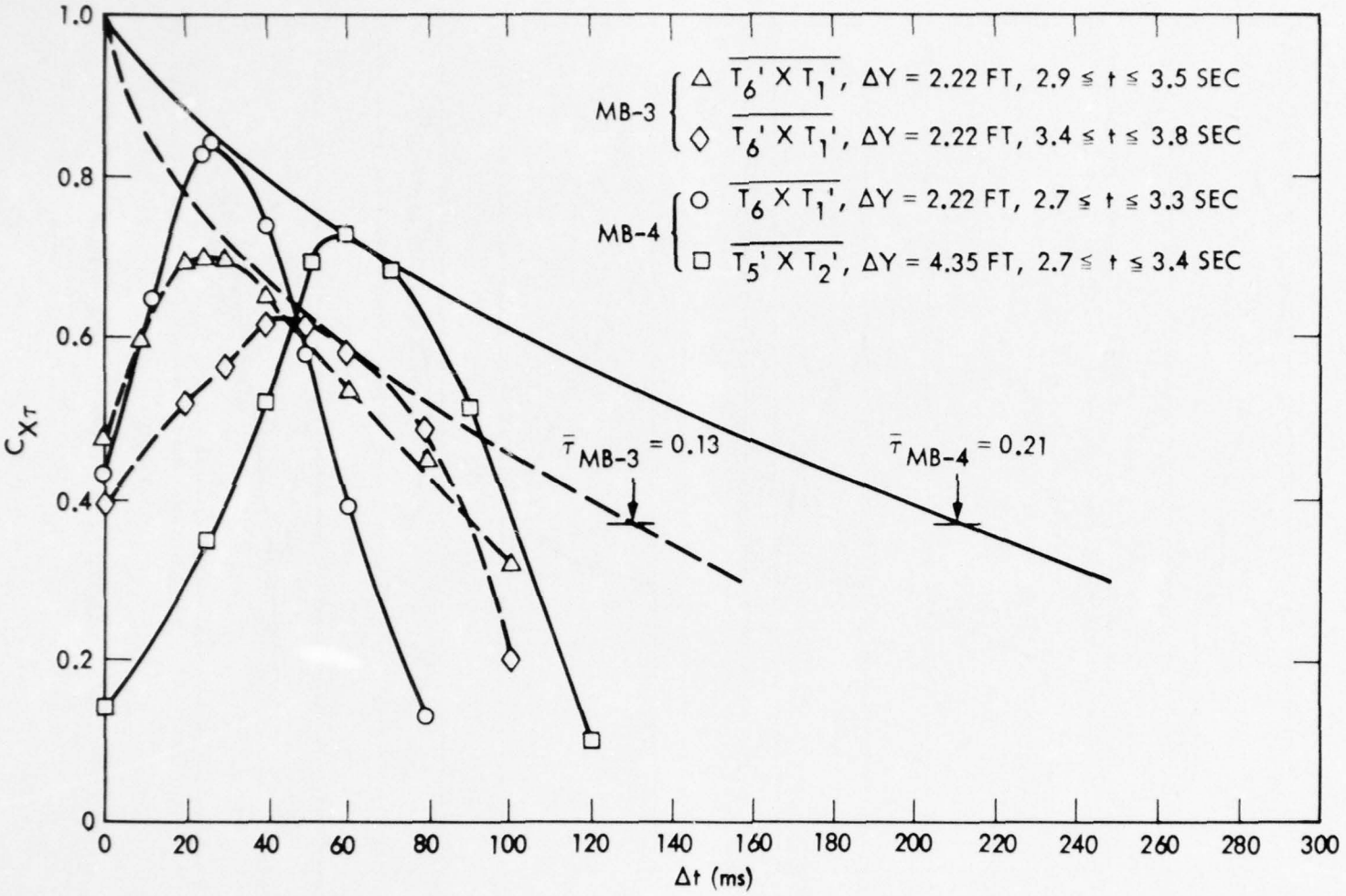

Figure 23. Moving Frame Autocorrelation Coefficient for Temperature Data ($2.7 \leq t \leq 3.4$ sec)

turbulent flows (2 to 5). This result suggests that the intensities and gradients associated with the fireball eddy structure exhibit a highly persistent nature, a finding which supports those radar models which postulate relatively slow "smearing" of early time electron density gradients.

3.6.2 Probability Density Distributions. Figures 24a and 24b show summarized histogram results for MB-3 and MB-4 using the locally stationary temperature data presented in Figure 19. The noted probability density distributions (pdf) are seen to be "spiky" in nature with some evidence of bimodel behavior. Ensembled averaged skewness ($\sigma_3 = \overline{T'^3}/\sqrt{\overline{T'^2}}^3$) and flatness ($\sigma_4 = \overline{T'^4}/(\overline{T'^2})^2$ factors for MB-3 and MB-4 were +.1805/2.677 and +.0308/2.697, respectively. Note that for a Gaussian pdf the skewness is zero and the flatness factor is three. Although the σ_3 and σ_4 data indicated on Figures 24a and 24b were all determined from use of TRW's turbulent statistics program (GEST-TS), results computed from the temperature conversion program (GEST-T) for core and wake conditions and using data uncorrected for the trend in mean temperature were comparable both in magnitude and in variations between channels. In general, the histogram data of Figure 24 are seen to be skewed to the negative side of their normalized values. These non-Gaussian histograms are representative of the extent to which the GEST fireballs approximate a homogeneous turbulent temperature field and thus provide a means to evaluate inherent uncertainties introduced by assuming a Gaussian probability density distribution in the fluid mechanical and/or chemical model for a turbulent fireball.

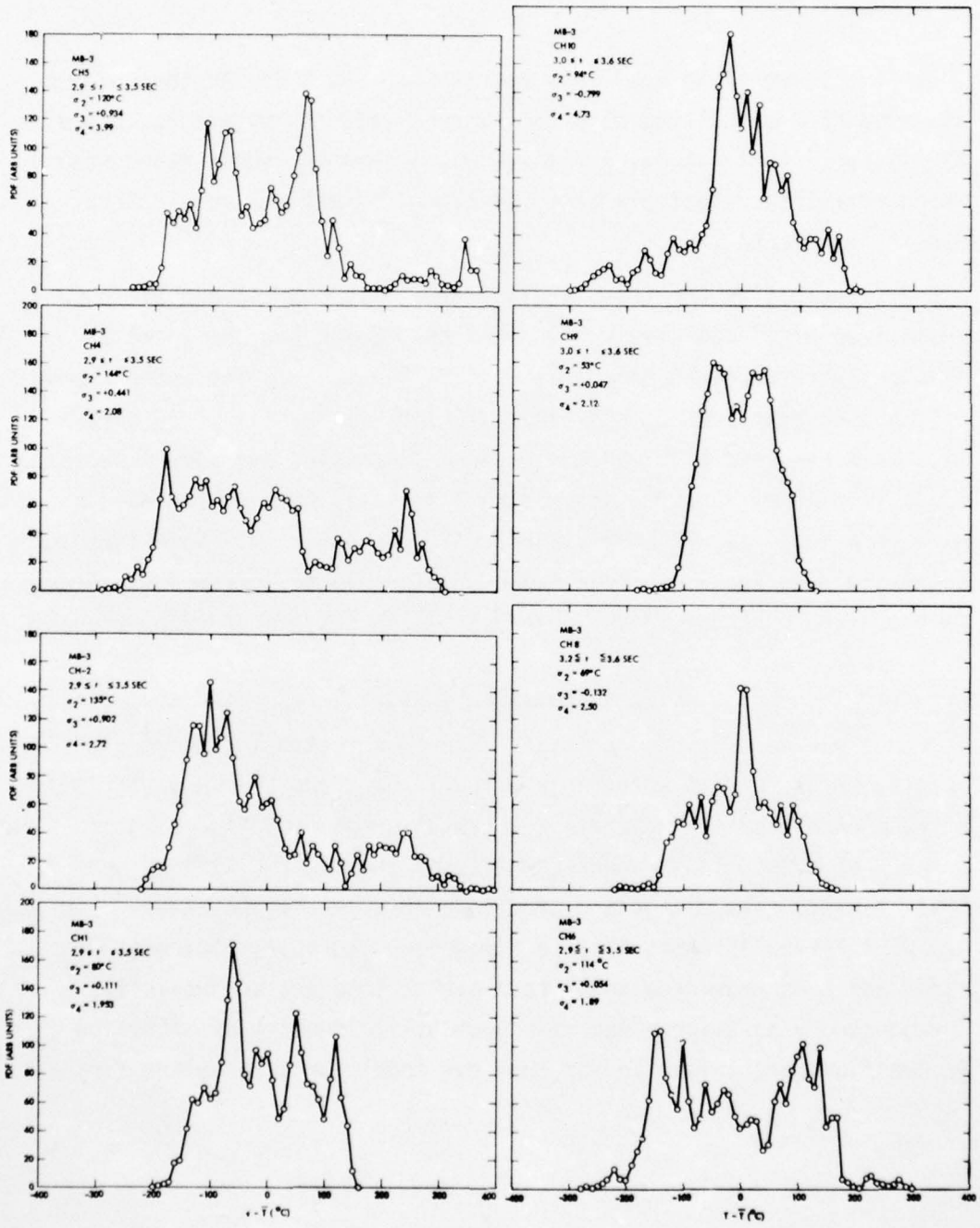

Figure 24a. Probability Density Distributions for Temperature Fluctuations: MB-3

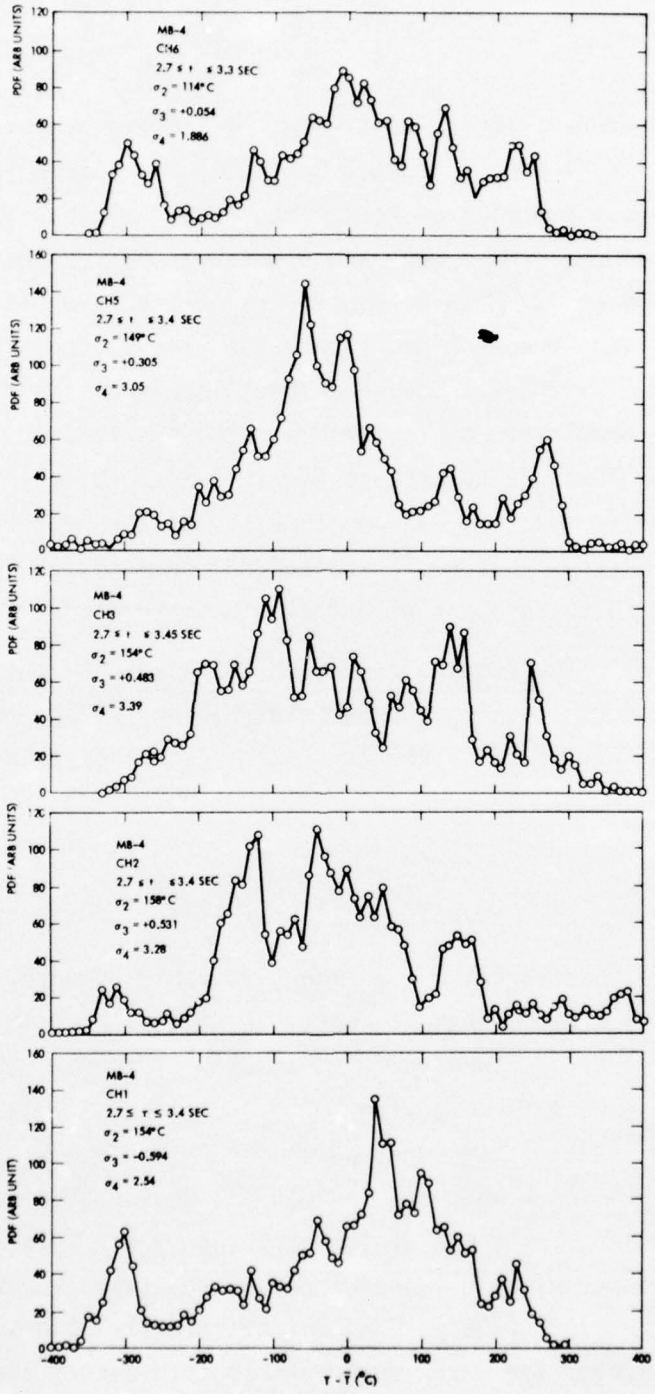

Figure 24b. Probability Density Distributions for Temperature Fluctuations: MB-4

3.6.3 Temperature Spectra. A summary of temperature spectra data for events MB-3 and MB-4 is presented in Figure 25. The data, as shown, are plotted as a function of normalized frequency, $n\tau$, where n corresponds to frequency and τ represents the measured autocorrelation time for a given channel. Also presented, as co-abscissa, is the normalized wavenumber given by $kL = 2\pi n\tau$. Since the wavenumber is typically defined by $k = 2\pi n/u$, the integral length scale L is approximated in the present formulation by Taylor's hypothesis, i.e., $L = u\tau$. In Section 3.6.1 Taylor's hypothesis was evaluated for the GEST fireballs and it was shown that spatial and time scales compared to within 20%. The data of Figures 25a and 25b correspond to fireball "wake" results as digitized (4000 cps) and with the mean temperature "trend" removed.

In general, the results of Figure 25 illustrate that the GEST temperature spectra follow approximately a $(n\tau)^{-5/3}$ falloff behavior. Shown also on Figure 25 is the familiar spectral distribution curve given by

$$\frac{E(n)}{E(o)} = \frac{1}{1 + (2\pi)^2(n\tau)^2}$$

Although this theoretical curve often favorably compares with spectra data for small scale turbulent flows, it is seen here to fall off $[(n\tau)^{-2}]$ more rapidly than measured results. The favorable comparison of the present spectra data with Kolmogoroff's -5/3's law, which holds for several decades of spectral power, is consistent with the large turbulence Reynolds number for the GEST fireballs (see Section 3.6.4 which follows) and with the homogeneous nature for those high frequency eddies associated with fully developed, large scale turbulent flows. The present result, illustrating that the inertial subrange $[(n\tau)^{-5/3}]$ "spread" is larger for large scale atmospheric events than that

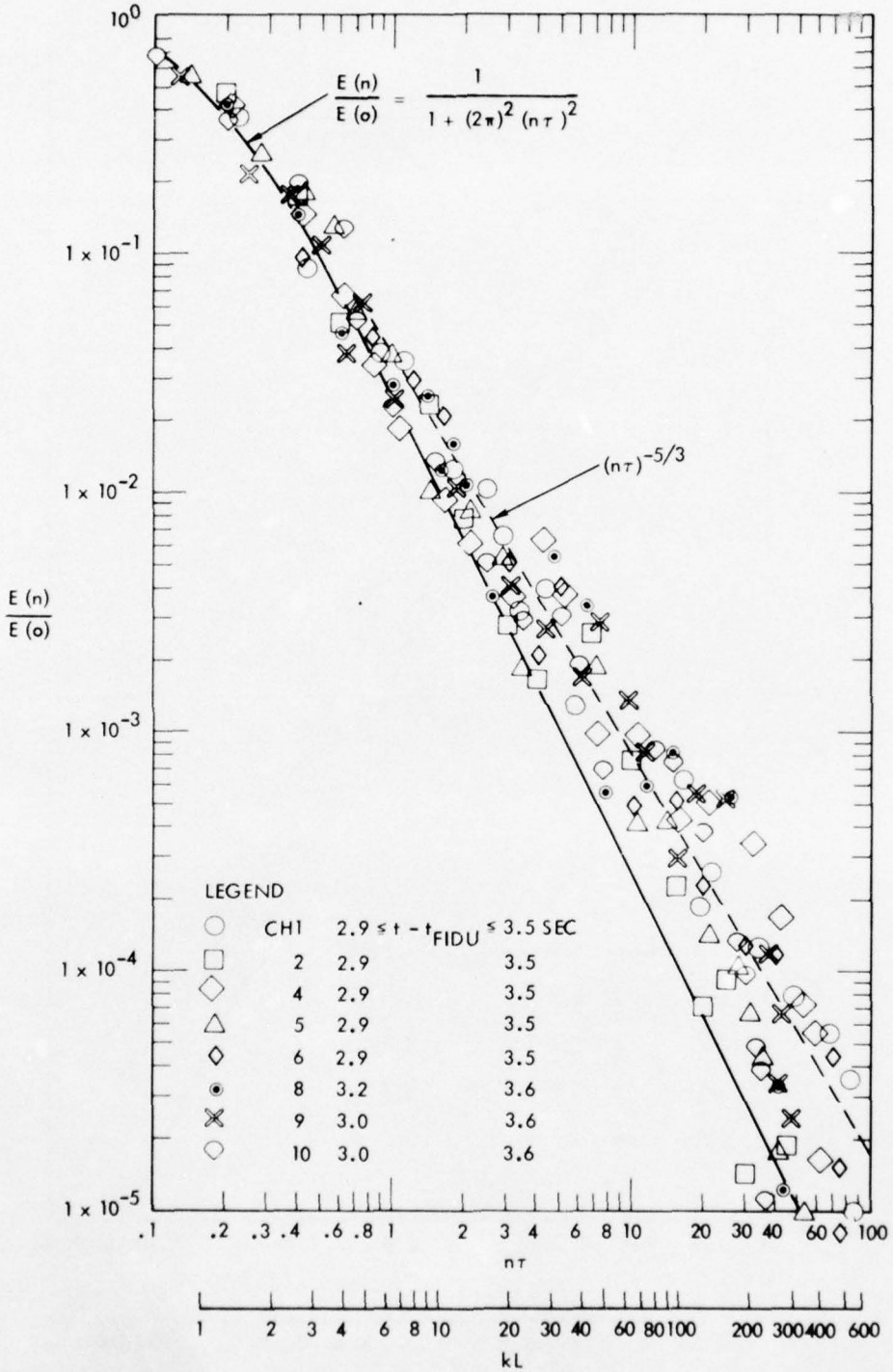

Figure 25a. Normalized Power Spectra for Temperature Fluctuations: MB-3 Wake

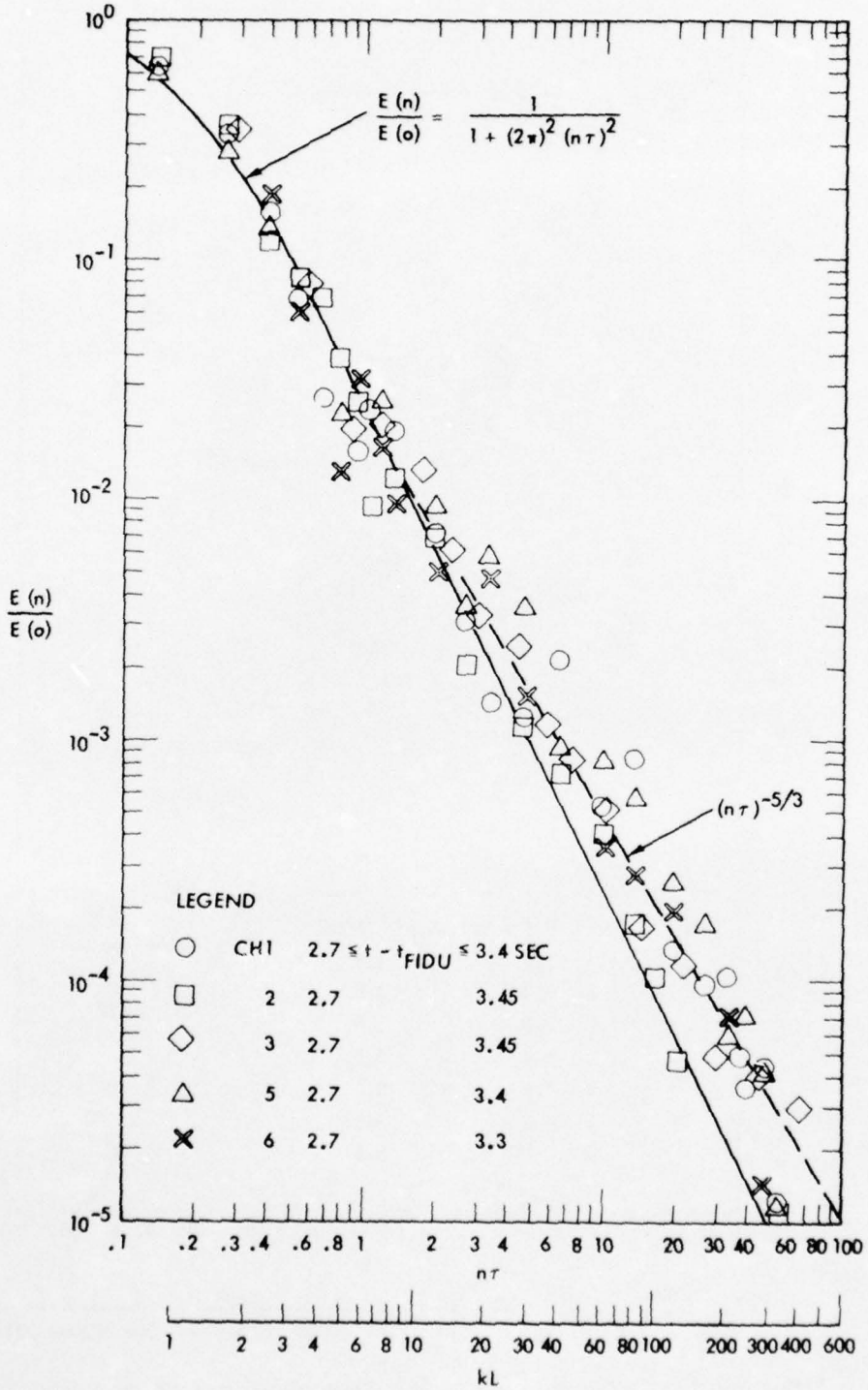

Figure 25b. Normalized Power Spectra for Temperature Fluctuations: MB-4 Wake

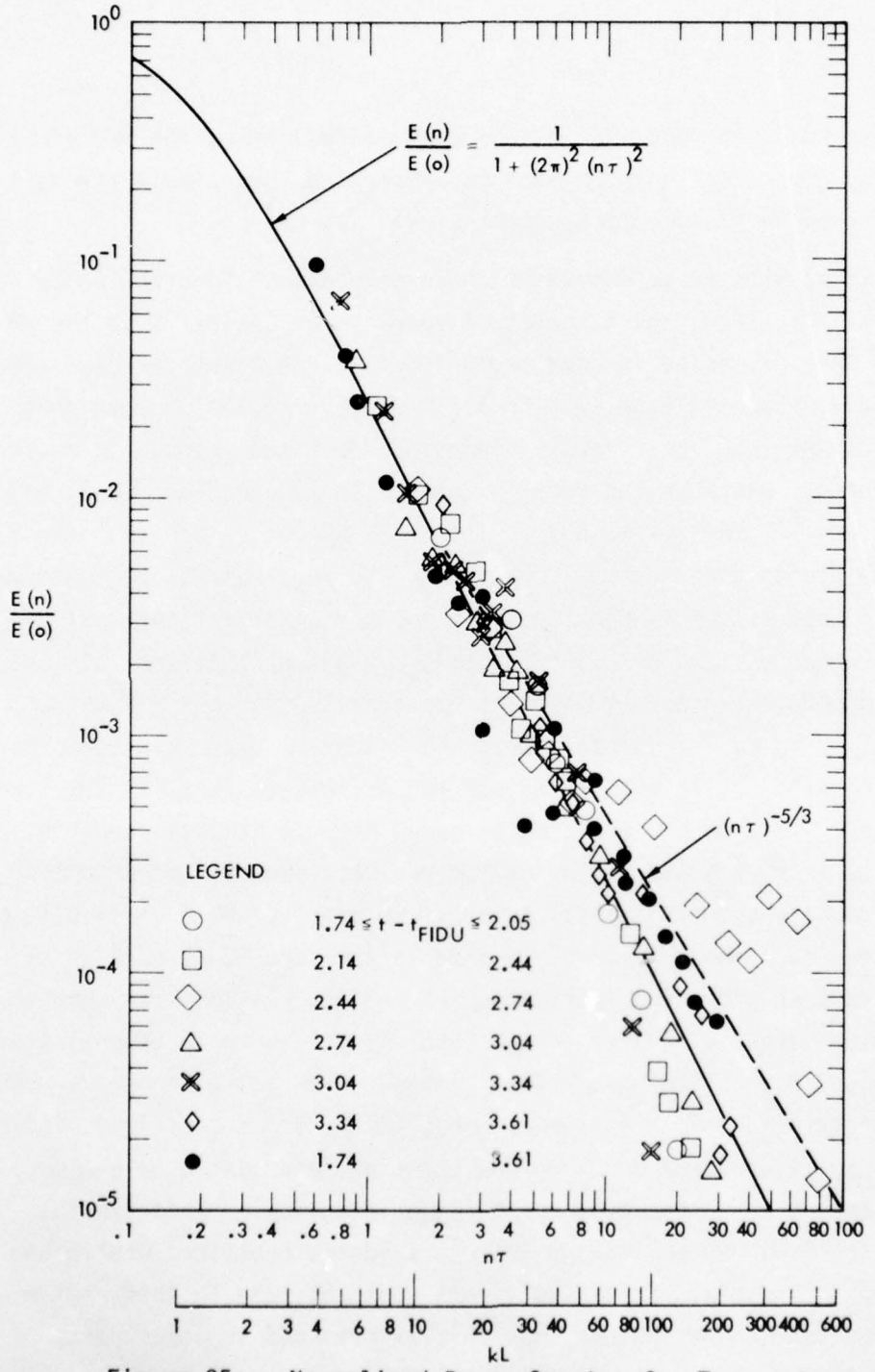

Figure 25c. Normalized Power Spectra for Temperature Fluctuations: MB-4 (Channel 2)

corresponding to small scale laboratory experiments, further demonstrates the relative importance in performing large scale fireball testing under field test programs similar to GEST.

In an attempt to determine the dependence of spectral power on fireball location, the temperature results for Channel 2 of the MB-4 event were processed in data segments of Δt = 0.3 sec for times from detonation ranging from 1.74 to 3.61 sec (Figure 25c). Note that these times span the fireball dimensions from the leading to the trailing edges. Although the data in general correspond more to a $(n\tau)^{-2}$ than $(n\tau)^{-5/3}$ falloff behavior, it should be recognized that the frequency response for Channel 2 (constant current resistance thermometer, f_c = 1 kc) was not as high as for the other channels (constant temperature hot wire, f_c = 5 kc) and therefore a somewhat faster fall off due to frequency response limitations was expected for the Channel 2 results. Note, for example, that the Channel 2 data in Figures 25a and 25b also consistently fall off faster than results for the other channels. Except for the time slice, 2.44-2.74 sec, all spectra results in Figure 25c including the one data segment corresponding to the complete set of fireball temperature data for MB-4 (1.74-3.61 sec) are seen to compare favorably. This latter result, as well as the spectra data presented in Figures 25a and 25b, illustrates that the turbulent spectral energy for the GEST fireballs is in general distributed in a well behaved/nominal manner over all wavenumbers. On the other hand, the MB-4 time segment for $2.44 \leq t \leq 2.74$ sec indicates that mid-fireball or core regions may experience detectable energy enhancement at large wavenumbers (high frequency). This finding suggests that the small high frequency eddies contained within the fireball core play a relatively more dominant role in this region's fluctuation energy content than that experienced in other parts of the fireball.

3.6.4 Microscale Data. In isotropic turbulence the Taylor microscale for temperature fluctuations is given by

$$\overline{\left(\frac{dT}{dt}\right)'^2} = \frac{2\,\overline{T'^2}}{\tau^2} \tag{7}$$

Based on this microscale formulation, the present digitized temperature data have been processed to provide approximate microscale data, as averaged and spatially transformed by the local velocity, for the GEST fireballs. For these calculations, the temperature conversion program was used along with the MB-3 and MB-4 nonstationary data (Figure 19). Results (within a factor of two) suggest that time microscales vary from 1 to 3 ms (Figure 22). As shown in Figure 22 corresponding spatial microscales, determined by the local velocity transformation, vary between 2 to 4 cm. Because of the sensitive dependence of the temperature time derivative $\left[\overline{(dT/dt)'^2}\right]$ to signal noise effects, some microscale results were also computed by subtracting the random-noise contributions (measured by non-fireball data) from the calculated raw data intensities. It was found that corrected scale data, at most, were only 20% larger than uncorrected results.

Microscale values can also be estimated directly from isotropic turbulence theory (Refs. 14 and 16) which provides the following microscale definition:

$$\lambda = (15)^{1/2}\ell\left(\frac{\tilde{u}\ell}{\nu}\right)^{-1/2} \tag{8}$$

In Equation (8), ℓ represents the integral scale of turbulence, $\tilde{u}$ is the RMS level for velocity fluctuations, and ν corresponds to the local kinematic viscosity. By assuming that the velocity intensity $(\tilde{u}/\overline{u})$ is comparable to temperature intensity $(\tilde{T}/\overline{T} \cong .2)$ and using

measured temperature data to determine the viscosity and length scales ($\ell \cong 3$ ft) a predicted microscale of about 3.2 cm is calculated for MB-3 and MB-4 corresponding to fidu times of 3.2 and 2.7 sec, respectively. Not only is this predicted result in fair agreement with measured scale data (3.6 cm, Figure 22) but measured trends generally behave in a consistent manner with the expected microscale dependence [Equation (8)] on intensity, viscosity (temperature) and velocity between the core/wake interface and the fireball base. The present favorable comparison between predicted and measured microscale data represents not only an interesting but a potentially very useful experimental verification of one aspect of turbulence modeling theory as applied to the early-time fireball. Since the turbulence Reynolds number

$$Re_\lambda = \frac{\tilde{u}\lambda}{\nu} \tag{9}$$

for $\lambda = 2$ cm is about 2000 for the current results, the ratio of the Taylor microscale to the dissipation or Kolmogorov microscale, given by

$$\frac{\lambda}{\eta} = 15^{1/4} R_\lambda^{1/2} \tag{10}$$

is approximately 90. It should also be noted that the indicated magnitude for the turbulence Reynold's number is "large" and suggests that spectra results should display an inertial subrange ($n^{-5/3}$) covering several decades in spectral power. The AFWL spectra data of Reference 6, as well as the TRW data of Section 3.6.3, indeed confirms that the five-thirds behavior holds true over a substantial range in wavenumber and thereby further substantiates the well developed turbulent nature of the early time GEST fireballs.

4.0 CONCLUSIONS

Using stationary rakes of hot wire anemometer probes, a series of temperature measurements have been conducted within rising fireballs created by detonation of large diameter (10 m) balloons filled with a methane/oxygen gas mixture (DNA's GEST Program). All measurements were performed after pressure equilibrium ($t > 1$ sec) but prior to completion of the toroid formation process and within the time required ($t < 4$ sec) for the fireball to rise one diameter. Based on an extensive processing/reduction of measured data for two single balloon events, MB-3 and MB-4, unique results describing the mean flow field and turbulent structure statistics for the early time large scale fireball have been determined.

Review of reduced temperature-time trace histories illustrate that the early time rising fireball is characterized by a highly intermittent irregular fireball top or cap, a constant (high) temperature core and a thermal wake exhibiting a linear decay in mean temperature. Not only are temperature fluctuations near the fireball "top" and bottom of the same order as local mean temperatures, but these fluctuations as well as temperature and temperature gradients are all higher at the leading edge of the fireball as compared to corresponding values at the trailing edge. This is evident, for example, in the "sudden" growth in temperature/intensity at the top of the fireball as compared to the gradual decay at the fireball base. Leading edges of "hot" eddies and the fireball core are generally characterized by steep temperature gradients relative to trailing edges which contain relatively shallow gradients. Hot fluid motion at the fireball top consists of steep gradient, large scale structure in combination with random pockets of intense turbulent activity. The presence of ambient air eddies embedded/entrained within the fireball top and wake is evident in the temperature history data as well as in available GEST

AD-A033 738 TRW SYSTEMS GROUP REDONDO BEACH CALIF F/G 15/6
HOT WIRE MEASUREMENTS OF TEMPERATURE FIELD STRUCTURE WITHIN GES--ETC(U)
MAR 76 R G BATT DNA001-74-C-0067
UNCLASSIFIED DNA-3936F NL

2 OF 2
AD A033738

END

DATE FILMED
2-77

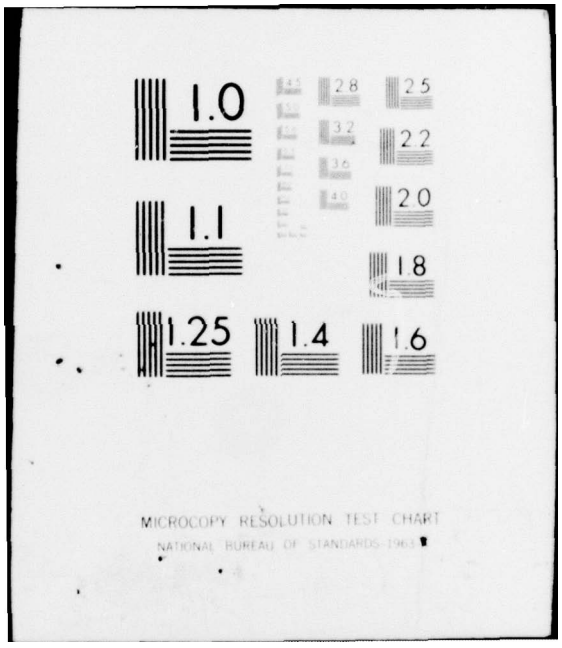
1.0
1.1
1.25
1.4
1.6
2.8
2.5
3.2
2.2
3.6
2.0
4.0
1.8
MICROCOPY RESOLUTION TEST CHART
NATIONAL BUREAU OF STANDARDS-1963

photographic results. This approximate thermal "picture" of a rising fireball agrees favorably with available laboratory data for buoyant thermals, as well as with fireball models which consider the fireball top to be "hard shelled" (capped) relative to the fireball base.

Specific results from the present investigation are as follows:

1. Reduced mean velocity data for the fireball core compare favorably with the optically-derived mean rise velocity (43 ft/sec). Thermal wake velocities were found to be twice as large as core velocities, a velocity increase somewhat smaller than that predicted for Hill's spherical vortex model ($\cong 2.5$).

2. Peak brightness temperature data determined from an IR measurements experiment (LASL) agree favorably with maximum fireball temperatures as measured herein ($T_{MAX} \cong$ 1100°C). Such a result substantiates the temperature measurement accuracy of the IR scanning technique and further justifies its use in measuring peak temperature data on other large scale detonation events. Trailing edge mean temperature gradients were approximately .4°C/cm whereas core leading edge gradients were 8.5°C/cm and 10°C/cm for MB-3 and MB-4, respectively. These mean gradient results contrast with instantaneous gradient data which were measured to be as high as 300°C/cm. Although MB-3 leading edge gradients are low relative to HULL code predictions (11°C/cm), the corresponding MB-4 data are in good agreement. Predicted temperatures from HULL code calculations compare poorly with the present temperature data in terms of maximum temperature (2000°C) and trailing edge gradients (3°C/cm).

These latter differences are partially explained by the substantial temperature attenuation caused by the fireball's turbulent mixing process, a feature not included in the "laminar" HULL code calculations.

3. Normalized temperature intensity data at the fireball top and within the thermal wake are comparable to mean temperature levels ($\tilde{T}/\overline{T} \leq .6$). Penetration of entrained ambient air into the fireball core region was limited as evidenced by the relatively quiescent (low level) core intensity data ($\tilde{T}/\tilde{T} \cong 0.10$).

4. Wake integral scales ($\Lambda \cong 3$ feet) determined from cross correlating data from vertically-aligned temperature probes were approximately 5% of the fireball mean radius. This result compares favorably to available scale results derived from optical data for an atmospheric nuclear detonation. Estimated scale data using measured autocorrelation times (41 ms) and the local convection velocity were approximately 20% larger than spatial scale results.

5. From moving frame autocorrelation results for the fireball thermal wake, an "e" folding decay time (eddy lifetime) of .17 $\pm$ .04 sec was measured. This time scale, which quantifies the decay behavior of the large eddies, is approximately a factor of four larger than measured autocorrelation times. The resulting time scale ratio is comparable to results for other turbulent flows and suggests that the intensities and gradients associated with the early time fireball eddy structure exhibit a

highly persistent nature, a finding consistent with those radar models which postulate relatively slow "smearing" of early time electron density gradients.

6. Probability density distributions for the fireball thermal wake were found to be "spiky" in nature, with some evidence of bimodal behavior, and slightly skewed to the negative side of their normalized values. Averaged values for skewness and flatness factors were approximately +.10 and 2.7, respectively.

7. Normalized spectra data, in general, followed Kolmogoroff's -5/3's falloff behavior for several decades in spectral power. Low wave number results, on the other hand, compared favorably with the formula

$$\frac{E(n)}{E(o)} = \frac{1}{1 + (2\pi)^2(n\tau)^2}$$

The noted large "spread" in the inertial subrange is consistent with the large turbulence Reynold's numbers for the GEST fireballs and with the homogeneous nature for the high frequency eddies associated with fully developed, large scale turbulent flows ($Re_D \cong 3 \times 10^7$).

8. Taylor microscale data were calculated from temperature and temperature gradient intensity data under the isotropic turbulence assumption. "Measured" results (within a factor of two) suggest that fireball wake microscales vary from about 2 to 4 cm. Predicted microscale magnitudes, although smaller, were of the same order as measured scale data, thus providing an "approximate" verification of turbulence modeling theory as applied to the early time fireball. For

a 2 cm microscale the turbulence Reynold's number was "large" (2000) and consistent with the large inertial subrange spread as observed in measured spectra results.

REFERENCES

1. Knapp, W. S., and Schwartz, K. "Aids for the Study of Electromagnetic Blackout," DNA 3499H, 25 February 1975.

2. Lin, S. C.; Tsang, T.; and Wang, C. P.; "Temperature Field Structure in Strongly Heated Buoyant Thermals," Physics of Fluids, 15, 2118, (1972).

3. Tsang, L.C.H., "Initial Formation Geometry and Evolution of Temperature Field in Buoyant Thermals," MSE Thesis, University of California - San Diego, 1974.

4. Mantrom, D. W., and Haigh, W. W., "Fireball Entrainment Study," DNA 3248F, also TRW Report No. 18895-6004-RU-00, June 1974.

5. Bigoni, R. A., and Matuska, D. A., "Gas Explosive Simulation Technique," AFWL TR-73-129, May 1973.

6. Bigoni, R. A., and Matuska, D. A., "Preliminary Report on Project Gas Explosive Simulation Technique," AFWL TR-74-252, October 1974.

7. Kovasznay, L.S.G., "Turbulence Measurements - Hot Wire Method," Physical Measurements in Gas Dynamics and Combustion, Princeton University Press, Princeton, New Jersey, 1954.

8. Corrsin, S., "Extended Applications of the Hot-Wire Anemometer," NACA TN 1864, April 1949.

9. Bradshaw, P., An Introduction to Turbulence and Its Measurement, Pergamon Press, 1971.

10. Carpenter, H. J., et al, "Blast Wave Boundary Layer Measurements, AFWL TR-73-211, (TRW Systems) March 1974.

11. Lamb, H., Hydrodynamics, Sixth Edition, Dover Publications, 1932.

12. Bendat, J. S., and Piersol, A. G., Random Data: Analysis and Measurement Procedures, Wiley Interscience, 1971.

13. Blackman, R. B., and Tukey, J. W., The Measurement of Power Spectra, Dover Publications, 1958.

14. Lumley, J. L., and Panofsky, H. A., The Structure of Atmospheric Turbulence, Interscience Publications, 1964.

15. Tennekes, H., and Lumley, J. L., A First Course in Turbulence, MIT Press, 1972.

16. Hinze, J. O., Turbulence, McGraw-Hill, 1959.

APPENDIX I

GEST - Temperature Measurements Task

Hot Wire Data Reduction Formulae

I. GEST - T (Temperature Conversion Program)

1. Constant Temperature Heat Transfer

$$\frac{e_w^2}{R_w} = \dot{q}_{NF} + \pi \ell \, Nuk(T_w - T)$$

where e_w = measured wire voltage

R_w = sensor resistance (constant)

$\dot{q}_{NF}$ = end loss (no flow) heat transfer (ambient conditions)

ℓ = sensor length

$Nu = .21 + .49\, Re^{.45}$ (Nusselt number, Ref. 12)

$Re = \rho ud/\mu$ (wire Reynolds number)

ρ, u, μ, k, T = density, velocity, viscosity, conductivity and temperature, respectively, of local flow

d = wire diameter

T_w = sensor temperature (constant)

2. Constant Current Temperature

$$T = \left((e_m + e_B) - e_A\right)(dR/de)(dT/dR) + T_A$$

where e_m = measured voltage

e_B = bucking voltage

e_A = ambient voltage

dR/de = electronics gain factor

dT/dR = sensor resistivity calibration

T_A = ambient temperature

3. Output from GEST-T Program

T; $\overline{T}$; dT/dt; $\overline{dT/dt}$; $\sqrt{\overline{T'^2}}$, temperature intensity; $\sqrt{\overline{(dT/dt)'^2}}$, temperature gradient intensity

$\overline{T'^3}/\sqrt{\overline{T'^2}}^3 = \sigma_3$, skewness factor; $\overline{T'^4}/(\overline{T'^2})^2 = \sigma_4$, flatness factor

II. GEST-TS (Turbulent Statistics Program)

1. Autocorrelation Coefficient

$$C_T(\Delta t) = \frac{\Sigma T(t)\ T(t + \Delta t)}{\Sigma T(t)\ T(t)}$$

i) Integral Time Scale

$$\tau_e \equiv \Delta t \text{ at } C_T(\Delta t) = e^{-1}$$

2. Cross-correlation Coefficient

$$C_{XT}(\Delta x, \Delta t) = \frac{\Sigma T(o,t)\ T(\Delta x, t + \Delta t)}{[\Sigma T(t)\ T(t)]^{1/2}\ [\Sigma t(\Delta x,t)\ T(\Delta x,t)]^{1/2}}$$

i) Integral Length Scale

$$\Lambda \equiv \Delta x \text{ at } C_{XT}(\Delta x, 0) = e^{-1}$$

ii) Convection Velocity

$U_c \equiv \Delta x/\Delta t$ determined from delay time for maximum C_{XT} correlation

iii) Eddy Life Time (Moving Frame Autocorrelation Time)

$\overline{\tau}_e$ = delay time for maximum C_{XT} correlation to decay to e^{-1}

iv) Power Spectral Density (PSD)

$$\overline{T'^2} = \int_0^\infty E(f)df$$

v) Time Microscale

$$\tau = 2\pi^2 \int_0^\infty Ef^2df^{-1/2}$$

$$\left(\cong\left(\frac{\overline{2T'^2}}{\overline{(dT/dt)'^2}}\right)^5, \text{ Section 3.6.4}\right)$$

vi) Probability Density Distribution Function

$$f(T): \overline{k} = \int_{T_1}^{T_2} k\ f\ dT$$

Note for Gaussian distribution

$$f(T) = \frac{1}{\sqrt{2\pi}\,\sigma} e^{-(T-\bar{T})^2/2\sigma^2} \quad , \quad \sigma_3 = 0 \quad , \quad \sigma_4 = 3$$

DISTRIBUTION LIST

DEPARTMENT OF DEFENSE

Defense Documentation Center
12cy ATTN: TC

Director
Defense Nuclear Agency
ATTN: RAAE
ATTN: DDST
3cy ATTN: STTL, Technical Library
ATTN: STSI, Archives

Commander
Field Command, Defense Nuclear Agency
ATTN: FCPR

Director
Interservice Nuclear Weapons School
ATTN: Document Control

Chief
Livermore Division, Field Command, DNA
Lawrence Livermore Laboratory
ATTN: FCPRL

OJCS/J-3
ATTN: J-3 WWMCCS, Mr. Toma

DEPARTMENT OF THE ARMY

Commander/Director
Atmospheric Sciences Laboratory
U.S. Army Electronics Command
ATTN: DRSSEL-BL-SY, F. E. Niles

Director
BMD Advanced Tech. Center
ATTN: CRDABH-O, W. Davies
ATTN: ATC-T, Melvin T. Capps

Program Manager
BMD Program Office
ATTN: DACS-BMS, Julian Davidson
ATTN: John Shea

Commander
Harry Diamond Laboratories
2cy ATTN: DRXDO-NP

Commander
TRASANA
ATTN: R. E. Dekinder, Jr.

Commander
U.S. Army Materiel Dev. & Readiness Command
ATTN: DRCDE-D, Lawrence Flynn

Commander
U.S. Army Nuclear Agency
ATTN: USANUA-W, J. Berberet

DEPARTMENT OF THE NAVY

Commander
Naval Surface Weapons Center
ATTN: WA501, Navy Nuc. Prgms. Off.

DEPARTMENT OF THE NAVY (Continued)

Director
Naval Research Laboratory
ATTN: Code 7701, Jack D. Brown
ATTN: Code 7750, Timothy P. Coffey
ATTN: Code 7720, Edgar A. McClean

DEPARTMENT OF THE AIR FORCE

AF Weapons Laboratory, AFSC
ATTN: DYT, Maj G. Ganong
ATTN: SUL
ATTN: SAS, John M. Kamm

AFTAC
ATTN: TF, Maj Wiley

HQ USAF/RD
ATTN: RDQ

SAMSO/SZ
ATTN: SZJ, Maj Lawrence Doan

ENERGY RESEARCH & DEVELOPMENT ADMINISTRATION

Los Alamos Scientific Laboratory
ATTN: Doc. Control for Eric Jones

DEPARTMENT OF DEFENSE CONTRACTORS

Aerospace Corporation
ATTN: V. Josephson

Calspan Corporation
ATTN: Romeo A. Deliberis

General Electric Company
TEMPO-Center for Advanced Studies
ATTN: Tim Stephens
ATTN: DASIAC

General Research Corporation
ATTN: John Ise, Jr.

Institute for Defense Analyses
ATTN: Ernest Bauer

Martin Marietta Aerospace
ATTN: Roy W. Heffner

McDonnell Douglas Corporation
ATTN: Robert W. Halprin

Mission Research Corporation
ATTN: M. Scheibe
ATTN: Dave Sowle
ATTN: P. Fischer
ATTN: Gary McCarter

Photometrics, Inc.
ATTN: Irving L. Kofsky

Physical Dynamics, Inc.
ATTN: A. Thompson